Flat plate pulsating heat pipes: A review on the thermohydraulic principles, thermal performances and open issues

Vincent Ayel, Maksym Slobodeniuk, Rémi Bertossi, Cyril Romestant, Yves Bertin

Flat plate pulsating heat pipes: a review on the thermohydraulic principles, thermal performances and open issues

Vincent Ayel[1*], Maksym Slobodeniuk[1,2], Rémi Bertossi[2], Cyril Romestant[1], Yves Bertin[1]

[1] Pprime Institute, CNRS – ENSMA – Université de Poitiers, UPR 3346, Futuroscope-Chasseneuil, France
[2] IPSA, Direction de la Recherche et de l'Innovation de l'IPSA, 92120 Ivry-sur-Seine, France

[*]Corresponding author: ENSMA, 1, av. Clément Ader, BP40109, 86961 Futuroscope-Chasseneuil, Phone: +33-5-4949-8112, Fax: +33-5-4949-8101, email: vincent.ayel@ensma.fr

Abstract

Thermal management of modern micro- and high-power electronic systems has become a progressively challenging problem due to current trends in miniaturization and increased heat generation. Conventional cooling methods, such as natural and force convection, have become insufficient to meet new challenges in electronics industries, transport and space applications where thermal management system size, mass, autonomy, high density and overall system reliability play a crucial role. Unlike active technologies, heat pipes are passive heat transfer devices without moving mechanisms which lead to greater reliability, even though they are limited by capillary, viscous and/or gravity factors. In contrast, the Pulsating Heat Pipe (also called Oscillating Heat Pipe) has recently become a source of increasing interest: first, due to fascination for the complexity of the internal two-phase phenomena; and secondly, due to novel applications, which are rapidly increasing the Technology Readiness Level of this device, for both ground and space environments. Pulsating heat pipe manufacturing can be divided into two categories: the classical tubular pulsating heat pipe, and the flat plate pulsating heat pipe. While the former is manufactured and developed from a single tube enrolled like a serpentine around heat and cold sources, the latter is obtained from a metallic plate including an engraved serpentine single channel, and hermetically closed on its top side by a second plate. These two manufacturing concepts lead to differences in operating behavior that are worth noting in order to better understand the functioning of the devices.

This paper presents a review of recent scientific experimental studies on thermal and flow behaviors of flat plate pulsating heat pipes, which present particular interest due to their structural dissimilarity compared to classical tubular pipes, leading to different thermo-hydrodynamic behaviors. The dissimilarities can be largely explained by the square or rectangular channels, leading to capillary pumping in the corners, and to the

thermal spreading effect associated with the geometrical continuity of the plate. Local studies of self-induced evaporation have demonstrated the faster evaporation process in square channels versus circular ones, which was confirmed later by comparison tests of channel shapes in FPPHPs. Furthermore, FPPHPs tested in horizontal orientation are more often subject to dry-out of the evaporator zone than tubular ones. Based on these considerations, a literature overview of local hydrodynamic visualizations and physical analyses is presented first in order to fully understand the phenomenological aspects, which will help to analyze the following sections on: the most influential parameters (channel dimension, fluid/material, geometrical aspects, operating conditions); thermal performances and attempts at significant improvements and, finally, the potentially promising fields of application and the processes applied in manufacture of flat plate pulsating heat pipes. Synthesis in appendix highlights the behavior of effective thermal conductivities of many papers with parameters such as the heat flux applied at the evaporator, figures of Merit from the literature or hydraulic-diameter-to-capillary-length ratio, showing its increasing trend with heat flux and diameter. Lastly, a table gathers all available material and geometrical characteristics and operating conditions of all devices tested in the presented literature.

Keywords

Flat Plate Pulsating Heat Pipes; Experimental; Slug flow; Annular flow; Heat transfer performances.

1 Introduction

In recent years, miniaturization of electronics components has induced high heat flux generation. Along with stringent requirements such as compactness, lightness and small energy consumption for the aerospace/transport/energy applications, this factor has led to challenging issues in thermal management. Among the highly efficient passive heat transfer devices for electronic equipment, one of the most promising cooling technologies is the Pulsating Heat Pipe (PHP). PHPs are thermally driven two-phase passive devices based on phase change-induced liquid motion and capillary forces. They can be defined as a single capillary tube or channel bent in several interconnected turns [Khandekar,02]. The tube is partially filled with a working fluid at the liquid/vapor saturation state, and distributed by means of surface tension effects in the form of liquid slugs and vapor plugs. Under the effect of the heat sources, pressure instabilities in the evaporation and condensation zones initiate complex two-phase flow, ranging from bubbly flow to slug/plug flow and annular flow, with effects on the total heat flux transferred by the PHP from the heated to the cooled zones.

Due to growing interest on the subject, many papers have been published in the literature about pulsating heat pipes since their initial appearance in the early 90's. Many details on their definition, fabrication process, thermal performance, hydraulic behavior, etc. can be found in the complete review papers or books including those of Ma [Ma,15], Bastakoti *et al.* [Bastakoti,18], Marengo and Nikolayev [Marengo,18] and [Nikolayev,18], and Khandekar *et al.* [Khandekar,10] with regard to hydraulic behaviour inside pulsating heat pipes and micro-channels, among others.

This paper will be specifically focused on a particular type of PHP known as the "Flat Plate Pulsating Heat Pipes" (FPPHP), which can be defined as: a flat plate with engraved/machined (or obtained by additive/etching manufacturing) single, generally square or rectangular channel forming a serpentine between one or more hot sources and one or more cold sources. This plate is sealed with a smooth plate cover to confine the channel. Figure 1 shows an example of copper plate with square serpentine channel machined on its top (a) and an example of micro-FPPHP designed and tested by Kamijima *et al.* [Kamijima,20] (b). It is essential to keep in mind two major issues that may differentiate a FPPHP from a capillary tube PHP; they have been discussed by Khandekar *et al.* [Khandekar,02] and thereafter by Yang *et al.* [Yang,09], Ayel *et al.* [Ayel,15a], as well as Qu *et al.* [Qu,12] regarding micro-FPPHPs. First, square shape channels engraved in the FPPHP plate have sharp angles in the corners, acting like capillary grooves assisting the liquid flow back to the evaporator zone; it may provoke premature rupture of the cross-sectional menisci, resulting in flow regime transition into annular flow. The liquid/vapor interface is thereby distributed over the edges and the corners of the channels. Operating in favorable vertical inclination, the FPPHP works quite efficiently in the capillary-assisted thermosiphon mode, even for the lowest heat power inputs, which is not the case with circular shape channels [Khandekar,02] [Qu,12]. Second, due to the geometrical continuity between channels, transverse thermal resistance is very low and thermal spreading occurs and tends to strongly decrease the thermal gradients between channels. This causes homogenization of the pressure differences in the channels, which

are the main drivers of oscillations under slug flow regime, particularly in horizontal inclination. The FPPHPs tested under such configurations consequently often shows premature dry-out [Khandekar,02][Chien,12][Ayel,14][Jun,18]. To sum up, with respect to capillary tube PHPs, FPPHPs should work more effectively under favorable vertical orientation (bottom heated mode, BHM), while they may come to a complete stop when functioning in a horizontal position. The distinction between the two systems has rarely been raised in the literature; even if their operations are based on the same physical principles, we are dealing with two different devices. As a result, taking into consideration the peculiarities of such device, tubular PHPs embedded in flat plate structures will not be considered according to the above definition as FPPHPS, and not be taken up in this review.

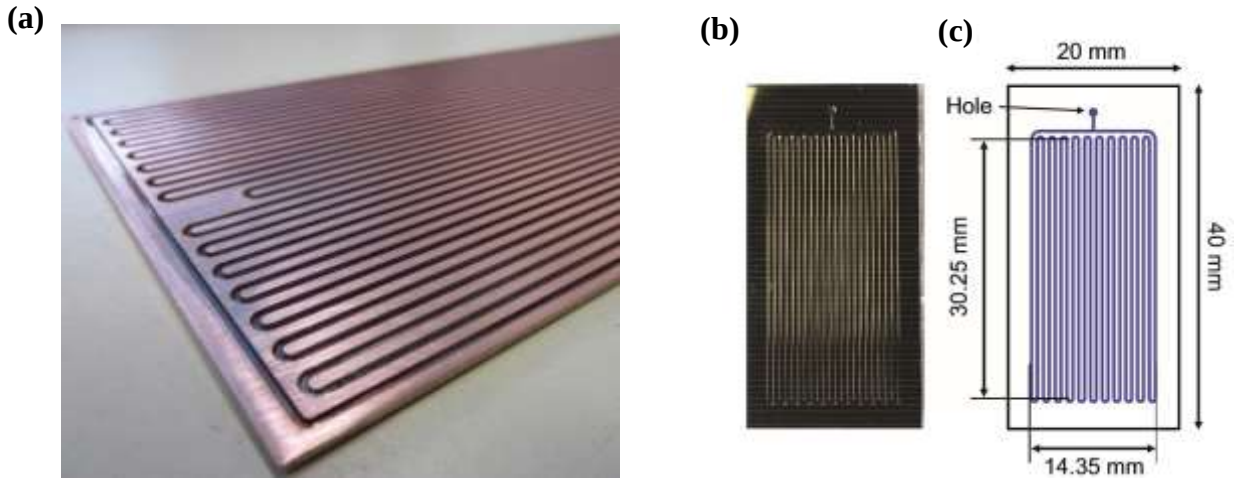

Figure 1: (a) Copper plate with machined engraved square channel forming U-turns;
(b) photograph and (c) schematic diagram of a micro-FPPHP [Kamijima,20]

Due to its specific design, in terms of applications the FPPHP does not have the same advantages and disadvantages as the tubular PHP; its flat and rigid shape does not allow integration capacity specific to the tubular structure, which can easily be wrapped around complex geometric shapes. On the contrary, due to its flat shape, good thermal contacts can be obtained with flat heat sources, which are favorable to heat transfer. Furthermore, its design is considerably more complicated than that of a tubular PHP and requires occasionally complex or expensive manufacturing techniques [Taft,15][Kearney,16][Betancur,20][Jung,20]. However, it is conducive to miniaturization, opening up the possibility of many applications in the field of micro-electronic cooling [Kearney,16][Guowei,19][Jang,19].

This paper will be focused exclusively on experimental studies conducted on flat plate pulsating heat pipes, and will be divided in four additional sections:

- First, the thermal and hydraulic behavior of FPPHPs will be described in section 2; starting from fundamentals on the main physical phenomena, followed by a focus on the peculiarities of capillary flows in channels with sharp corners, the hydrodynamics analyses of the flow patterns observed inside the FPPHP channels will be presented with global visualizations.

- Section 3 will be dedicated to the main parameters influencing the thermal performances of such devices, including the operating conditions (heat power, filling ratio and orientation), the geometrical aspects, particularly concerning the hydraulic channel diameter and shape, and the thermophysical properties of the working fluid.
- Section 4 will focus on how the different authors have tried more or less effectively to enhance FPPHP performances, by modifying the internal structure or design (using alternated channels, Tesla valves, multilayer channels…) or by modifying fluid properties (binary mixtures, self-rewetting fluids, addition of nanoparticles).
- Finally, in section 5, the main application fields for which these devices have been built and tested by the authors will be presented (from classical electronic cooling applications to space, transport and renewable and conversion energy applications), and the different manufacturing processes for this particular device will be shown.

A comparison of the effective thermal conductivities of the devices drawn from the literature will be presented in appendix A.1 as a function of influencing the operating or geometrical parameters exerting an influence, such as heat fluxes, figures of Merit and diameter-to-capillary-length ratio. In appendix A.2, table A1 will bring together the main geometrical parameters and operating conditions of all the FPPHPs tested by the different authors in their respective studies.

We have sought to present the most complete and relevant bibliographic study possible. Unfortunately, there will necessarily be some inadvertent oversights for which we wish to apologize to the concerned authors.

2 Thermal-hydrodynamic behavior of operating flat plate pulsating heat pipes

This section deals with the general physical phenomena involved in the operating of FPPHP. It presents a general overview of the studies contributing to the characterization of device behavior.

2.1 Main physical phenomena in PHPs

The basic physical operations of pulsating heat pipes are now relatively well-known. However, the complexity of the phenomena involved and the multiplicity of intense transfer sites along the tubes/channels make modelling approaches difficult. The objective of this section is to underline the main basic physical phenomena responsible for both heat and mass transfer inside PHPs, in view of better understanding the analyses and considerations to follow. An important work detailing PHP physics was written by Nikolayev and Marengo [Nikolayev,18], subsequent to the reviews authored by Zhang and Faghri [Zhang,08] and Ma [Ma,15]. In general, fluid flow pattern in capillary tube/channels of pulsating heat pipes is assumed to be slug flow (or “Taylor bubble flow”); liquid slugs and vapor plugs are initially distributed in the partially filled tube, moving according to the various driven forces between them. This is rendered possible when the channel hydraulic diameter becomes smaller than a threshold value called critical diameter, D_{crit}, characterized by

most authors using the Bond number defined in static isothermal conditions as the ratio between gravitational forces and surface tension ones ($Bo = (\rho_l - \rho_v)gD^2/\sigma < 4$):

$$D_{crit,Bo} \approx 2\sqrt{\frac{\sigma}{(\rho_l - \rho_v)g}} \quad (1)$$

When the channel diameter becomes inferior to $D_{crit,Bo}$, surface tension forces dominate and vapor bubbles and liquid plugs are separated by menisci [Marengo,18]. The values of critical diameters have been discussed by some authors [Ma,15], and can be called into question, particularly insofar as they do not take into account either the viscous or inertial forces concerning fluid motion or the variation of the gravity/acceleration field. As analyzed by Mangini *et al.* [Mangini,15], these factors are obviously not applicable to microgravity conditions. In PHPs, liquid plugs and vapor bubbles move with velocity of which the order of magnitude ranges from 0 to 1 m.s^{-1}, and due to its higher density, liquid inertia has been accepted as the predominant force between the two phases. In this case, new criteria considering inertial forces based on the Weber number ($We = \rho_l u_l^2 D/\sigma < 4$) were proposed by Gu *et al.* [Gu,04] (eq (2)), or considering both inertial and viscous effects, based on Garimella number ($Ga = \sqrt{Bo}Re < 160$), leading to the more relevant criterion proposed by Harichian and Garimella [Harichian,10], defining the diameter limitation for reduced gravity fields (Eq. (3)). More details can be found in [Mangini,15] and [Mangini,17].

$$D_{crit,We} \approx 4\frac{\sigma}{\rho_l u_l^2} \quad (2)$$

$$D_{crit,Ga} = \left[\frac{160\mu_l}{\rho_l u_l}\sqrt{\frac{\sigma}{(\rho_l - \rho_v)g}}\right]^{1/2} \quad (3)$$

First, considering the liquid slug motion, two main phenomena are necessary to model them: momentum and heat transfer represented by the Nusselt number. The main forces acting on slug-bubble system are due to surface tension, viscosity, inertia, tangential shear stresses and the force associated with the disjoining pressure at the molecular level. The non-dimensional numbers of interest in such configurations are the Reynolds number ($Re = \rho_l u_l D/\mu_l$), Capillary number ($Ca = \mu_l u_l/\sigma$), Bond and Weber numbers (see above), etc. For example, in the context of a PHP, in common working fluids such as water, acetone, and common refrigerants etc., typical Ca will ranging from 10^{-4} to 10^{-1}. The integrated momentum equation over the channel cross-section S of a moving liquid slug of length L_s is given by ($S = a.b$ for a square/rectangular channel of width a, and height b; or $S = \pi R^2$ for a circular channel of radius $R = D/2$):

$$\frac{d(m_l u_l)}{dt} = [(P_r - P_a) - \Delta P_c \pm \rho_l g dh]S - (F_\tau + F_{turns}) \quad (4)$$

In Eq. (4), m_l represents the liquid plug mass ($m_l = S.L_s$) and u_l the liquid slug velocity. ΔP_c is the capillary pressure drop arising from hysteresis between advancing (θ_a) and receding (θ_r) contact angles during the motion of the slug ($\Delta P_c = (2\sigma/R)(-\cos(\theta_a)+\cos(\theta_r))$). This additional resistance is additive and gets

amplified if several slugs are simultaneously located in a channel (figure 2). The cumulative pressure gradients damp oscillations and, when contact angle hysteresis is too large, an excessive number of liquid plugs may rapidly block the flow, especially if the driving force is not sufficient [Khandekar,10]. $\rho_l g dh$ represents gravity pressure drop, which is positive or negative according to the inclination of the tube and the direction of the slug motion. F_τ represents the viscous shear stress term (classically, $F_\tau = \Lambda(L_s/D)S(\rho_l u_l^2)/2$, with $\Lambda = 64/Re$ the Poiseuille flow friction for laminar flows); (it will be noted in section 2.2 that the "oscillating" motion and the vortices at the proximity of the menisci have additional effects on conventional viscous pressure drops), and F_{turns} a supplementary force coming from the pressure drop when the plugs in part or in their entirety enters inside the curved part of the tubes [Nikolayev,18]. For liquid slugs of high length-to-diameter ratio ($L_s/D >> 1$), the viscous shear stress terms becomes preponderant relative to the capillary ones. Finally, the pressure difference $(P_r - P_a)$ in Eq. (4) is guided by the pressures of both vapor bubbles surrounding the liquid slug, and appears to be the main driver of the liquid slug motions inside tubes of pulsating heat pipes. Relevant modelling of mass and momentum transfer inside PHPs consequently necessitates precise evaluation of the vapor thermodynamic state, which add further difficulty.

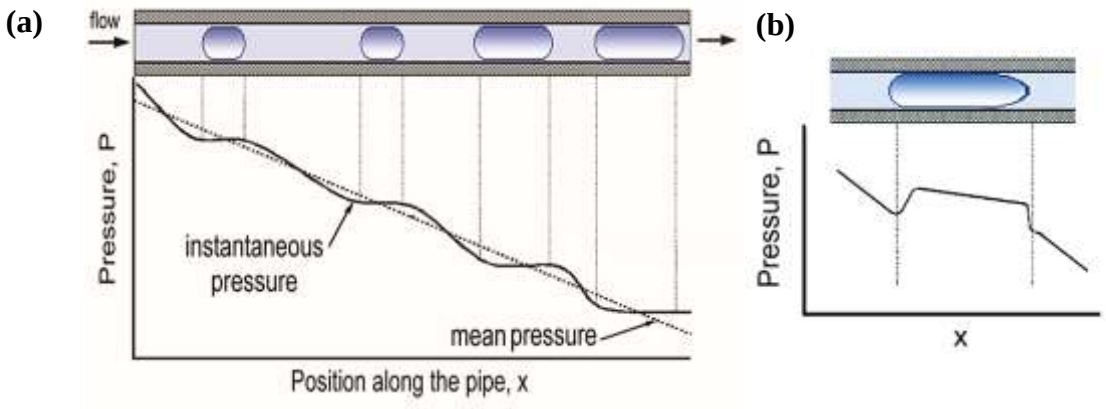

Figure 2: Pressure drop in Taylor bubble flow assuming (a) no pressure in individual bubbles; (b) liquid plug advancing angle lower than $\pi/2$ [Khandekar,10].

Some of the following is derived from [Nikolayev,18], who drew up from the literature concerning PHPs a complete and comprehensive review of the modeling approaches of the vapor thermodynamic phase, especially as regards the spring that provides oscillations. A major issue concerns thermodynamics: Is the vapor at saturation state or superheated state? On the one hand, according to Kim and Kim [Kim,20], vapor pressure can be regarded as the saturation pressure corresponding to the vapor temperature if the vapor plug is entirely covered by the liquid film (saturation state only). On the other hand, other authors showed that vapor can be superheated [Gully,15][Jun,18][Jun,19][Mameli,19]. Jun and Kim [Jun,18] measured fluid temperature in different micro-FPPHP locations; with a sufficiently long vapor plug, they highlighted both a superheated region in the evaporator zone, and a saturated temperature region in the adiabatic zone of the same bubble. This means that there can exist a wide temperature gradient in a vapor plug, with local superheated zones. In

addition, testing their hybrid thermosiphon / tubular PHP under microgravity conditions, Mameli *et al.* [Mameli,19] analyzed local thermodynamic states by measuring vapor temperatures at both ends of a tube between condenser and evaporator zones. They showed that the evaporator was mainly superheated and the condenser mainly subcooled, with increasing subcooling level with heat input in both zones. According to the authors, the fluid can be metastable (superheated liquid phase for temperatures above saturation, and subcooled vapor phase for temperatures below saturation). The level of energy that separates the fluid thermodynamic state at saturated equilibrium is exchanged as sensible heat (or latent heat in the metastable state), and should be taken into account in the overall energy balance of a pulsating heat pipe.

Nevertheless, according to [Nikolayev,18], vapor behavior may be assimilated to that of the ideal gas law:

$$P_v = \frac{m_v R_v T_v}{V_v} \tag{5}$$

In Eq. (5), m_v, R_v, T_v and V_v are, respectively, the mass, specific gas constant, temperature and volume of the vapor plug. This equation can be used as the exact equation of gas states of closely approaches the ideal gas law, rather than more sophisticated laws (the deviation from the ideal gas law can be corrected using the compressibility factor Z [Kim,20]). According to [Nikolayev,18], and contrary to what has been assumed by many authors, the vapor cannot be simultaneously and continuously both saturated and superheated. For example, in the author's own words, during compression phases, if the vapor is compressed quickly enough and its compression is not strong, liquid drop nucleation does not occur and the vapor evolves in the metastable state. When superheated vapor is compressed or dilated, the pressure changes along the isothermal curve create a restoring force for oscillations. Concerning heat exchanges, they occur between vapor and dry walls, following:

$$\dot{Q}_v = h_v \pi D L_v (T_w - T_v) \tag{6}$$

h_v is the vapor heat transfer coefficient, L_v the vapor bubble length and T_w the inner wall temperature. In order to summarize the evolution of the vapor bubble pressure, the energy equation is used, starting from the first law of thermodynamics, for superheated vapor:

$$m_v c_{v,v} \dot{T}_v = R_v T_v \dot{m}_v - P_v \dot{V}_v + \dot{Q}_v \tag{7}$$

$c_{v,v}$ is the vapor heat capacity at constant volume. Generally, this term can be neglected, simplifying the above Eq. (7), as in [Noh,20], but there is still some controversy concerning on the term which is sometimes replaced by a much larger quantity h_{lv}, overestimating the power injection into the vapor and the consequent mechanical response. In any event, one important term in Eq. (7) is the vapor mass derivative, which comes mainly from the mass exchange rate due to evaporation/condensation processes, particularly through the thin deposited liquid film from receding menisci, as will be described below: one of the most important terms in

vapor bubble pressure variation inside evaporator comes from the vapor formation due to evaporation from thin film deposited on the walls of the capillary. Further details can be found in [Nikolayev,18] on the complex operation of the vapor thermodynamic state.

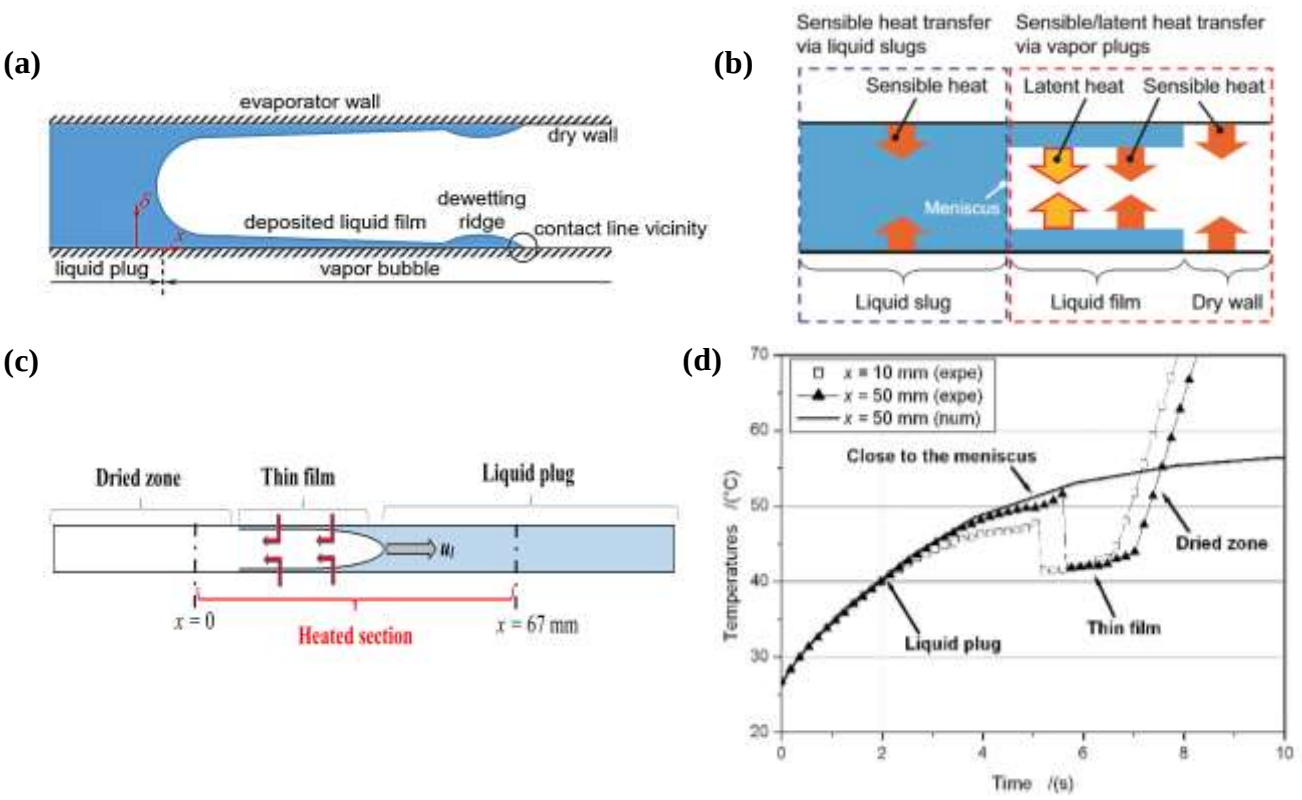

Figure 3: (a) Schema of the film shape following receding in the PHP evaporator [Nikolayev,18]; (b) corresponding heat transfer in different zones [Kamijima,20]; (c) Schema of an evaporating thin film in heated copper tube; and (d) film infrared thermography of the outer wall temperature of the heated copper tube wherein water flows –the continuous line corresponds to numerical calculations on the basis of establishing laminar liquid flow- ($T_{sat} \approx 42$°C, u_l = 69 mm.s^{-1}, $\dot{q}_{ev}$= 17200 W.m^{-2}) [Ayel,15b]

A slug flow pattern appears when a liquid plug, separated by two (advancing and receding) menisci, flows inside a capillary tube, and a thin liquid film is deposited on the wall surrounding the vapor bubbles. The liquid film seems to be a result of competition between viscous and capillary forces in a transition region adjacent to the liquid meniscus [Nikolayev,18]. While viscous friction tends to immobilize the fluid near the wall, increasing its thickness, the surface tension forces tend to decrease the meniscus area, thereby decreasing its thickness. This competition is illustrated by the capillary number ($Ca = \mu_l u_l/\sigma$), which has been developed in previous studies following the theory of lubrication by Bretherton [Bretherton,61], and establishing that the deposited film thickness δ follows the scaling $(\delta/R) \approx Ca^{2/3}$ (for Ca ranging from 10^{-3} to 10^{-2}, R being the radius of the channel). Figures 3a and b provide an overview of the key parameters affecting heat and mass transfer between a receding meniscus and its neighboring vapor bubble: liquid plug momentum, thin liquid film deposition, evaporation/condensation, contact line vicinity, dewetting effect and vapor thermodynamic

state. It is well-known that during phase-change heat transfer across menisci, as in PHPs, a major contribution comes from the thin films covering part of the interior of the capillaries [Khandekar,10]. These films strongly contribute to the motions of slugs and plugs due to rapid evaporation from heat transfer through their exceedingly low thickness (δ, few tens of micrometers) by providing a large amount of vapor in the closed volume bubbles, through which they are widened.

However, in the early PHP studies PHPs, it was repeatedly established that vapor evaporation/condensation contributes to slug/plug flow motion mainly as a motor for PHP oscillations, and that a major part of the heat exchanged comes from the sensible heat of the liquid slugs flowing in both the heated and cooled PHP sections. More recently, it was experimentally proven that latent heat was predominant in the heat exchanges of pulsating heat pipes (see section 2.3.3 below, and analyses from [Jo,19], [kamijima,20] and [Jung,21], where it appears that between 55% to more than 80% of heat is transferred by latent heat exchanges in both evaporator and condenser).

First, when considering the heat transfer through thin film evaporation, the mass evaporation flux is guided by:

$$\rho_l \frac{d(\delta)}{dt} = -J \qquad \text{and} \qquad h_{lv} J = \frac{\lambda_l (T_w - T_i)}{\delta} \tag{8}$$

In Eq. (8), J is the mass evaporation flux (per unit area), T_w the inner wall temperature and T_i the liquid/vapor interface temperature, nearly always equal to the saturation temperature T_{sat} corresponding to the vapor pressure (for a pure fluid). In the above equation, sensible heat flux in the vapor has been neglected with respect to the latent heat exchange [Nikolayev,18]. Heat transfer during thin film evaporation is consequently guided by heat conduction through thin film thickness δ. As mentioned above, the very low thickness leads to very high heat transfer coefficients (HTC), ranging from 10^3 W.m^{-2}K^{-1} for refrigerants at $\delta \approx 100$ µm to more than 50x10^3 W.m^{-2}K^{-1} for water at $\delta \approx 10$ µm. These values are considerable when compared to those obtained with sensible heat exchanges in liquid slugs in laminar flows and vapor plugs, even for temperature differences higher in sensible heat than in latent heat. For example, considering single liquid phase heat transfer measurements from Han *et al.* [Han,12], the Nusselt numbers tend to the classical value of 4.36 for established laminar flow, when the length of the liquid plugs L_s *is* very long ($L_s/D >> 1$), but it may increase by one order of magnitude when the velocity increases and/or the length is close to the tube diameter ($L_s/D \approx 1$) [Nikolayev,18]. In the best conditions (common alcohols, ethanol or acetone, having intermediate values), one thereby obtains HTC values ranging from around 1 W.m^{-2}K^{-1} for refrigerants up to less than 10^2 W.m^{-2}K^{-1} for water. As regards sensible heat exchanges in the vapor phase under the same conditions, the maximum HTC obtained is lower than 1 W.m^{-2}K^{-1}, meaning that it is possible to neglect these aspects of heat exchanges in the overall heat balance of pulsating heat pipes.

To illustrate this, Chauris *et al.* [Chauris,15] performed thermal measurements of thin liquid film evaporation in a 2 mm capillary copper tube (see figures 3c-d). It consisted of the flow of semi-infinite liquid

slugs (terminated by receding menisci, depositing thin film and followed by vapor phase theoretically at saturation state) inside a capillary tube heated by Joule effect, and painted in black on its outer surface (tube wall thickness: 0.2 mm). Infrared thermography allowed calculation of the temperature field at the top line of the tube and clearly distinguished the four heat transfer areas during the transient phase of heating, when the liquid slug crosses the heated area; on figure 3d, the transient temperature curve initially shows a temperature increase of the tube cooled only by classical convective cooling from single-phase liquid flow (the experimental results are quite congruent with numerical CFD calculations of single phase liquid convection); after which, the region named "close to the meniscus" begins when the experimental and numerical curves are separated from each other (after 3.6 s); as discussed in section 2.2, the lower experimental temperature tends to prove that the Nusselt number increases in the region near the meniscus. The third zone corresponds to the liquid thin film evaporation phase; there is a sudden drop in wall temperature curves (linked to heat storage release). Due to the marked intensification of heat transfer in this area, the wall temperature seems to be almost constant in time, and its minimal value is very close to the vapor saturation temperature T_{sat}. The last zone corresponds to the sharp linear increase of temperature ("dried zone", right-hand side of the curves). It starts when the thin film is completely evaporated, namely when the contact line passes through the corresponding abscissa. These results, which are also obtained with n-pentane and ethanol, confirm the above-mentioned assertion that latent heat transfer via the liquid films accounts for a considerable portion of the total heat transfer rate in pulsating heat pipes.

However, as has been observed in experiments, this affirmation requires reconsideration when nucleate boiling occurs in liquid plugs,. In that case, heat transfer during boiling of liquid flows inside small diameter tubes and mini-channels as described by Kandlikar [Kandlikar,02] appears to attain the same order of magnitude of HTCs as during thin film evaporation (10^3:10^4 $W.m^{-2}K^{-1}$). It then becomes necessary to insert a wall temperature trigger criterion for the appearance of nucleated bubbles with the corresponding heat transfer coefficient. When the wall temperature becomes higher than the wall superheat necessary to onset nucleation, the cavity on the capillary wall inner surface becomes active, and a small entrapped hemispherical vapor nucleus starts to grow. In their model, Qu and Ma [Qu,07a] included the classical criterion of superheated vapor temperature necessary to grow the vapor bubble, and found it to be associated with the size of the cavity (of radius r_c) at the wall, evaluating the influence of r_c on the degree of superheat as follows:

$$T_n - \mathrm{T}_v = \frac{RT_nT_v}{h_{lv}} \ln\left[1 + \frac{2\sigma}{P_v}\left(\frac{1}{r_c} - \frac{1}{r_m}\right)\right] \tag{9}$$

In Eq. (9), T_n, and T_v, represent the small vapor nucleus temperature and the temperature in the vapor bubble next to the liquid slug where nucleation occurs, respectively; r_m is the radius of curvature of the liquid-vapor cross-sectional interface in the capillary channel. In the subsequent study by Senjaya and Inoue [Senjaya,13], the degree of superheat was taken as a fitting parameter, initially set at 5 K. Bae *et al.* [Bae,17], and Noh and Kim [Noh,20] took into account the roughness of the channel's inner walls (also noted r_c), using

the Howel and Siegel correlation [Howel,67] to calculate the wall superheat criterion in their modeling approaches:

$$T_w - \mathrm{T}_{sat}\,(P_v) > \begin{cases} \dfrac{4\sigma T_{sat}}{h_{lv}\rho_v\left(\frac{\lambda_l}{h_{l-s}}\right)} & r_c \geq \dfrac{\lambda_l}{h_{l-s}} \\ \left(\dfrac{2\sigma T_{sat}}{h_{lv}\rho_v r_c}\right)\dfrac{1}{1-r_c/\left(\frac{\lambda_l}{h_{l-s}}\right)} & r_c < \dfrac{\lambda_l}{h_{l-s}} \end{cases} \tag{10}$$

In Eq. (10), $h_{l\text{-}s}$ is the liquid slug convective heat transfer coefficient, and ($\lambda_l/h_{l\text{-}s}$) represents the thermal boundary layer thickness.

Finally, many other local phenomena occurring during phase change may likewise have an influence on heat transfer during evaporation and/or condensation; they include heat transfer at the contact line, involving contact line dynamics, or dewetting phenomena, as can be seen on figure 3a with the dewetting ridge. Similarly, thermal coupling with the solid walls of the PHP is of major importance, particularly when the evaporator is massive, as is the case for FPPHPs. The authors invite the readers to consult the papers by Bae *et al.* [Bae,17], Noh and Kim [Noh,20] and the book by Nikolayev and Marengo [Nikolayev,18] for further details concerning all these phenomena. However, these considerations become less relevant when the fluid flow regime turns into annular flow, leading to different physical phenomena, in which latent heat exchanges also predominate.

2.2 Peculiarity of capillary flows in square/rectangular channels

While several authors have used circular channels [Lin,08][Lin,09][Ibrahim,17][Facin,18][Betancur,20], most have preferred FPPHPs with square or rectangular channels due to manufacturing facilities (machining); moreover, sharp angles induce capillary pressure imbalance between the edges and the corners. Compared to studies on two-phase flows in circular tubes, research works on two-phase flows square channel remain limited. One example: Having measured liquid film thickness in a micro-square channel, Han and Shikazono showed that it varies along the channel perimeter, rendering a theoretical approach of two-phase flow more complicated [Han,09]. Essential information about the distribution of the film thickness along the perimeter, its minimum and maximum values, etc. is still elusive despite its pronounced interest for two-phase microfluidic systems, as stated by [Magnini,20], who performed a numerical analysis of the gas bubbles propagating in square capillaries. The first consequence of the presence of corners is that the trapped liquid films provide paths between the bulk meniscus and the neighboring vapor bubble (see figure 4a-c). Even in dry-out conditions or with non-moving bubbles, the liquid is transported within the films under the action of the pressure gradient induced by capillary effect (variation of the meniscus curvature along the interface). This efficient self-induced transport mechanism of liquid by the films is naturally absent in circular tubes.

Gurumarthy *et al.* present examples of numerical visualizations of spontaneous rises against gravity of polydimethylsiloxane (PDMS) menisci along the corners of a 3 mm square tube, at t = 5 s after starting from

flat interface, according to the contact angle θ (figure 4a, between 0° -left- and 60° -right-) [Gurumarthy,18]. They showed that at the early stages of capillary rises, the corner rise precedes the bulk rise against gravity for contact angle values $\theta < 45°$. Corner capillary rise can reach at least as many as 20 millimeters. By the same token, figure 4b show photographs of two successive menisci in a FPPHP tested during a parabolic flight campaign (2 mm square channel, FC-72, vertical orientation, without applied heat power). During transition between hypergravity ($\approx 1.8g$) and microgravity (μg) phases, the menisci, initially barely curved under the major effect of gravity forces *vs.* relatively low capillary ones (step 1), immediately undergo a decrease of their bulk radius of curvature (step 2). At the same time, liquid films start to flow along the corners of the square cross-section in the direction depicted by red arrows (steps 3-4) due to capillary forces and to the high wettability of FC-72 with copper. Due to the incompressibility of the liquid phase [Ayel,19] and coupled with thermodynamic instabilities in vapor phases, this phenomenon subsequently causes displacement of both menisci in two opposite directions (yellow arrows), . This capillary flow can help to improve the wetting of the evaporation zone, which is located at the top part of the schema of figure 4c.

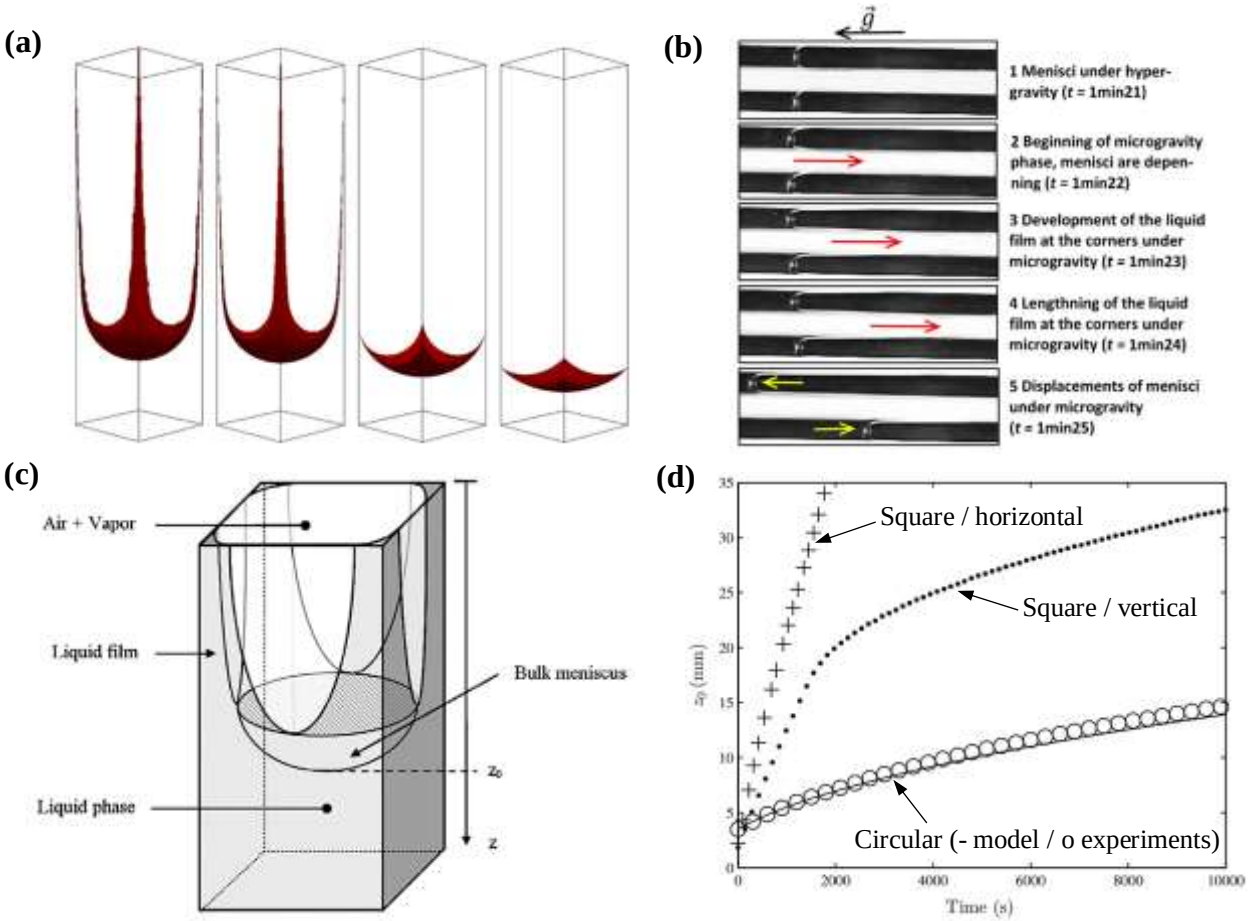

Figure 4: (a) Meniscus shapes in capillary square tube with different contact angles and at time t = 5 s (D_h = 2 mm, PDMS, from top to bottom: θ = 0°, 15°, 45° and 60°) [Gurumurthy,18]; (b) sequences of two isolated menisci during a transition between hyper -and micro-gravity phases (D_h = 2 mm, FC-72, vertical, Q = 0 W) [Ayel,19]; (c)

schema of liquid films in a capillary square tube; (d) bulk meniscus position *vs.* time: comparison between square and circular tubes (D_h = 2 mm, n-hexane) [Chauvet,10].

Figure 4c illustrates a schema of a bulk meniscus with thick capillary films in the corners of a square capillary tube and dried edges. In their experimental study, Chauvet *et al.* [Chauvet,10] tested self-induced evaporation of n-hexane in capillary tubes of square or circular cross-section and open to stagnant ambient air (D_h = 1 mm). Their results confirmed a tendency indicating that evaporation in a channel with corners can be several orders of magnitude faster than in a circular channel with the same dimensions (figure 4d); evolution of the bulk meniscus position z_0 *vs.* time (z_0 = 0 starting from the top of the tube), which is due exclusively to progressive evaporation of the fluid in the tube, is faster in horizontal than in vertical orientation for the square channel, and under the same conditions, both are much faster than in the circular tube. Whatever the tube orientation, the corner films considerably accelerate evaporation; as stated by the authors, the location of the phase change is not (in contrast with circular channels) at the bulk meniscus, and the evaporation rate is much greater owing to capillary pumping through the corner films, which results in phase change location closer to the evaporating zone than would be the case from a circular cross-section.

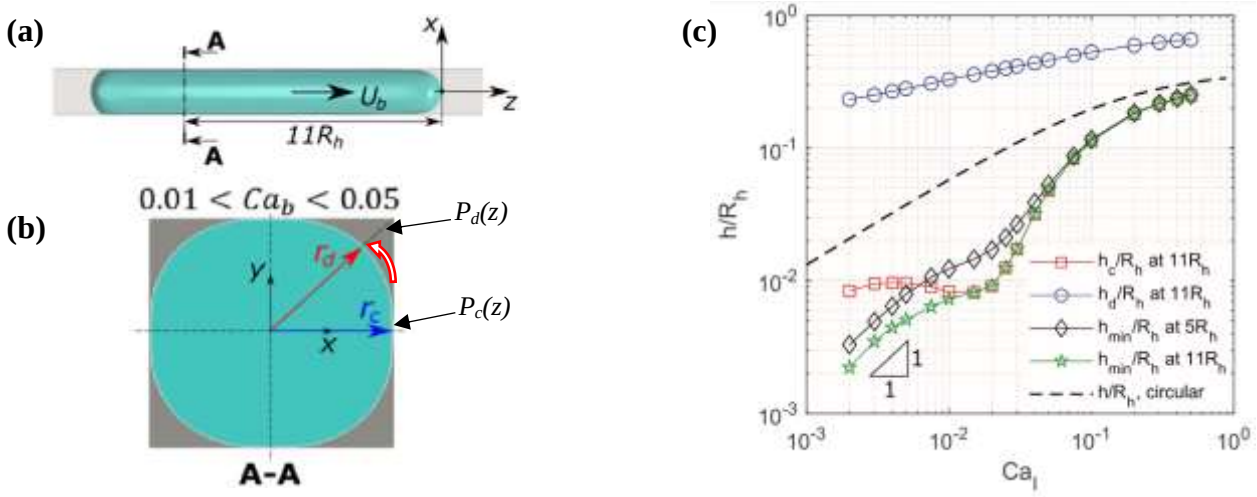

Figure 5: (a) Elongated bubble travelling in a square capillary, and (b) representative cross-sectional bubble shapes; (c) channel center (h_c), diagonal (h_d) and minimum (h_{min}) film thicknesses *vs.* *Ca* (*We* << 1) [Magnini,20]

As regards the liquid film deposited on the channel walls by the receding menisci of moving liquid slugs, its morphology in the transverse cross-section is, of course, very different from that found in circular tubes. Han and Shikazono [Han,09] measured the film thicknesses of water, ethanol and FC-40 deposited in square channels with hydraulic diameter ranging from 0.3 to 1 mm as functions of capillary and Weber numbers. They observed that the liquid tends to move towards the corner due to non-uniform pressure distribution at small capillary number. Liquid film thickness at the channel center (ex: along *x*-axis of figure 5a) decreases and remains much thinner than in an equivalent circular tube of the same diameter. On the other hand, the liquid film thickness at the channel corners tends to increase after deposition, approaching an asymptotic

value; given the variation of curvature radii from centers to corners, the deposited liquid film flows from channel centers to corners due to pressure gradient along the channel perimeter. In a numerical study of the morphology of long gas bubbles propagating in square capillaries, Magnini and Matar [Magnini,20] explained that the radius of curvature is higher in the channel center (r_c, figure 5a) than in the corners ("diagonal", r_d, figure 5a), so that the pressure in the centerline zone ($P_c(z)$) remains higher than in the corners ($P_d(z)$). The transversal pressure gradient drives a transverse flow of liquid that drains the thin-film region (see red arrow of figure 5b), thereby explaining a progressive thinning of the liquid from the center towards the corners. Figure 5c displays the liquid film thickness along the cross-section diagonal in the corners (h_d), the channel center (h_c) and minimum thickness (h_{min}) as functions of the capillary number *Ca* calculated with numerical simulations (R_h being the channel hydraulic radius) [Magnini,20]. Minimum thickness h_{min} corresponds to the formation of a dimble on the interface between center and corner, and has been numerically identified for low capillary numbers ($Ca \leq 0.01$); the interface curvature changes and exhibits a saddle shape at the channel center. Figure 5c confirms that the diagonal (corner) film thickness is considerably larger than the uniform thickness measured in circular channels (dotted black line), with a difference of one order of magnitude when $Ca \leq 0.01$. On the other hand, film thickness at the channel center is always below the value for circular channels, with a smaller order of magnitude when $Ca \leq 0.01$. Thinning film can attain critical values with regard to the stability of the film of partially-wetting liquids, and may lead to rupture and the formation of dry-out patches along the channel walls [Khodaparast,18].

To quantify the mass/heat transfer performances in square capillaries, it is also imperative to study wall shear stress in capillaries. Pressure drop in a slug/droplet couple could be modelled as the sum total of the frictional pressure drops in the liquid slug, in the gas bubble, and of the interface pressure drop over the bubble. The pressure drop in the bubble region and the thin surrounding film can be modelled as annular flow, but only when the length of the bubble is at least as much as the channel diameter [Abdollahi,20]. While Khandekar *et al.* [Khandekar,10] drew up a wide-ranging inventory of hydrodynamic phenomena occurring inside pulsating heat pipes, from the influence of the three-phase contact line to the oscillating menisci inside capillaries, most other studies have dealt with circular tubes. The propagation of long bubbles inside a square capillary is naturally different from that observed in circular capillaries, especially at low *Ca* numbers. In circular capillaries, the flow assumes a cylindrical symmetry, acting like a tight-fit piston with liquid film lubricating the bubbles. Whereas for square sections, the flow is symmetric (along planes perpendicular to *x*-axis, and *y*-axis, figure 5a, if gravity forces are neglected), but not axisymmetric [Taha,06]. It is essentially three-dimensional and in this case, the bubbles act like a leaky piston. At low *Ca*, the bubbles are not axisymmetric, flattening out against the walls and the liquid lenses at the leaky corners. At moderate and high capillary numbers, once the liquid film becomes thicker and the front meniscus sharper, resembling those inside circular tubes, the bubble bodies become more and more cylindrical and axisymmetric [Taha,06]. Figure 6a and b shows streamline patterns around bubbles rising inside a 2 mm capillary square channel filled with silicone oil, here for $Ca = 0.06$, and along two directions: side and diagonal of the square cross section

(ex: along r_c, and r_d, respectively, of figure 5a). Two vortexes are clearly noticeable ahead of the bubble, but they tend to disappear as *Ca* increases; this results in detachment of the back flow from the interface, producing a new recirculating flow pattern in which the recirculating rigs shrink toward the symmetry line. In figure 6a-b, the two views are quite similar, except that the liquid film close to the wall surrounding the vortex and the bubble is thicker and more discernable from the diagonal view (b). As it lacks cylindrical symmetry, the vortex in square capillaries is not toroidal, and its diagonal view is wider than its side view [Taha,06].

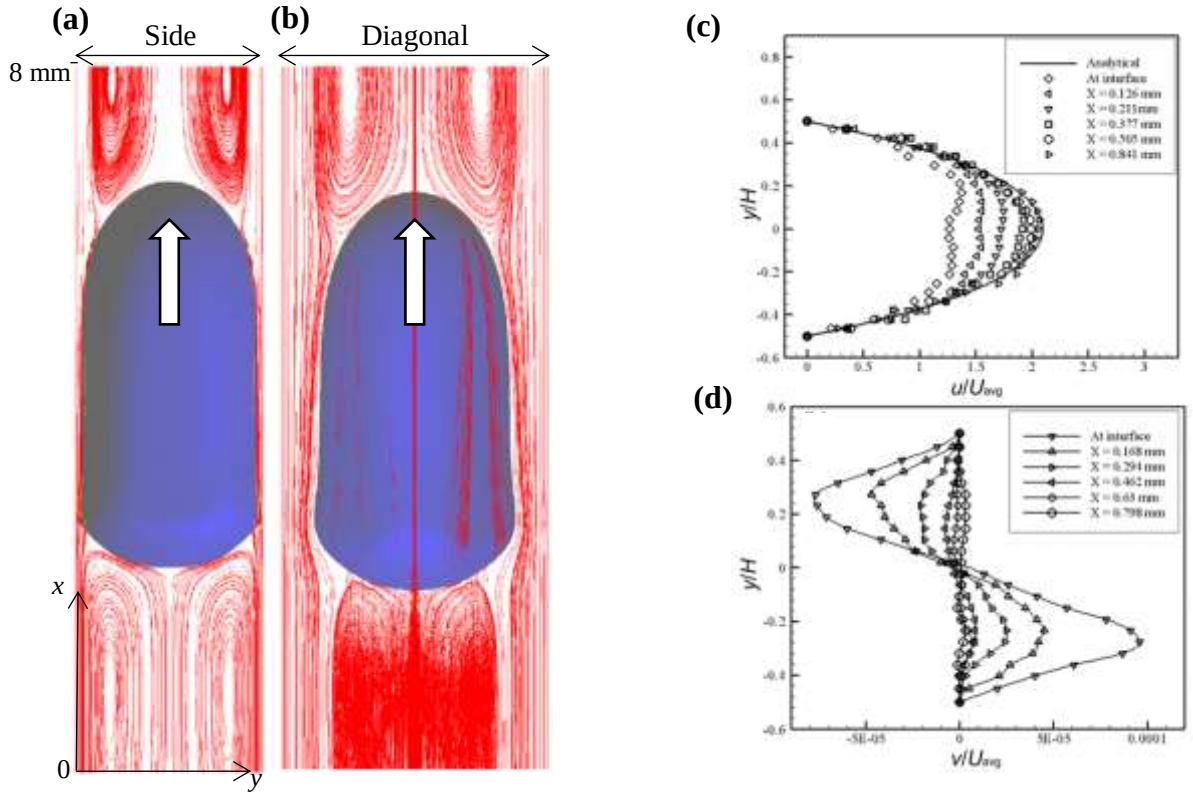

Figure 6: Flow velocity field around a gas bubble rising inside a 2 mm square capillary: (a) side direction, (b) diagonal direction (silicone oil, *Ca* = 0.06; arrows: flow direction) [Taha,06]; variation of non-dimensional components of velocities *vs.* distance from the advancing meniscus of a liquid plug in a 1 mm horizontal square channel: (c) u/U_{avg} and (d) v/U_{avg} (U_{avg} = 0.277 m.s^{-1}, *Ca* = 3.7x10^{-6}) [Rana,14]

Rana *et al.* [Rana,14], performed micro-PIV measurements and numerical simulations of the velocity field and its distribution near moving liquid/air interfaces flowing in a 1 mm square capillary tube. They demonstrated that the *u*-velocity profile along the *x*-axis of the channel is not parabolic in nature, but that it is flatter, and particularly close to the meniscus (from "interface" to "*x* = 0.377 mm", figure 6c). Indeed, far from the interface, deeper in the liquid domain ("*x* = 0.841 mm", figure 6c), it satisfies the Poiseuille flow condition. Close to the meniscus, the flow clearly becomes three-dimensional with both *v* (along *y*-axis) and *w* (along *z*-axis) velocities showing a double vortex. This leads to enhanced local transport of momentum. Figures 6c-d show the variation of velocity components *u* and *v* along the channel height at various locations of the liquid/gas interface (here, water and air) for a capillary number of 3.7x10^{-6}. Both velocities are dimensionless, applying the average liquid supply velocity U_{avg} based on the total cross-section far from the

interface. While the *u*-velocity profile adheres to the parabolic Poiseuille distribution when sufficiently far from the interface (figure 6c), a significant drop in magnitude is seen at the center region close to the front meniscus. In fact, obstruction of fluid flow at the meniscus offers a free-surface boundary with only tangential velocities possible. This leads not only to the flatter profile close to the interface, but also and on the contrary, to a considerable increase of *v*-velocity magnitude, qualitatively varying like a sinusoid (figure 6d) [Rana,14]. They maintain that the characteristic of the flow field in the meniscus wake is the most important parameter affecting the viscous stress generated due to its motion. That said the complexity of slug flow in such geometry is particularly high and necessitates further studies regarding the parameters.

Slug flows are even more complex when considering oscillations or intensified velocities leading to a change in flow patterns. In 2018, Youn *et al.* [Youn,18] performed liquid film thickness measurements of water and ethanol from oscillating liquid slug in a 1 mm diameter circular capillary tube, thereby depicting the influence of oscillating frequency (1-10 Hz); film thickness deviates from that found in steady conditions and becomes thinner when accelerated and thicker when decelerated. Similar trends are expected in channels with square or rectangular shapes. Shekhawat *et al.* [Shekhawat,09] measured the radii of curvature and contact angles of an oscillating meniscus of water (0.25-0.5 Hz) in a 2 mm square channel, and showed variations of contact angle along the stroke length; the advancing contact angle is higher than the receding one, with a difference increasing with frequency. This effect is attributed to inertial and viscous forces. Similarly, Srinivasan *et al.* [Srinivasan,17] and, later, Rahatgaonkar *et al.* [Rahatgaonkar,18] showed that a change in the oscillation frequency of a liquid slug in a 1 mm square channel drastically affects the nature of the hysteresis between advancing and receding curvature radii, even at low Capillary and Weber numbers. As a result, inertial effects play a significant role in deformation of the dynamic meniscus. PIV visualizations by [Srinivasan,17] showed that the vortices appearing near the meniscus (like in figure 6d), which change their direction according to the meniscus flow direction, can lead to an alternating recirculation pattern inside the liquid plug and be a major factor in the estimation of the pressure losses in such a flow pattern. This is particularly true when too many small liquid slugs are present in the capillary and are liable to rapidly block the flow if the driving force is not sufficient to counterbalance the cumulative pressure gradients damping oscillations due to large dynamic contact angle hysteresis [Khandekar,10].

The influence of non-circular channels on transfer, and specifically on heat transfer, remains an open question. Considerable work has been done on such geometry by Khandekar *et al* [Khandekar,10] [Majumber,13][Mehta,14][Gatapova,19]. For example, even without latent heat of evaporation, Taylor bubble flows tend to increase the transport of heat up to 1.2-1.6 times more than laminar single-phase liquid flow [Majumber,13]. Gatapova and Khandekar also highlighted strong thermo-hydrodynamic coupling between the tube wall (thermal conduction) and the moving Taylor liquid plug through local thin film hydrodynamics and its subsequent evaporation [Gatapova,19]. That said the specificity of heat transfer in square/rectangular channels *vs.* circular ones has only sparsely been covered in the literature. Except for self-induced evaporation open to ambient air cases (see figure 4c-d [Chauvet,10]), the influence of heat power or heat flux on FPPHP

operation (see section 3.1.1) and the influence of the channel shape on the thermal performances of FPPHPs (see section 3.2.1), heat transfer have generally been treated as in conventional PHP tubes.

In this section, a discussion was initiated on slug flow pattern, but as regards its transition to other flow patterns, such as annular flow (when inertial or viscous forces increase and lead to breaking menisci or droplet flow), it is considered not here but in the literature, for example in [Wu,19] for liquid/liquid flows in square capillary.

2.3 Flow visualizations and hydrodynamics analyses

One of the major advantages of flat plate pulsating heat pipes is that the entire fluid flow can be visualized by placing a transparent window on the top face, while preserving the metallic substrate. Many experiments have been performed since the precursor tests by [Miyazaki,99], [Khandekar,02] or [Kim,03]. As observations in the literature are few and far between, the main fluid flow regimes will be presented in the following parts, with a particular focus on the vertical and horizontal orientations, which lead to different fluid flow modes, particularly for this kind of device. A distinction will be made concerning the definition of "normal" FPPHPs (with channel diameter of about 1-4 mm) and "micro" FPPHPs (with channel diameter below 1 mm) as defined in [Qu,10]. Quantitative information will also be summarized at the end of this section. That said, all observations transcribed below depend on the geometrical and operating conditions of each test (particularly concerning channel dimensions, filling ratios and working fluid), and must be analyzed in relative terms.

2.3.1 Flow regimes in vertical bottom heated mode

The vertical bottom heated mode (BHM, i.e. evaporator below the condenser) is an orientation favorable to the functioning of FPPHPs, except sometimes concerning the start-up phases: due to some observed liquid accumulation in the bottom part of the channels (see figure 7a, from [Markal,20a]), the minimum heat input for the start-up of oscillations requires initiation of nucleation, at internal wall temperatures sometimes higher than that obtained at low heat fluxes: the wall temperature of the channels has indeed to be higher than the saturated temperature of the working fluid. In the case of [Kim,03], the generation and growth of vapor bubbles continuously occurred when heat was applied to evaporating section in a 4-turns FPPHP filled with ethanol (channel: 1.5x1.5 mm²). But, according to Takawale *et al.* [Takawale,19], the minimum heat flux required for the start-up of oscillations increases with increasing filling ratio (17 turns, 1.2x1.2 mm², ethanol): the initial oscillations were observed for 49% *FR* at input power of 80 W, whereas, for 60% and 80% *FR*, it starts above 106 W. In the case of micro-FPPHP, as described by [Qu,10] (7 turns, D_h = 352 or 394 µm, FC-72), during the start-up process, no obvious nucleation was observed. The vapor plugs are mainly formed at the evaporator due to break-up of liquid slugs. The temperature difference between evaporator and condenser increases and induces some pressure difference, mainly due to the increase of $(\partial P/\partial T)_{sat}$. As long as this pressure difference is large enough to overcome the flow frictional and capillary forces, oscillation motion

begin within the channels. Then, for a further increase of oscillation amplitudes, the fluid start to move across the U-turns and migrate into adjacent channels, eventually extending the oscillating flow to all channels, leading to the final stage of start-up.

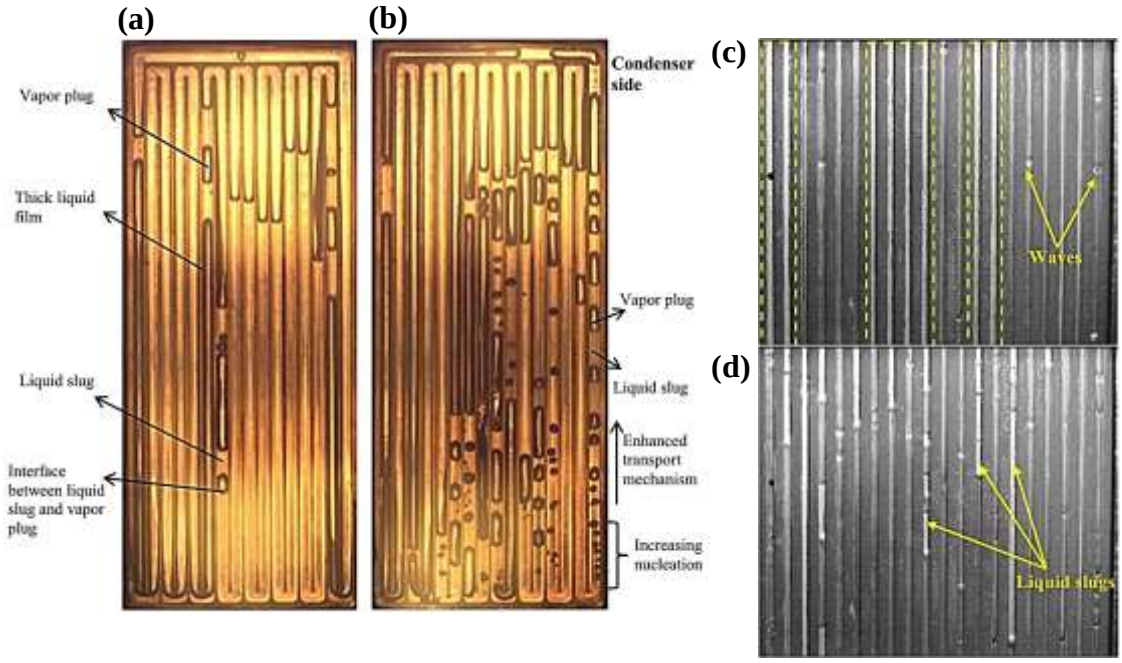

Figure 7: Flow regimes in copper FPPHPs (square 2x2 mm² channels): (a) $\dot{Q}$ = 21 W; (b) $\dot{Q}$ = 49 W (methanol, *FR* = 40%, BHM, $T_{II°}$ = 20°C): [Markal,20a]; and visualizations in the adiabatic section: (c) annular flow, $\dot{Q}$ = 40 W; (d) semi-annular flow, $\dot{Q}$ = 100 W (ethanol, *FR* = 50%, BHM, $T_{II°}$ = 20°C) [Ayel,14]

Once started, the bubbles grow and coalesce to become vapor plugs, and small bubbles continue to be generated in the liquid plugs. Different operating modes can be observed according to operating conditions. Yang *et al.* [Yang,09] described several operating modes with increasing filling ratio. At low filling ratios (below 20%), the spreader behaves as an interconnected array of two-phase thermosyphons. This operating mode is specific to the sharp angles of square channels and was not distinctly observed in previous studies with circular channels/tubes [Khandekar,02]. This trend was confirmed by [Ayel,14], [Manno,15], [Kearney,16], [Takawale,19] and [Markal,20b], where it appeared that the flow pattern was annular, even for a filling ratio close to 50%, the situation being reinforced by capillary pumping in the corners of the square channels. The vapor rises through the center of the channel and the condensed liquid returns as a liquid film along the corners (also see section 2.1). However, in [Ayel,14] and [Manno,15], the annular flow was prevalent in the central and lateral channels and distributed along the whole length of the FPPHP, whereas excess liquid was trapped in adjacent channels, therefore not contributing to in heat transfer, as can be seen in figure 7c (dotted yellow rectangles). The waves visible in figure 7c show some instability at the liquid/vapor interfaces caused by counter-current vapor flow. This trend is all the more pronounced as the diameter is high, as in [Ayel,18], testing a FPPHP with a hydraulic channel larger than the critical diameter for FC-72 at 20°C (2.5 mm / 1.65 mm, respectively).

For higher filling ratios, there is a transition from classical thermosiphon mode to pulsating slug flow regime [Yang,09], which represents the true pulsating mode and is the most efficient in terms of thermal performance. This situation is the same for increasing heat fluxes with filling ratios around 50%. with higher heat fluxes, in bottom-heated orientation, the flow pattern is a mixture of classical thermosiphon-type counter-current annular flow in some channels and capillary slug flow in others. In this case, liquid plugs are carried away by the vapor flow (figure 7d), with a random and rapid movement [Ayel,14]. They arise from the entrapped excess of liquid which, as they start their motion, contribute to the heat transfer by addition of a significant portion of sensible heat to total heat transfer [Khandekar,04]. For Takawale *et al.* [Takawale,19], in their FPPHP (17 turns, 1.2x1.2 mm², ethanol), tested in vertical orientation, slug flow was found to be the dominant flow regime, particularly for higher heat inputs. At times, slug flow was mixed with rapid boiling and thin film condensation in the bottom part of the evaporator [Ayel,18][Ayel,19]. Otherwise, a circulation occurs, enhancing the capacity of the working fluid to transport heat from both sections [Kim,03a]. According to Yang *et al.* [Yang,09], when filling ratio is more than 70%, the excessive liquid reduces (a) the degree of freedom of the system and (b) the effective advantage of the sharp angle corners. It becomes almost impossible for the vapor to reach the condenser area without encountering liquid plugs on the way. As a result, oscillating/pulsating action markedly decreases or even disappears [Markal,20]. Lastly, the increase of heat input causes dry-out in the evaporator region; the entire evaporator section remains dried-out and most liquid plugs oscillate in the condenser/adiabatic sections [Takawale,19].

Similar observations has been made for micro-FPPHPs. Qu *et al.* [Qu,12] observed in their devices (5 or 7 turns, D_h = 251 to 394 µm, FC-72 and R113) that at lower power inputs (below 5.4 W), the bottom of the evaporator was flushed with the liquid pool, even with low channel hydraulic diameters, and that the pool was decreased with increasing heat inputs. Nucleate boiling occurred suddenly (after 8.7 W) with tiny bubbles being generated and expanding rapidly and continuously from the nucleation sites. The bubbly flow quickly turned into slug flow, with induced bulk circulation throughout the microchannels. For higher heat power inputs, nucleate boiling became more intense, and dry-out occurred in the evaporator. However, for the lowest channel diameters (251 – 352 µm), intense film evaporation was observed instead of nucleate boiling, and neither nucleate boiling nor bulk circulation was observed, even at relatively high power inputs. Figure 8a shows representative flow behavior in the micro-FPPHP of Kamijima *et al.* [Kamijima,20] (11 turns, 0,35x0,35 mm², FC-72); liquid slugs and vapor plugs appear alternatively along the flow channel. The condenser contains many liquid slugs, while liquid films are formed along the channel due to the counter-current vapor flow from the evaporator. In this zone, dry walls without liquid films are present, as is rapid boiling in the bottom part of the channels. In another configuration, the authors observed two different modes for the same heat power ($\dot{Q}$ = 12 W, figure 8b-c); in mode 1 (b), the evaporator is dried, and the amplitude of self-oscillations is quite small and the liquid slugs are constantly stopping. By contrast, in mode 2 (c), the working fluid self-oscillates, leaving a significant amount of liquid film on the channel wall. This difference

in flow behavior results in a pronounced difference in heat transfer performances, the second mode being obviously the most efficient.

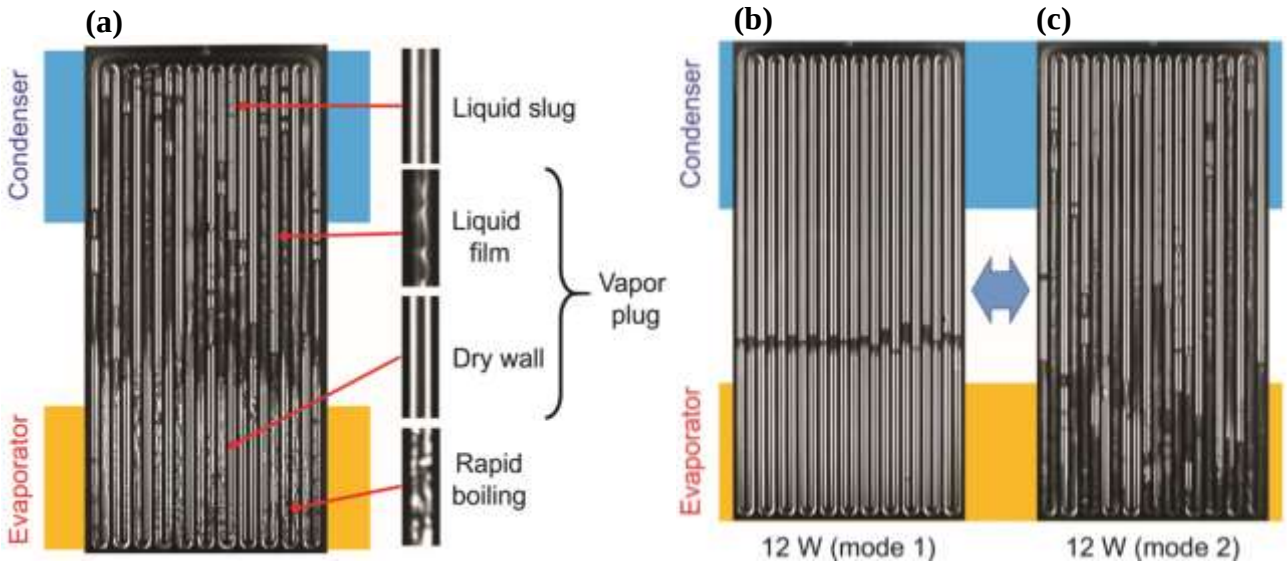

Figure 8: Examples of an internal flow images in a micro-FPPHP (square 0.35x0.35 mm² channels): (a) T_{II° = 20°C / $\dot{Q}$ = 20 W; and T_{II° = 20°C / $\dot{Q}$ = 12 W: (b) dry-out mode 1; (c) self-oscillation mode 2 (FC-72, *FR* = 48%, BHM) [Kamijima,20]

2.3.2 Flow regimes in horizontal orientation

In horizontal orientation, without the help of gravity driving forces, the flow pattern can only be slug flow. If in some cases the devices operated efficiently [Yang,09] [Qu,12] [Betancur,18] [Winkler,20], for many others, operations in horizontal inclination lead the FPPHP to unstable operation and low thermal performances caused by intermittently long-term stopover phenomena (momentary stops of liquid slugs oscillations [Jun,16]), or even to a complete stop of operation due to early dry-out of the evaporator [Khandekar,02][Chien,12] [Ayel,14][Jun,18][Ayel,18]. This is more specifically attributed to a lack of pressure perturbations and/or other mechanisms on account of a low number of turns [Markal,20a]. Figure 9a-c shows successive photos of a FPPHP tested in a horizontal position at 30 W of applied heat power (8 turns, 2x2 mm², water) [Chien,12]. Oscillations occur only for short time periods and completely stopped at steady-state. As a result, heat transfer takes place by conduction from evaporator to condenser, thence the very poor thermal performance of the device. In 2002, Khandekar *et al.* [Khandekar,02] provided their own explanations for such unsatisfactory performances; as mentioned in the introduction, the very thin wall between neighboring channels in the massive metallic plate is conducive to exceedingly low transverse thermal resistance, particularly when compared to disconnected tubes of tubular PHPs. The low resistance quickly equalizes the thermally created pressure gradients, which represent the primary driving potential for stable PHP operation. Furthermore, if sharp-angled edges act as capillary structures, thereby enhancing heat transport capability, their effect is in all likelihood negligible for high filling ratios, under which multiple

liquid plugs prevent a direct vapor flow from the evaporator to the condenser. Authors also lay blame on the capillary resistance due to dynamic contact angle hysteresis (see section 2.1), and the effect of latent heat which, once it reaches a high level, no longer effectively contributes to the oscillation motions (bubble volume change has become insufficient). On the one hand, capillary pumping may be efficient, once the liquid plugs are not too far from the evaporator; on the other hand, when the filling ratio is too low, as in figure 9d, the liquid slugs are too far from the evaporator to be transported by capillary forces into the evaporator zone.

In a channel with a hydraulic diameter higher than the critical one, which is calculated by means of the Bond number, channel dimensioning yields fluid stratification; acting like a hybrid loop thermosiphon under normal gravity and a PHP under microgravity conditions, the FPPHP of [Ayel,18] (11 turns, 2.5x2.5 mm², FC-72), is dried out in horizontal inclination, even though gravity and capillary-assisted flow helps the liquid to flow back close to the evaporator zone, like an open-channel flow. Furthermore, capillary pumping in the corners gives rise to liquid film flowing closer to the evaporator direction, thereby improving thermal performances compared to those of classical dry-out FPPHPs with smaller channels and sharp liquid/vapor frontier imposed by capillary forces, as in the previous studies.

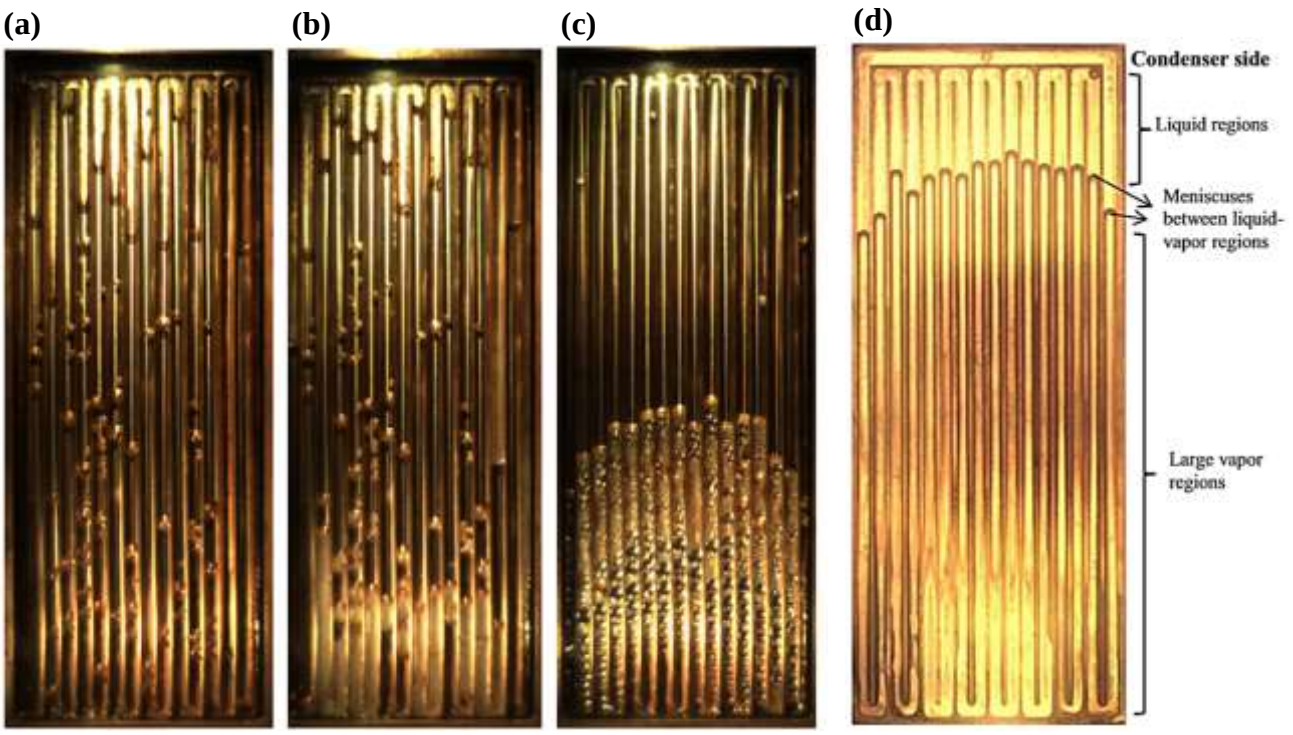

Figure 9: High speed internal flow images in horizontal FPPHPs (square 2x2 mm² channels): (a) initial state; (b) after 1 min of heating; (c) steady-state operation ($\dot{Q}$ = 30 W, water, *FR* = 70%, horizontal) [Chien,12]; and (d) dry-out FPPHP ($\dot{Q}$ = 42 W, methanol, *FR* = 25%, horizontal, $T_{II°}$ = 20°C) [Markal,20a]

However, starting from a dried-out configuration (*i.e.* long liquid slugs accumulated in the cold edge of the channels, forming U-shaped liquid columns of approximately the same length, as in figures 9c or d), several authors have observed fluid flow reactivation processes, which are associated with different sources of

instability; for example, the FPPHP of Jun and Kim [Jun,18] (10 turns, 1x0.5 mm², ethanol) exhibited amplitude oscillation defined by the authors as short-large, followed by a relative and repeated long-term stopover phenomenon. During the stopover periods, the vapor plugs are always superheated. The channels in the evaporator zone are totally occupied by vapor plugs exposed to dry wall without liquid film, and they are more superheated, until subsequent instability, which is attributed to a mathematically unstable mass-spring system. When the fluid starts to flow, the ends of a U-shape liquid column oscillate in opposite directions. If the amplitude of oscillations is sufficient, liquid flow into the evaporator and vapor flow into the condenser occur, completing the circulation cycle. As the heat load increases, oscillations become larger, with the liquid occasionally overflowing into neighboring turns. Because the phases of liquid column oscillations are not independent from one another, they vary continuously and the menisci at each end move in a waveform [Miyazaki,99]; due to the spring effect of the vapor bubble, the fluid motion is sequentially transmitted from one branch to another along the FPPHPs. Figure 10a depicts a rapid waveform interconnecting the ends of long liquid slugs at each flow channel [Kim,03]. In one case [Kim,03a], waves are generated from the right, grow as they propagate to the left, and are finally damped and disappear until the next cycle. Oscillation frequency is influenced by the heat flux and heat energy accumulated in the solid walls. Ayel *et al.* [Ayel,18], tested their large-channel FPPHP (11 turns, 2.5x2.5 mm², FC-72) under microgravity conditions (during an ESA parabolic flight campaign) and observed an alternation of stopover periods and waveform fluid flow reactivations, with exceedingly high amplitude oscillations, until the menisci ruptured. In the absence of gravity forces, even with large-dimension channels, the flow pattern turns into slug flow: low capillary forces are strong enough to maintain liquid slugs between two vapor bubbles. Otherwise, due to very low capillary and friction forces, both of which are linked to the large hydraulic diameter, the liquid slugs move quite impulsively, the menisci break, and the flow pattern evolves into a more chaotic condition. Under such conditions, the fluid tends quickly and spontaneously to dry out in the evaporator, while isolated liquid plugs can easily move, even under the influence of small pressure variations, thereby enhancing the heat transfer during the operating periods.

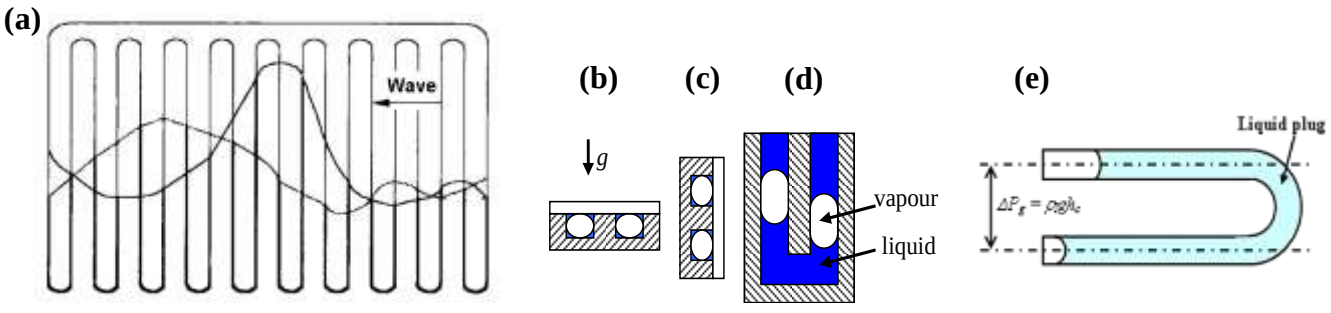

Figure 10: (a) Schematic diagram of oscillating wave in a 10 turns FPPHP [Kim,03a]; FPPHP orientation regarding gravity vector: (b) horizontal; (c) edge, (d) vertical and (e) gravity pressure drop in one bend in edge orientation [Ayel,14]

Another configuration was tested by [Ayel,14], [Manno,15] and [Pagnoni,18a]: the so-called “edge”(or “side”) orientation; in this case, the FPPHP is oriented vertically, but with horizontal channels, as in figure 10c. Pressure imbalance in the liquid slugs is occasioned by difference in height at each U-turn (see figure 10e), leading to a particularly high gravity pressure head for the last surrounding bend; this can drive a continuous long-term oscillatory motion between all liquid slugs, even for the lowest heat powers applied, without encountering any dry-out at the evaporator. As in [Miyazaki,99] and [Kim,03a], the liquid slugs oscillate in a waveform from top into bottom, through the vapor phase into the evaporator region, as oscillation velocities and amplitudes increase with heat input augmentation.

On the basis of the literature, a systematic description of the parameters (heat power input, filling ratio, U-turn number…) influencing the horizontal operation of FPPHPs is depicted in section 3.1. Several authors managed to exceed such operating limits by employing different parameters: alternated channel dimensions in [Chien,12][Shi,16], fluid mixtures in [Markal,20b], etc. This is explained in detail in section 4.

2.3.3 Quantitative analysis

With image post-processing, the displacements of multiple liquid slug motions have been calculated by several authors, contributing to quantitative analyses of the relationships between hydraulic behavior and thermal performances. For example, Borgmeyer and Ma [Borgmeyer,07] measured the positions and velocities of menisci oscillating in a horizontal FPPHP (2x14 turns, 1.59x1.59 mm², ethanol/Flutec PP2/water), and found that the nature of the working fluid significantly affects the oscillating motion of liquid slugs. With water, no oscillating motions were observed, whereas the largest amplitudes and velocities were created with ethanol compared to other fluids in the same operating conditions (see velocity curves of figure 11a). When heat power increases, displacement, velocity and frequency correspondingly increase, but with highly irregular oscillating motions. When velocity measurements yielded maximum values up to 50 $mm.s^{-1}$, in this case with ethanol (at 160 W), Pagnoni *et al.* [Pagnoni,18a] found maximum velocities of around 0.6, and 1 $m.s^{-1}$, and frequencies from 2.5 and up to 4 Hz, for heat powers of 80 W, and 200 W, respectively, in their edge-oriented FPPHP (11 turns, 2.5x2.5 mm², ethanol). These velocity values are particularly high and one order of magnitude higher than the classical value of 0.1 $m.s^{-1}$ used in the literature to classify the critical diameter based on Weber or Garimella criteria.

(a) **(b)** **(c)**

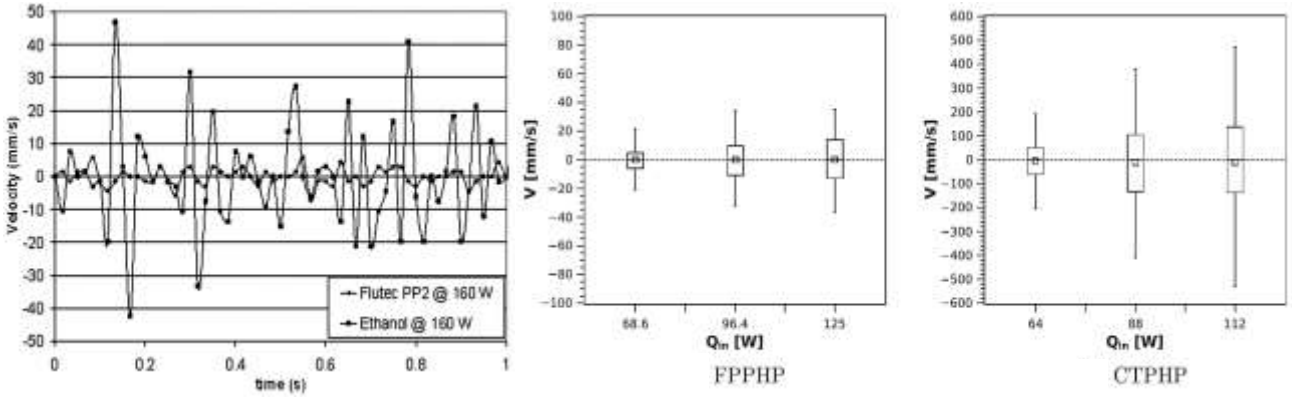

Figure 11: (a) Liquid slug velocity measurement in a FPPHP (N = 2x14, 1.59x1.59 mm², $\dot{Q}$ = 160 W, FR = 50%, horizontal, T_{II° = 20°C) [Borgmeyer,07]; and velocities of liquid slugs inside (b) FPPHP and (c) CTPHP for various heat power inputs (N = 17, 1.2x1.2 mm², ethanol, FR = 60%, BHM, T_{II° = 22°C) [Takawale,19]

Similarly, Takawale *et al.* [Takawale,19] measured positions and velocities of liquid plugs oscillating in both FPPHP and capillary tube PHP ("CTPHP") with similar geometries (17 turns, 1.2x1.2 mm², ethanol) under the same operating conditions. They observed that oscillation amplitude goes up with increasing heat power, but that the amplitude is several times larger in CTPHP. Figure 11b-c shows a comparison of liquid slug velocities between FPPHP and CTPHP for three heat power inputs; the boxes contain 50% of the total values, whereas the bars contain 90%. Absolute velocities measured in the CTPHP (case (b)) are about 8-10 times higher than those inside FPPHP (case (a)). While slug flow pattern is the dominant flow regime observed in both PHPs, the CTPHP is seen to have vigorous large-amplitude self-sustained oscillations as compared to FPPHP.

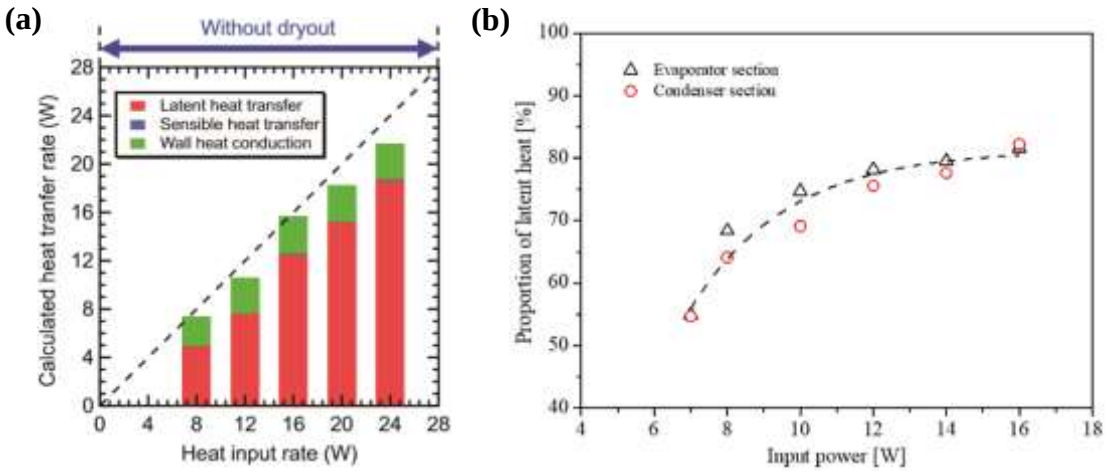

Figure 12: (a) Calculated heat transfer rates in a micro-FPPHP (N = 11, 0.35x0.35 mm², FR = 48%, BHM, T_{II° = 40°C) [Kamijima,20]; and (b) proportion of latent heat to overall heat at various input powers (N = 5, D_h = 0.84 mm, ethanol, FR = 45%, BHM, T_{II° = 30°C) [Jung,21]

Lastly, some authors have coupled the flow mapping obtained from visualizations with the synchronized temperature measurements and heat fluxes obtained from thermocouples arranged on the outer wall of the

device ([Lee,18],[Jamijima,20]) or from infrared thermography ([Jung,21]), the common objective being to define sensible heat influence on heat transfer performance. Based on a modeling approach of heat transfer through the different parts of the mapped bubble/slug train, taking into account not only sensible heat through liquid and vapor slugs and latent heat through the thin film (see figure 3a-b in section 2.1), but also heat conduction through the walls, Jo *et al.* [Jo,19], Jamijima *et al.* [Jamijima,20] and Jung and Kim [Jung,21] reconstituted the decomposition of heat transfer rates from the fluid to the wall, according to heat flux (figure 12a) or heat input (figure 12b). It can be seen, as already maintained in section 2.1, that latent heat transfer via the liquid films accounts for a considerable portion of the total heat transfer rate by the fluid [Kamijima,20]. For [Jo,19], the proportion of latent heat reaches 74% at the evaporator and 66% at the condenser, for a 14 W heat power input. For Jung and Kim [Jung,21], the proportion of latent heat reaches more than 80% in both evaporator and condenser sections for the highest heat inputs: in their study, the proportion of latent heat increases from around 55% to 82% with input power increasing from 6,5 W to 16 W (figure 12b). Two conclusions emerge from these findings: first, latent heat transfer not only induces an oscillating flow, but also significantly contributes to overall heat transfer, while sensible heat is a by-product of the oscillating flow [Jo,19]. Second, it is necessary to take into account the thin film evaporation and condensation phenomena when modeling heat and mass transfer inside pulsating heat pipes.

3 Thermal performances of flat plate pulsating heat pipes: the influential parameters

Based on the same physical phenomena as for tubular PHPs, FPPHPs are often subject to the same influential parameters. For example, for both devices it has been shown by most researchers that PHP with closed ends (Closed Loop PHP) show better heat transfer performances than those with open ends [Kim,03a][Zhang,04][Mehta,16]. This point will not be developed here, and the main observations will be presented below, based on parametrical investigations on channel dimensions, the working fluid, the geometrical aspects and/or the operation conditions (particularly applied heat power, orientation and filling ratio). A parameter widely used by authors to characterize the thermal performances of pulsating heat pipes is given by thermal resistance:

$$R_{th} = \frac{\bar{T}_{ev} - \bar{T}_{cd}}{\dot{Q}} \tag{11}$$

where $\bar{T}_{ev}$ and $\bar{T}_{cd}$ are, respectively, evaporator and condenser (or secondary cold source) temperatures averaged in space and time, and $\dot{Q}$ the heat power applied, at times taking into account the heat losses, and/or heat conduction through the plate of the device. In certain cases, the authors use equivalent thermal conductivity for purposes of comparison with the thermal conductivities of heat conductive materials such as copper, aluminum, etc. It can be defined as:

$$\lambda_{eff} = \frac{\dot{Q} L_{eff}}{A_t(\bar{T}_{ev} - \bar{T}_{cd})} \quad (12)$$

where L_{eff} is, according to the authors, an effective length between evaporator and condenser zones or a length defined between two temperature measurements in the adiabatic zone; and A_t is the FPPHP transverse cross-section.

An attempt will be made below to identify the main parameters influencing on the working operation of flat plate pulsating heat pipes. However, such an analysis appears to be highly complicated insofar as many of the parameters are interconnected with one another. In appendix A.1 have been brought the main values of effective thermal conductivities found, when possible, in the literature. They are relevant only to FPPHPs with one layer of channels, with evaporator and condenser disposed at both ends of the device, and having been tested in horizontal and vertical BHM positions. Figure A.1-2 presents all values in the same graph as functions of heat flux density at the evaporator; it highlights the strikingly scattered values of effective thermal conductivities, ranging from a few tens of $W.m^{-1}K^{-1}$ up to more than ten thousands of $W.m^{-1}K^{-1}$. Effective thermal conductivities have also been plotted as functions of Figures of Merit extrapolated from the analyses of [Kim,20] in figure A.1-3a and those of [Noh,20] in figure A.1-3b. Conclusions can be drawn on some tendencies, but sometimes are hardly conclusive. With that in mind, the main trends from the literature will be evoked in the following parts.

3.1 Operating conditions

3.1.1 Heat power, heat flux, start-up conditions

This parameter is the most often and the most systematically studied, insofar as all authors have tested their device(s) sweeping heat power from the lowest to the highest values provided by the power supply or the operating limits of the FPPHPs. The influence of heat power remains very similar to tubular PHPs, as soon as the oscillating operation occurs.

Several authors have discussed the start-up conditions of their devices. As regards the minimal heat power triggering the start of FPPHP operations, the results are too dispersive to be comprehensively mentioned. Section 2.3.1 introduces some observations made on start-ups in vertical BHM mode through visualizations. From the experimental point of view, a start-up has been established when the thermal energy accumulated in the evaporator is high enough for the pressure instabilities to overcome the self-excited flow resistance of liquid/vapor slug flow and consequently to transport heat from evaporator to condenser zones [Qu,12]. The initial start-up phase is accompanied by a smooth increase of evaporator wall temperature. Betancur *et al.* [Betancur,20] attribute this mode to conductive heat transfer. Occasionally, fluid presents random isolated temperature oscillations, mainly in a horizontal position; the liquid slugs' displacements are characterized by high amplitude and low frequency and tend to disappear over time.

Above a certain heat input value, thermally-driven two-phase oscillating flow begins to occur; concerning micro-FPPHPs, this threshold value was found for heat powers higher than 4 W for [Jung,21] (5 turns, 1.1x0.5 mm², ethanol, 45%, BHM), 4.8 W for [Qu,12] (5 turns, D_h = 251 μm, R-113, 50%, BHM), 6 W for [Yoon,18] (5 turns, 1x0.5 mm², ethanol, 55%, BHM) and 6.9 W for [Qu,10] (5 turns, D_h = 394 μm, FC-72, 50%, BHM). The micro-FPPHPs of Qu *et al.* did not start using water or ethanol as working fluids [Qu,12]. Jo *et al.*, similarly to [Yoon,18], observed an oscillation of liquid slugs with an amplitude of several millimeters from 6 W heat power applied [Jo,19] (5 turns, D_h = 835 μm, ethanol, 50%, BHM). After start-up, the oscillation amplitude increased with increasing power, resulting in decreased thermal resistance. Concerning classical FPPHPs, the threshold values also obviously vary among authors. According to [Li,13], the FPPHP started at heat input of 12 W for acetone and 18 W for ethanol under the same operating conditions (10 turns, 1x1 mm², 50%, BHM). For Ayel *et al.* [Ayel,15], in vertical orientation, the heat input necessary for FPPHP start-up differed in some tests, according to the initial distribution of the fluid. In the initial phase of the start-up, the formation and expansion of the vapor bubbles at the evaporator provide the driving force triggering the fluid flow motion. It has been observed that the minimum heat power level needed to trigger such motion increases with increasing filling ratio [Shi,17][Betancur,20][Markal,20a]; start-up occurred at 40 W, 60 W and 80 W, for filling ratios of 25%, 37,5% and 50%, respectively [Betancur,20] (5 turns, D_h = 2.5 mm², water, BHM). In the case of [Markal,20a], small differences were noted between 25% and 40% filling ratios (5 turns, D_h = 2.5 mm², water). They argued that the adverse effects of the liquid excess are clearly present and can be associated with a restriction of motion or pumping action. Lastly, few authors have observed nucleation during start-up conditions; in some cases, it seemed as though some liquid pool remained accumulated in the bottom region of the evaporator, as in [Markal,20a-b] (8 turns, 1-2x2 mm², methanol, 40%, BHM) (see figure 7a, section 2.2.1).

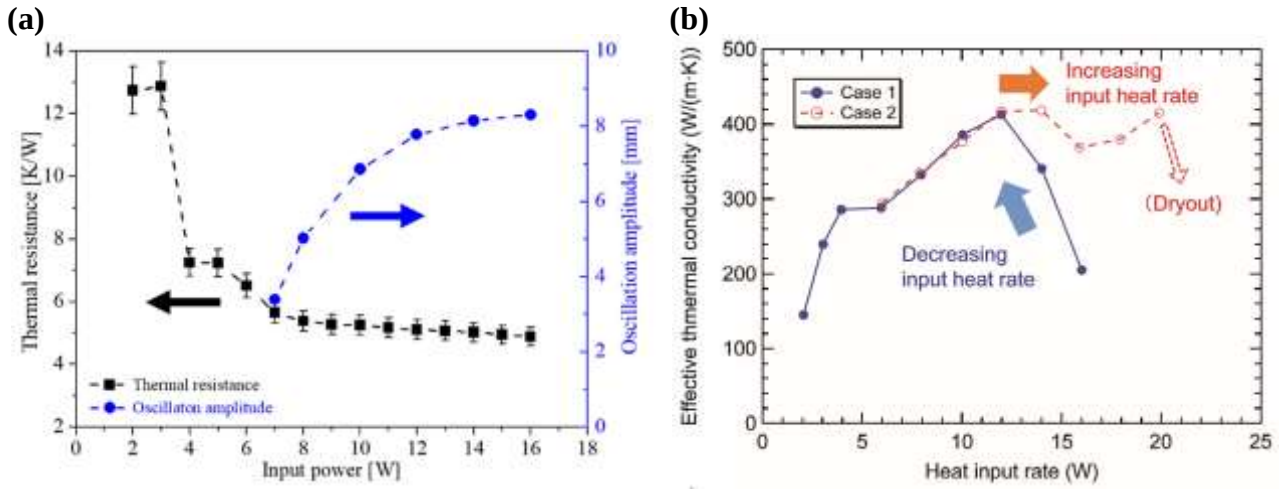

Figure 13: (a) Thermal resistance and oscillation amplitude of micro-FPPHP (N = 5, D_h = 0.84 mm, ethanol, FR = 45%, BHM, $T_{II°}$ = 30°C) [Jung,21]; and (b) effective thermal conductivity hysteresis (N = 11, 0.35x0.35 mm², FR = 39%, BHM, $T_{II°}$ = 40°C) [Kamijima,20]

Generally speaking, whatever the conditions, thermal performances increase with increasing heat power/heat flux due to an intensification of driven forces caused mainly by evaporation/boiling and condensation processes, and also ascribed to the thermophysical properties of the fluids. The main conclusions are given in the sections and figures below (and appendix A1), and confirm this overall trend insofar as the device works "nominally" under slug flow up until operational limits, which are mainly due to the appearance of dry-out in the evaporator zone. Intriguing trends concerning micro-FPPHP operation are indicated in figure 13a; Jung *et al.* [Jung,21] have superimposed the thermal resistance curve with quantitative estimation of oscillation amplitudes based on visualizations (see section 2.3.3 for details). For heat power less than 4 W, no oscillation was detected and most of the heat is transferred by conduction alone through the silicon substrate. Above 4 W, the micro-FPPHP starts to operate and thermal resistance decreases pronouncedly. After 7 W, thermal resistance continues to slightly decrease, whereas mean oscillation amplitude increases in such a way as to favor heat transfer. On the other hand, figure 13b presents the hysteresis effect observed in the micro-FPPHP of Kamijima *et al.* [Kamijima,20], suggesting that for large heat inputs, the device exhibits two different self-oscillation modes with different resulting effective thermal conductivities, even for identical heat input rates, depending mostly on whether heat power is delivered increasingly or decreasingly. All relevant heat power or heat flux ranges in the literature (from 0.3 up to 43 $W.cm^{-2}$) are given in appendix A.2 (table A.1).

3.1.2 Filling ratio

Even though the influence of filling ratio has been experimentally studied by many authors, it remains quite difficult to reach definitive conclusions insofar as optimal filling ratios strongly depend on operating conditions, particularly as regards orientation (horizontal or vertical, BHM or THM, inclinations), on the nature of the working fluid, on the distance between evaporator and condenser, on their respective lengths, etc. The influence of filling ratio was discussed in section 2.3.1, particularly concerning vertical BHM; Yang *et al.* [Yang,09] explained that below or close to 20% of filling ratio, the FPPHP behaves as an interconnected array of thermosyphons. Increasing *FR* leads to transition to semi-annular flow including liquid slugs in the channels. Figures 14a-c present the influence of filling ratio on the thermal resistance of a FPPHP (N = 20, 2x2 mm^2, ethanol) tested under three orientations. Under vertical BHM, the device can operate under a wide range of *FR* (from 5% to 95%), whereas the ranges are reduced under horizontal (30-85%) and vertical THM (45-75%). All in all, the influence of *FR* decreases as heat input increases. It seems that in BHM, the higher the *FR*, the lower the performance. In horizontal and THM, there seems to exist an optimal value, around 50-60%, leading to lower thermal resistances.

Under vertical BHM (N = 8, 2x2 mm^2, methanol, $T_{II°}$ = 20°C), Markal *et al.* [Markal,20], who tested filling ratios ranging from 10% to 85%, confirmed this trend, finding that 30% *FR* provides more outstanding thermal performances than 60%. At 30%, annular or semi-annular flow characterizing thin film evaporation is dominant, and rapid bubble growth following explosive boiling in narrow channels play an active role. At

60%, bubbly or slug flow becomes dominant, but most of the channels are covered by an inactive liquid zone (motionless liquid, see figure 7a in section 2.3.1), liquid plugs further restricts low flexibility, given that vapor pressure in some channels do not suffice to drive heavier liquid mass. This was also the case of Kearney *et al.* [Kearney,14] [Kearney,16] who found better thermal performances in BHM when the FPPHP (N = 26, 1.9x1.55 mm²) was filled with 30-40% of fluid (Novec® 649, Novec® 774 or ethanol) than with 50-70%. For Takawale *et al.* [Takawale,19], a filling ratio between 40% and 80% had low influence on the performances of their FPPHP (N = 17, 1.2x1.2 mm², ethanol, $T_{II°}$ = 22°C). As for micro-FPPHPs, figures 14d-e show that the best performances were obtained for *FR* close to 50% (48-54% at $T_{II°}$ = 20°C and 48% at 40°C), particularly in the operating range of heat inputs prior to dry-out [Kamijima,20]. Similarly, in [Qu,12], optimum filling ratios were found around 40-60%. Higher optimal *FR* in micro-FPPHPs under vertical BHM is probably due to an increased ability to remain on slug flow due to lower hydraulic diameters leading to higher capillary forces.

Kim and Kim [Kim,20] observed that the contribution of latent heat transfer was dominant in the evaporator section but became reduced in the condenser section of their micro-FPPHP (N = 10, 1x0.5 mm², ethanol, *FR* = 50%, BHM). Flow visualizations showed that the thin liquid film enclosing vapor bubbles remained mainly located in the evaporator section, while the liquid slugs stayed in the condenser section. In the evaporator section, thin film evaporation occurred in the vapor bubbles, and nucleate boiling in the liquid slugs. In the condenser section, however, film condensation in the penetrating vapor bubbles was the only latent heat transfer. Therefore, in the authors' opinion, the increase in the latent heat transfer region in the condenser is the most important factor in the enhancement of the thermal performances of their micro-FPPHP. The optimal filling ratio is a compromise based on this type of assessment, at once avoiding dry-out with overly low values of *FR*, and an excess of liquid that would prevent vapor from reaching the condenser with overly high values.

(a) **(d)**

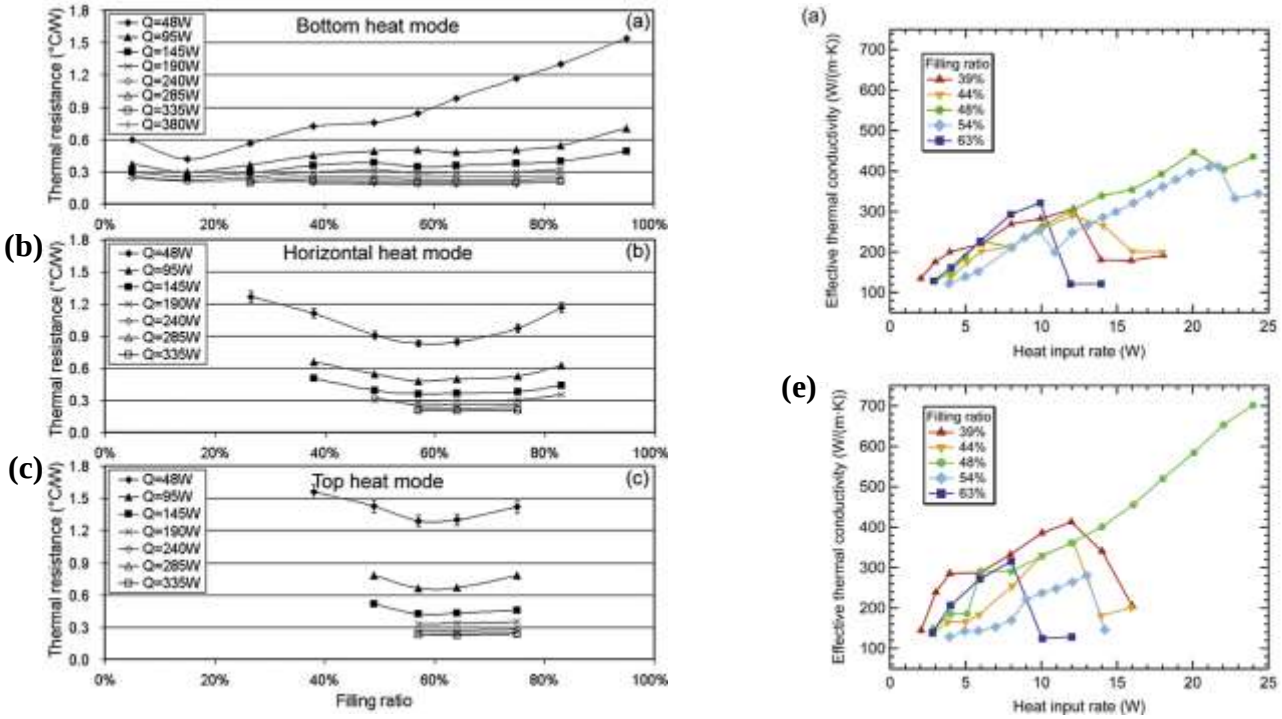

Figure 14: Effect of filling ratio on: the thermal resistance of FPPHP (N = 20, 2x2 mm², ethanol, $T_{II°}$ = 20°C) (a) bottom heated mode, (b) horizontal, (c) top heat mode [Yang,09]; and on effective thermal conductivities of a micro-FPPHP (N = 11, 0.35x0.35 mm², FC-72, BHM) (d) $T_{II°}$ = 20°C, (e) $T_{II°}$ = 40°C [Kamijima,20]

Obviously, in horizontal inclination (and up to THM), the optimal *FR* will be different than in vertical BHM, as can be seen in figure 14b. As in tubular PHPs, in this configuration most authors found optimal filling ratios close to 50%, with a variably wide range according to their operating conditions.

3.1.3 Orientation / gravity field

Influence of orientation was mentioned in section 2.3 with regard to fluid flow patterns. While in some studies the FPPHP failed to operate in horizontal inclination, in the cases where it does operate, the best performing conditions have always been found in the vertical bottom-heated mode. As mentioned in the previous section and in figures 14a-c, the FPPHPs tested by Yang *et al.* [Yang,09] (N = 20, 2x2 mm² or N = 33, 1x1 mm², ethanol, $T_{II°}$ = 20°C) can operate well in all orientations, even in top heat mode; that said, the gravity vector augments the driving forces, improving performance in BHM orientation as compared to all other orientations. Figure 15a depicts the performances of the FPPHP tested by Laun and Taft [Laun,14] (N = 20, 1.3x1.3 mm², acetone, *FR* = 80%); before oscillatory start-up at power levels from 100 to 200 W, and due to a high filling ratio, which markedly hinders performance, the BHM presents lower resistance, creating natural convection, which acts like a thermosyphon. Once oscillations begin (after 250 W), the orientation has no longer has any effect on thermal resistance. On the contrary, in figure 15b, Ayel *et al.* [Ayel,14] (N = 10, 2x2 mm², ethanol, *FR* = 50%) found that thermal performances strongly depended on inclination, from horizontal, where it was dried-out, to the best performing vertical BHM, while the above-mentioned "edged" inclination (see section 2.3.2) showed intermediate performances between horizontal and vertical BHM. The

FPPHP of Gu *et al.* [Gu,04] (N = 48, 1x1 mm², R-114, $T_{II°}$ = 25°C) was tested during parabolic flight campaign, under vertical and microgravity conditions, and was shown to operate whatever the inclination (even THM) and the level of gravity.

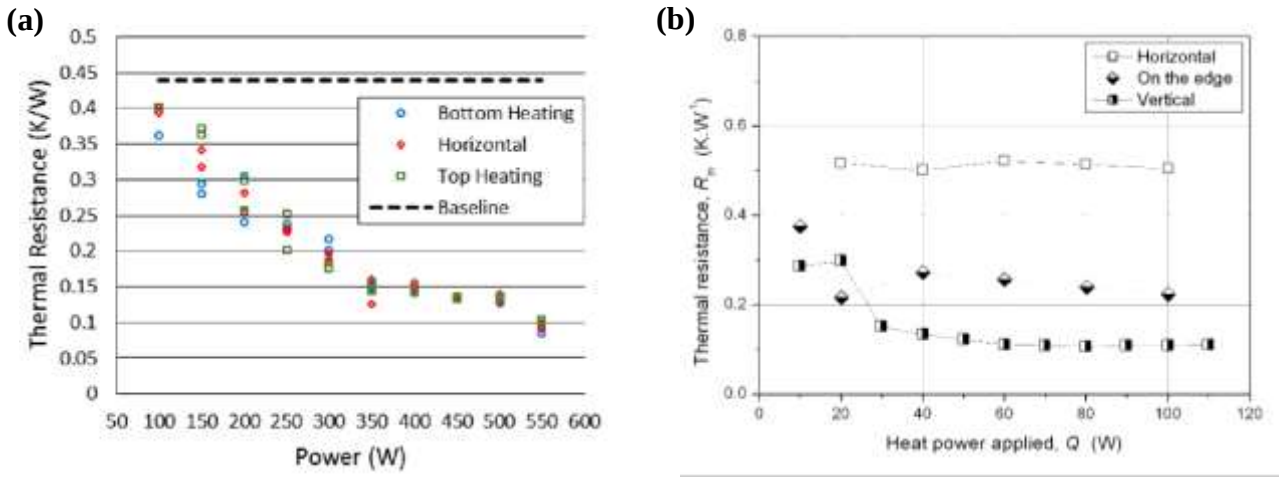

Figure 15: (a) Thermal resistances curves of FPPHP for three orientations: (N = 20, 1.3x1.3 mm², acetone, FR = 80%) [Laun,14]; and (b) (N = 10, 2x2 mm², ethanol, FR = 50%) [Ayel,14]

To illustrate the change of flow regime between vertical BHM and horizontal orientations, figure 16a shows the transient responses of the evaporator temperature of the FPPHP of [Yang,09] for the three tested inclinations; if the temperature fluctuations are very low in BHM and begin after 100 W (specific to annular flow), they are more pronounced in horizontal and particularly in vertical THM. After 250 W, temperature levels and fluctuations are very similar in the three orientations. In figure 16b, one can observe the fluid flow pressure fluctuations in the condenser zone of the FPPHP of [Ayel,18] for two orientations; the pressure fluctuations are much larger in amplitude and period in horizontal inclination, and also much more irregular than in vertical inclination. These fluctuations are the result of hydraulic instabilities, which are particularly large in slug flows.

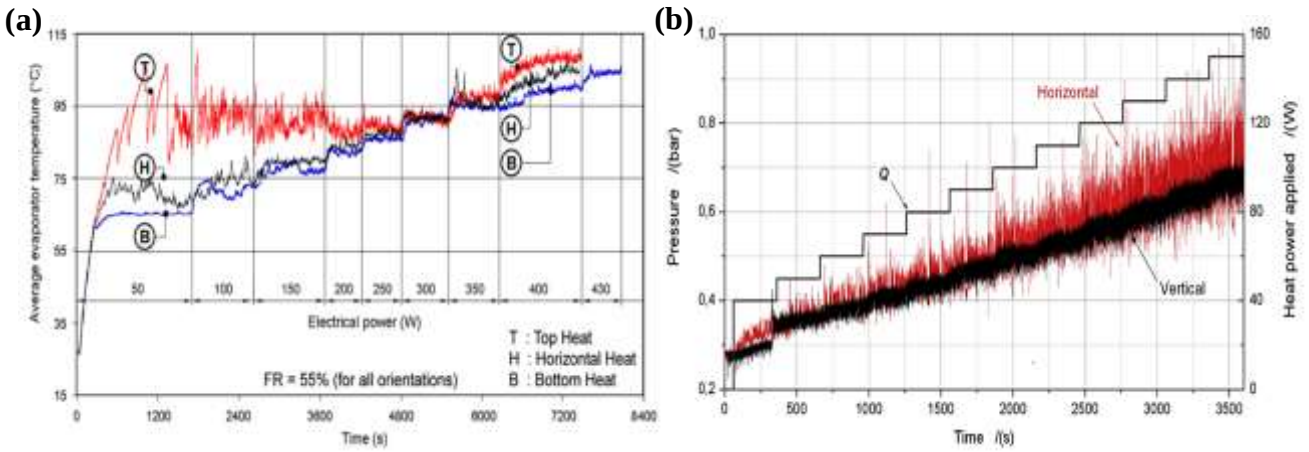

Figure 16: (a) Transient responses of: evaporator temperature (N = 20, 2x2 mm², ethanol, FR = 55%, $T_{II°}$ = 20°C) [Yang,09]; and (b) pressure in the condenser zone (N = 12, 1.6x1.7 mm², FC-72, FR = 50%, $T_{II°}$ = 20°C) [Ayel,18]

Regarding micro-FPPHPs, Qu *et al.* [Qu,12] and Lee *et al.* [Lee,18] tested their device under several orientations (from horizontal to vertical BHM). As was the case with conventional FPPHPs, the best thermal performances were recorded under vertical BHM, and as the devices turned from the horizontal orientation to BHM, thermal resistances tended to decrease, and the occurrence of dry-out was delayed, findings indicating that the influence of gravity could not be ignored, even in micro-FPPHPs with hydraulic diameters as small as 251 µm [Qu,12]. In the case of [Lee,18], figure 17a shows not only the same trend for the 5-turn device but also, and more remarkably, that the curves of figures 17b register very good performances and are perfectly superimposed for a 20-turn micro-FPPHP, whatever the inclination angle. Furthermore, the maximum allowable heat fluxes for the five inclinations are almost the same, and are largely extended compared to the 5-turn device. In view of these results and of those obtained in conventional FPPHPs by [Yang,09] and [Laun,14], it appears that flat plate pulsating heat pipes with a large number of turns (20 turns or more) have orientation-independent thermal performances and maximum heat fluxes.

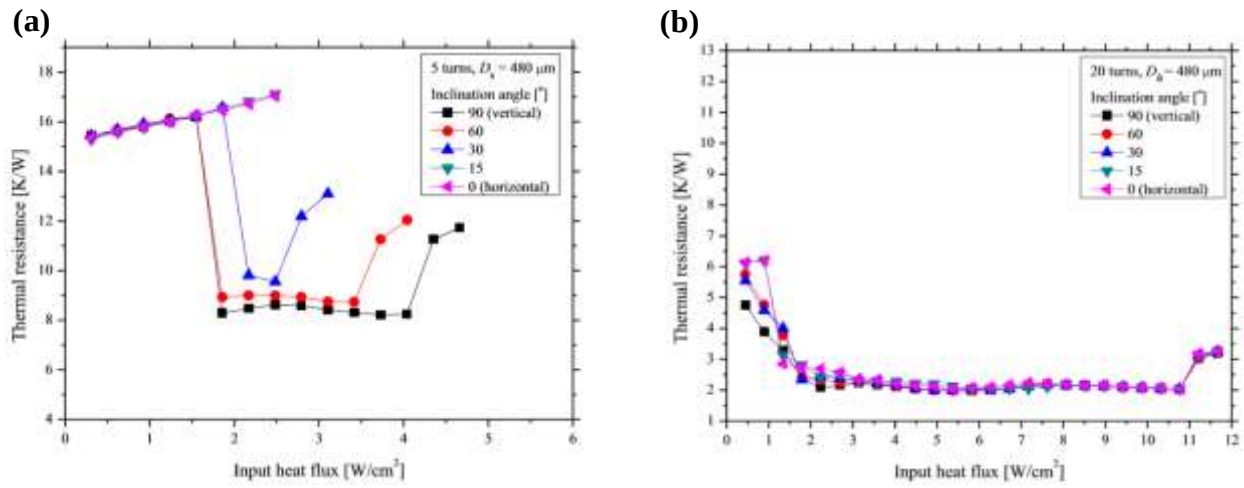

Figure 17: Thermal resistances curves of micro-FPPHP for different orientations (D_h = 480 µm, FC-72, FR = 50%): (a) N = 5; and (b) N = 20 [Lee,18]

3.2 Geometrical aspects

3.2.1 Channel dimension and shape

First, considering square or rectangular channels, it appears that the critical diameter governed by the Bond number (see section 2.1, Eq. (1)) is inappropriate for channels with sharp-angled corners. As the flow regimes are governed by an interplay of gravity, capillary, viscous and inertia forces, the relative magnitude of the forces is clearly affected by the hydraulic diameter of the tube cross-section as well as its shape [Yang,09]. It is to be expected that the larger the hydraulic diameter, the better the performances, as long as the above

criteria are not exceeded. In terms of channel dimension influence, Winkler *et al.* [Winkler,20] compared the heat transfer performances of two FPPHPs with the same overall dimensions (50x100 mm², acetone, *FR* = 50%) but with two channel dimensions and number (1x1 mm² / *N* = 13 and 1.5x1.5 mm² / *N* = 10), their objective being to reach a maximum channel density per surface. They found that a larger channel diameter leads to lower thermal resistances, in both horizontal and vertical BHM, but with premature dry-out appearing in horizontal inclination at 130 W, whereas it was not observed with the 1x1 mm² channel up to 180 W. As soon as heat input increases, the amplitude and velocity of liquid plugs oscillations increase. This is all the more significant insofar as the diameter is large, which brings the slug menisci diameters closer to the critical diameter, as seen in section 2.1. Both FPPHPs have operations becoming independent of orientation for heat inputs above 50 W.

During a parabolic flight campaign, Ayel *et al.* [Ayel,18] tested four FPPHPs of the same length (200 mm) but with width depending on channel dimension (*N* = 11, 1.5x1.5 mm² / 2x2 mm² / 2.5x2.5 mm² and 3x3 mm², FC-72, *FR* = 50%). They tested the behavior of the device under normal vertical BHM and microgravity conditions. They observed that thermal performances increase with increasing diameter, both in vertical BHM (interconnected thermosyphon mode, with the hydraulic diameters being above the critical diameter for this fluid) and microgravity transient phases. As explained in section 2.3.2, during those phases, for which the one possible flow pattern is slug flow, the fluid was subjected to alternated phases of stopover and reactivations. The larger the channel diameter, the higher the number and cumulated time of reactivation or active phases, up to a limit that seemed to be situated between 2.5 mm and 3 mm of diameter. This suggests that there exists an optimal hydraulic diameter in such a configuration beyond which performance will not necessarily increase, due to higher inertial forces and/or the lower capillary forces necessary to maintain the menisci in slug/plug distribution. Concerning micro-FPPHPs, Lee *et al.* [Lee,18] compared three 5-turn devices with different hydraulic diameters (0.39x0.39 mm² / 0.48x0.48 mm² and 0.57x0.57 mm², FC-72, *FR* = 50%). Figure 18a shows that the maximum allowable heat flux increases with hydraulic diameter, and also with orientation, from horizontal to vertical BHM. Generally speaking, thermal performances were also better with larger diameters. Figure A.1-4 (appendix A.1) shows the effective thermal conductivities of micro-FPPHPs from the literature plotted as functions of the ratio D_h/L_{cap} ($L_{cap} = \sqrt{\sigma/(\rho_l - \rho_v)g}$ the capillary length). It shows that the range of effective thermal conductivities strongly increases with this ratio, confirming the global trend that increasing the channel diameter enhances the thermal performances of FPPHPs, until a critical value defined in section 2.1.

(b)

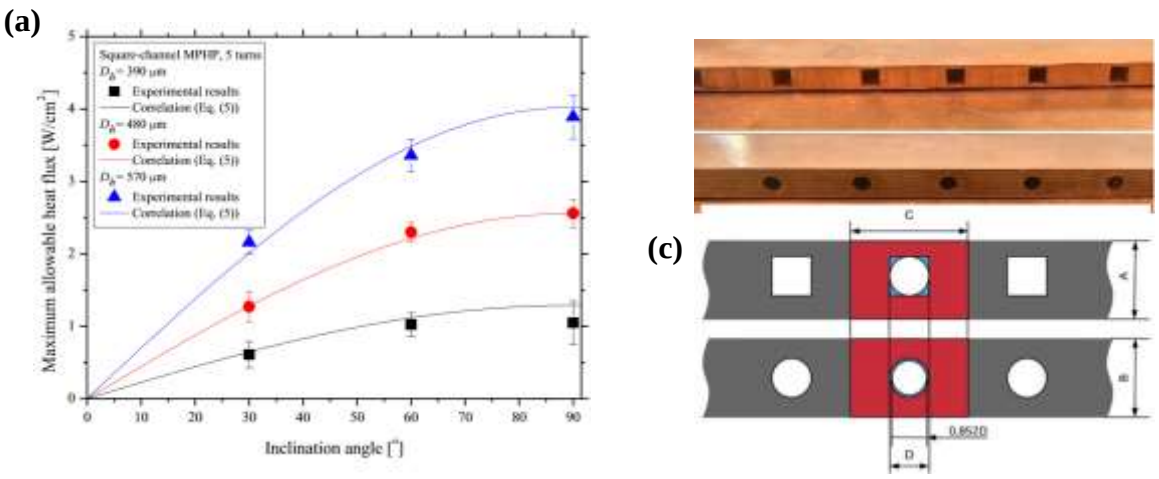

Figure 18: (a) Maximum allowable heat flux *vs.* inclination angle for three channel hydraulic diameters (N = 5, FC-72, FR = 50%, $T_{II°}$ = 20°C) [Lee,18]; and square and circular channels of same hydraulic diameter: (b) photograph of cut sections, and (c) scheme of the fluid distribution at FR = 22% [Facin,18]

Taking account the shape of the channels, Yang *et al.* [Yang,09] and subsequently Facin *et al.* [Facin,18] commented on the differences between circular and square channels of the same D_h. Even if they share the same hydraulic diameter, the volume per unit length of the square channel is $4/\pi$ higher than that of the circular one. In figure 18b-c, if a square channel is filled below 22%, the liquid will tend to accumulate in the corners, giving rise to capillary action generated due to sharp angle corners, and the menisci will recede if the filling ratio is lower. Such phenomena are obviously not to be expected in circular channels. The probability of distinct liquid plug formation is much higher in circular than in square channels, the hydraulic diameter being much reduced by the presence of the liquid film in the former configuration [Yang,09]. For this purpose, Facin *et al.* [Facin,18] compared two similar FPPHPs (N = 5, D_h = 3.18 mm, water, FR = 40-60%) with square or circular cross-section channels (figure 18b). They observed that generally, a square cross-section FPPHP works better than a circular FPPHP in terms of thermal resistance and evaporator temperature, especially in horizontal orientation, but also that for low power inputs (below 60 W), the thermal resistance in the square channels is higher than in the circular channels, the reason being that the oscillations have yet to start (figure 19a). Similarly, Lee and Kim [Lee,16][Lee,17] compared six different micro-FPPHPs of the same dimensions but with either square or circular channels, with three hydraulic diameters (N = 5, D_h = 390-480-570 µm, FC-72, FR = 50%). They found that when tested in vertical BHM, the square channel FPPHP obtained not only lower thermal resistances, but also a wider range of input powers than the circular one. This trend was confirmed by the faster self-induced evaporation observed in an isolated square channel compared to a circular one, under the same operating conditions, as discussed in section 2.2 (figure 4d [Chauvet,10]).

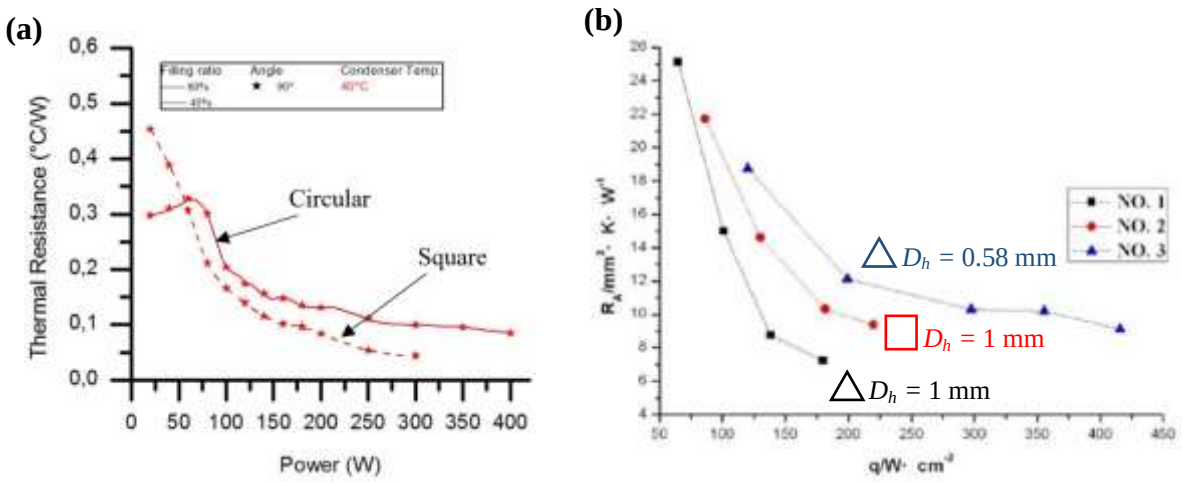

Figure 19: (a) Best thermal resistance comparing square and circular cross-section channels (N = 5, water, FR = 40-60%, BHM, D_h = 3.18 mm, $T_{II\circ}$ = 40°C) [Facin,18]; and (b) comparison between square and triangular cross-section channels (N = 10, acetone, FR = 50%, BHM, D_h = 1-1.7 mm, $T_{II\circ}$ = 32°C) [Li,13]

Qu *et al.* [Qu,07b] and Li and Jia [Li,13] compared four FPPHPs of the same dimensions but with square or triangular channels with two hydraulic diameters (N = 4, D_h = 1-1.5 mm, water, FR = 30% for [Qu,07b] and N = 10, D_h = 0.58-1 mm, acetone, FR = 50% for [Li,13]). It appears that the thermal performances of the triangular-shape FPPHP of [Qu,07b] always operate more effectively than the square-shaped FPPHP, whatever the channel diameter. By the same token, in the paper by [Li,13], figure 19b shows that the thermal performances of the square channel FPPHP tested in vertical BHM are lower and with premature dry-out than those of a triangular channel of the same hydraulic diameter (1 mm). Moreover, the device with a triangular channel diameter of 0.58 mm appears to operate less effectively than the previous ones. According to the authors, the triangular cross-section has a larger capillary force than the square cross-section, which causes evaporation of a larger amount of liquid, more intense phase transition and an increased driving force at the same hydraulic diameter and heat flux. Concerning specific cases of flat plate pulsating heat pipes, it seems that the presence of sharp corners enhances their heat transfer performances and capabilities when compared with circular channels.

3.2.2 Considerations on external geometry

Very few authors have studied the influence of condenser and/or adiabatic lengths on heat transfer. Winkler *et al.* [Winkler,20] tested their FPPHP (N = 10, 1.5x1.5 mm², acetone, FR = 50%) with five different condenser lengths, ranging from 10 to 50 mm. Results can be seen in figure 20a-b: a larger condenser area leads to lower evaporator temperatures (here, "heater" temperature, T_H) for both horizontal (figure 20a) and vertical (figure 20b) inclinations, due to increased probability of liquid formation closer to the evaporator; the increased cold plate length delays the occurrence of dry-out; at 40 and 50 mm condenser lengths, no dry-out occurred and the FPPHP worked similarly to vertical orientation. Pagnoni *et al.* [Pagnoni,18b] tested three adiabatic lengths (5.8, 8.7 and 10.8 cm) on their FPPHP (N = 12, 1.6x1.7 mm², ethanol, FR = 50%) simply by moving the 100 mm long cold plate at different abscissa from the evaporator. They found that adiabatic

lengths also play an important role in PHP behavior and performance; as in [Winkler,20], thermal resistances are decreased when condenser is moved towards evaporator, and at the minimal tested distance, gravity seems no longer to affect the thermal performance, as the resistance curves are superimposed for the highest heat power inputs (above 90 W).

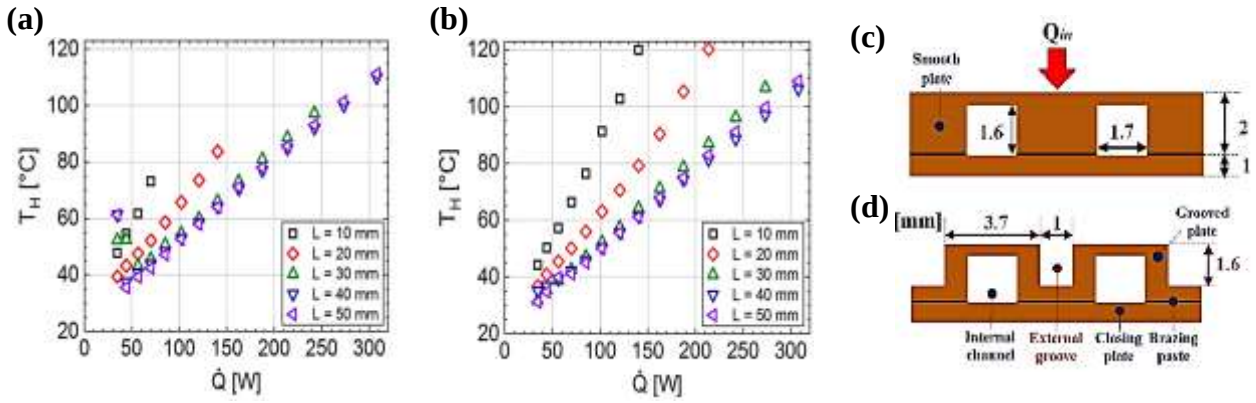

Figure 20: Influence of the condenser length L on the heater temperature T_H (N = 10, 1.5x1.5 mm², acetone, FR = 50%,) (a) horizontal, (b) vertical BHM [Winkler,20]; and schematic geometry of grooved (c) and smooth (d) FPPHPs (N = 12, 1.6x1.7 mm², ethanol, FR = 50%,) [Pagnoni,18b]

Pagnoni *et al*. [Pagnoni,18b] also attempted to reduce the effect of transverse conduction by introducing separating grooves between the channels, as can be seen in figure 20c-d. As stated by Khandekar *et al.* [Khandekar,02] (see section 2.3.2), the inter-channel heat balance plays a negative role, particularly in horizontal orientation, insofar as it reduces the local temperature gradient, which decreases the pressure instabilities degrading thermal performance. For this purpose, the authors compared two similar FPPHPs, one with separating grooves ("grooved FPPHP"), the other without ("smooth FPPHP") (N = 12, 1.6x1.7 mm², ethanol, FR = 50%). Against all odds, it appeared that the overall thermal performances of the grooved FPPHP were invariably degraded compared to the smooth FPPHP. In horizontal orientation, it was totally dried-out with performances close to the empty device. According to the authors, this specific point calls for further study.

3.3 Working fluid properties

"A suitable fluid should have a larger $(\partial P/\partial T)_{sat}$ than water or ethanol, thereby creating large pressure fluctuations with smaller heat input". Since this sentence by Khandekar *et al.* [Khandekar,02], many assertions or assumptions have been put forward by many authors on ways of enhancing FPPHP performances , particularly in horizontal orientation. For example, Kearney *et al.* [Kearney,14] and [Kearney,16] wrote that higher surface tension increases the critical channel diameter, allowing pulsation in larger tubes, resulting in increasing heat transfer capacity. A fluid with low latent heat of vaporization will evaporate more quickly, creating more vapor, which in turn increases vapor flow and pumping power. The second consequence is that it allows for start-up at lower heat powers. Furthermore, a fluid with low liquid viscosity will have more

vigorous pulsations. Increased heat capacity will increase the sensible heat capacity of liquid slugs. Obviously, large $(\partial P/\partial T)_{sat}$ is desired, since pressure rise due to increasing temperature drives pulsations; this assertion was deduced from the knowledge of the main physical phenomena driving the operation of PHPs. Section 2.1 gives a brief overview of such phenomena, including thin film deposition (through the Capillary number, requiring low surface tension σ and quite high liquid viscosity μ_l for increased thickness), thin film evaporation (through heat conduction across the film, Eq. (8), involving high liquid thermal conductivity λ_l), liquid slug momentum (through Eq. (4), requiring low liquid viscosity μ_l, moderate surface tension σ and low liquid density ρ_l when considering inertial and gravity forces), and vapor thermodynamic state and energy (through Eq. (5) to (7), requiring not only high $(\partial P/\partial T)_{sat}$ as previously mentioned, but also low density ρ_v and low latent heat h_{lv} to maximize the driving forces). However, it has also been demonstrated that latent heat through thin film evaporation is of major importance for many operations in pulsating heat pipes involving large latent heat of vaporization.

These diversified combinations are difficult to gather under a single Figure of merit, as in capillary heat pipes; as the multiplicity of phenomena is sizable and hardly conducive to classification. However, Kim and Kim [Kim,20] recently developed a highly interesting analysis leading to the establishment of a Figure of merit of particular relevance under their operating conditions. Based on observations and quantitative analyses carried out on their micro-FPPHP (N = 10, 1x0.5 mm², FR = 50%, BHM) and tested with several working fluids (ethanol, FC-72, HFE-7000, R-245fa and R-134a), they developed their analysis from a series of following assumptions:

- First, each vapor bubble is entirely covered by a thin liquid film. Vapor pressure can consequently be regarded as the saturation pressure corresponding to its temperature, and can be expressed using the Clapeyron equation and the ideal gas law (Eq. (3)) corrected with compressibility factor Z:

$$P_v = \left(\frac{\partial P}{\partial T}\right)_{sat} \frac{ZRT_{sat}^2}{h_{lv}} \tag{13}$$

- Second, as the pressure difference $(P_r - P_a)$ of the vapor bubbles surrounding a liquid slug appears to be the main driver for its motion (Eq. (4)), and considering that the terms of Eq. (13) can be assumed to be evaluated at $T_{sat} = (T_{sat,r} + T_{sat,a})/2$, the pressure difference is given by:

$$\Delta P_v = (P_r - P_a) \approx 2\left(\frac{\partial P}{\partial T}\right)_{sat} \frac{ZRT_{sat}}{h_{lv}}\left(T_{sat,r} - T_{sat,a}\right) \tag{14}$$

- Third, the frictional pressure drop due to viscous forces in the vapor phase is assumed to be negligible compared to liquid phase pressure. The motion of the liquid slug is assumed to be laminar and fully developed (like the force F_τ of Eq. (4) in section 2.1).
- Fourth, the velocity u_l of the liquid slug is related to the sensible heat transfer rate due to convective heat transfer of the moving liquid slug ($u_l \approx \dot{Q}_{sens}/\rho_l c_{pl} S(T_{ev} - T_{cd})$ with ρ_l and c_{pl} the density and

specific heat of the liquid phase, *S* the cross-sectional area of the channel; *(T_e – T_c)* corresponds to the mean evaporator-to-condenser temperature difference); according to Kim and Kim, the sensible heat transfer rate can be expressed by multiplying the total heat input $\dot{Q}$ by a certain ratio ($\dot{Q}_{sens} = \gamma_{sens}\dot{Q}$, γ_{sens} being obtained from experimental quantification) [Kim,20].Thus, the frictional pressure drop can be expressed as follows:

$$\Delta P_\tau = 32\mu_l \left(\frac{L_s}{D^2}\right) u_l \approx 32\mu_l \left(\frac{L_s}{D^2}\right) \left[\frac{\gamma_{sens}\dot{Q}}{\rho_l c_{pl} S(T_{ev}-T_{cd})}\right] \quad (15)$$

- Finally, the Figure of Merit is assumed to be proportional to the ratio of the driving pressure for fluid motion ΔP_v to the frictional pressure drop ΔP_τ, as can be seen in comparison of the experimental thermal resistance of the Micro-FPPHP with the inverse of the pressure ratio, in figure 21a, for the five tested fluids. The trend of $(\Delta P_v/\Delta P_\tau)^{-1}$ with operating temperature is consistent with the change in R_{th}, whatever the working fluid, making the pressure ratio suitable for characterization of the Figure of Merit:

$$\frac{\Delta P_v}{\Delta P_\tau} \approx \frac{\left(\frac{\partial P}{\partial T}\right)_{sat} ZRT_{sat}\left(T_{sat,r}-T_{sat,a}\right)}{16 h_{lv}\mu_l\left(\frac{L_s}{D^2}\right)} \left(\frac{\rho_l c_{pl} S}{\gamma_{sens}}\right) \frac{(T_{ev}-T_{cd})}{\dot{Q}} \quad (16)$$

According to the definition of the thermal resistance of Eq. (11), from previous equation (16), this leads to:

$$R_{th} = \frac{(T_{ev}-T_{cd})}{\dot{Q}} \approx \left[\frac{\rho_l c_{pl}\left(\frac{\partial P}{\partial T}\right)_{sat} ZRT_{sat}}{h_{lv}\mu_l}\right]^{-1} \left(\frac{16 L_s \gamma_{sens}}{SD^2\left(T_{sat,r}-T_{sat,a}\right)}\right) \quad (17)$$

First term of right-hand side of Eq. (17) brings together all the fluid thermophysical properties from the pressure ratio, while the second term corresponds to the residual term. Therefore, the Figure of Merit for working fluid selection in a FPPHP having the same operating conditions as in [Kim,20] has the following simplified relation:

$$M_{PHP} = \frac{\rho_l c_{pl}\left(\frac{\partial P}{\partial T}\right)_{sat} ZRT_{sat}}{h_{lv}\mu_l} \quad (18)$$

Figure 21b presents the variations of M_{PHP} as functions of the operating temperature for several working fluids. This figure highlights an initial qualitative selection of fluids when considering operating conditions similar to those of Kim and Kim [Kim,20]. Here, R134a presents the highest value of M_{PHP} among all working fluids, which is confirmed by its lower thermal resistance value among the five tested fluids in figure 21a. However, this analysis is not suitable for all situations, as it implies that the criterion of predominant capillary forces (Eq. (1-3)) is always effective. If the FPHP operates with dried walls in the evaporator zone, leading to

the superheated vapor phase, or if boiling appears in some liquid slugs, or if liquid slug velocity appears to be so large as to cause the rupture of menisci, then the set of equations (11-16) is no longer relevant. The driving forces to be considered are not the same when operating under annular flow pattern (favorable inclinations) or slug flow patterns (horizontal and unfavorable inclinations). This is particularly true in larger devices with higher heat fluxes. In such conditions, for the highest heat fluxes tested and the highest operating temperatures, it has often appeared that, contrary to what is shown in figure 21b, water is the best performing fluid. All in all, it remains difficult to conclude when comparing one fluid to another in the specific and complex context of pulsating heat pipes.

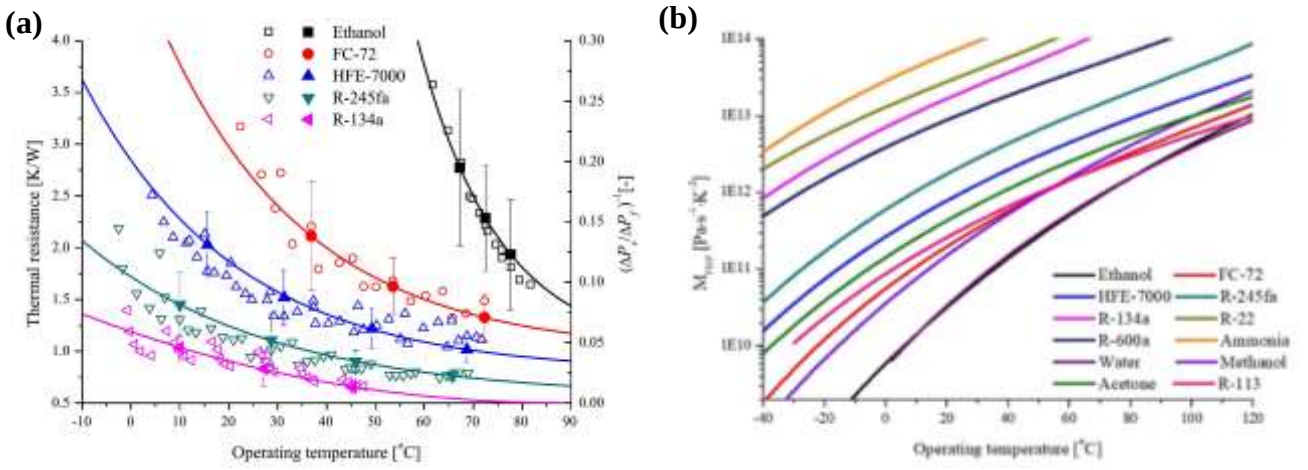

Figure 21: (a) Comparison of the thermal resistance (markers) of the Micro-FPPHP with the inverse of the pressure ratio $(\Delta P_v/\Delta P_\tau)$ (continuous lines) at various operating temperatures; and (b) change in the value of the proposed figure of Merit M_{PHP} with operating temperature and working fluid (N = 10, 1x0.5 mm², FR = 50%, BHM) (corrected from [Kim,20])

Some authors have tested their devices with different working fluids, comparing the performances according to the nature of the fluid and the operating conditions. Kearney *et al.* [Kearney,14] and [Kearney,16] compared the thermal performances of an FPPHP filled with acetone, ethanol, Novec® 649 and Novec® 7200. Curves of $(\partial P/\partial T)_{sat}$ are plotted in figure 22a for the four fluids. The device showed particularly good thermal properties for Novec® 649 (with the highest values of $(\partial P/\partial T)_{sat}$), which manifested significant potential as an appropriate dielectric fluid for operation in a FPPHP. Li and Jia [Li,13] compared acetone and ethanol in their device tested in vertical BHM. They found that the thermal resistance curves of acetone was lower than that of ethanol. Qu *et al.* [Qu,12] compared R-113 and FC-72 in their different devices, but were unable to determine the best performing fluid according to the different operating conditions. Once they were filled with water and ethanol, their micro-FPPHPs could not be activated at all; even though these two fluids are widely used in traditional-sized PHPs.

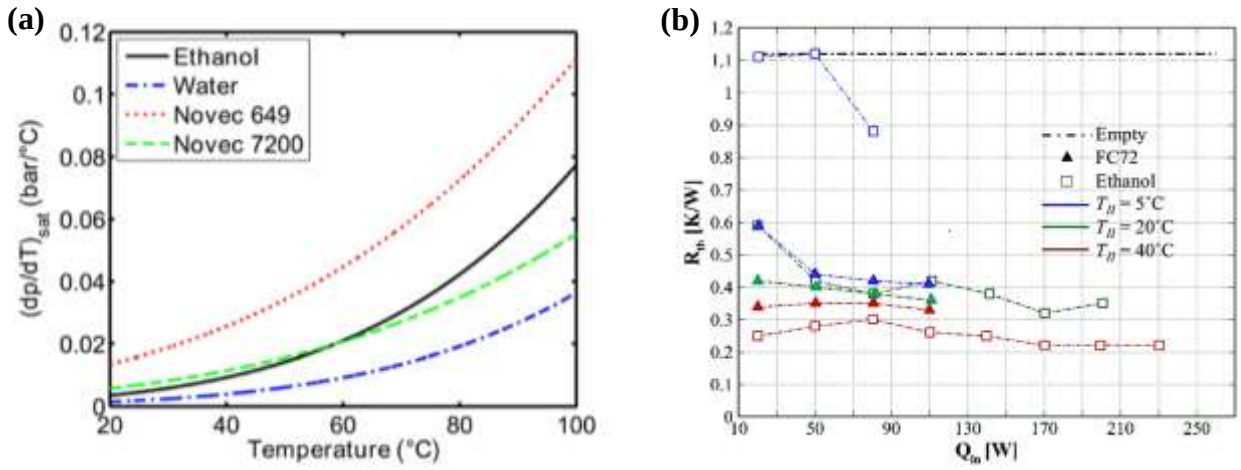

Figure 22: $(\partial P/\partial T)_{sat}$ of various working fluids as function of temperature [Kearney,14] (left) and effect of T_{II° on the thermal performance of a FPPHP (N = 12, 1.6x1.7 mm², FR = 50%, edge) [Pagnoni,18b] (right)

Another interesting way of observing the influence of thermophysical properties consists in varying the cold source temperature, T_{II°, thereby orienting the set of properties in one direction or another; increasing temperature will not only cause decreased latent heat, liquid viscosity, surface tension, liquid density and increased $(\partial P/\partial T)_{sat}$, all of which are favorable to higher driving forces, but also increased vapor density, which is unfavorable to driving forces. Generally, increased T_{II° leads to better thermal performances of FPPHPs. But the counterpart can be lower critical heat flux before dry-out, due for example to lower capillary forces. The single influence of T_{II° lies in the variation of thermophysical properties of the working fluid inside the device. Testing their FPPHP with water, Facin *et al.* [Facin,18] observed lower thermal resistance at 40°C cold source temperature than at 20°C; in horizontal inclination, however, the device started operating only when power inputs was higher than 200 W. For higher cold source temperatures, the device would start up more easily. The same conclusion was reached by Pagnoni *et al.* [Pagnoni,18b], as can be seen on figure 22b; between 5°C and 40°C cold source temperature, the device operates more proficiently with increasing temperature, particularly in the case of ethanol, compared with FC-72, for which, contrary to the trend shown in figure 21b, thermal resistance variations are rather low. In their micro-FPPHP, Kamijima *et al.* [Kamijima,20] compared the performances of their device at 20°c and 40°C. The results, presented in figure 14b of section 3.1.2, confirm the better results obtained at 40°C compared to 20°C. However, premature dry-out also occurred at the higher temperature.

Lastly, in addition to efficiency, safety, compatibility with the solid substrate, environmental and security issues have got to be considered when choosing the working fluid according to a specific application. This can drastically reduce choice, one example being the use of dielectric fluid for electronic cooling applications. Long-life operation is also a key point, and Taft tested the influence of non-condensable gases (NCG) appearing during one year on non-operation. It was found that while the addition of NCG did not prevent operation, it degraded thermal performances, producing an overall rise in the steady-state evaporator temperature and thermal resistance [Taft,13].

4 Performance improvement

Some of the multiple attempts to enhance heat transfer intensification on pulsating heat pipes are proposed below. This presents the interest of showing different ways of improving heat transfer performances of such devices on the basis of the main parameters exerting a physical influence on their operating behavior. One of the great interests of flat plate pulsating heat pipes is that the design and configuration of the channels can be easily formed by machining while remaining two-dimensional. However, now 3-D structures can be easily obtained by additive manufacturing, which opens a wide range of improvements.

4.1 Structural design

4.1.1 Non-uniform channels

Some authors have striven to improve FPPHPs heat transfer performances, particularly given the fact that PHPs with fewer turns generally fail to operate at horizontal orientation because they are lacking in gravity assistance [Shafii,01]. For this purpose, Chien *et al.* [Chien,12] proposed a new concept by varying the channel hydraulic diameter of the PHP; additional un-balancing capillary force may consequently prevail in bundles of adjacent channels, thereby promoting fluid motion along the PHP and amending the loss of gravity contribution. Fig. 23 presents a schematic view of alternate channel configuration ([Jang,19], figure 23a-c) and a representation of various forces acting on a bubble located at a bend between two channels of different dimensions ([Yang,15b], figure 23d). Yang *et al.* explain that increased pressure P_{vap} of a growing bubble under evaporation causes bubble growth. As viscous ($F_{f,Dh}$) and capillary ($F_{cap,Dh}$) forces are two major hindrances to the forward motion of the slugs, the narrower channel (figure 23d) causes higher flow resistance and capillary forces, thereby blocking the expanding vapor slug interface. The bubble is consequently forced to grow along the wider channel, leading to a preferential flow in a specific direction. Chien *et al.* have compared two similar devices - one with uniform channels (2x2 mm²) and the other with alternating dimensions ("non-uniform": $(w_1\text{-}w_2)$xh on figure 23b: (1-2)x2 mm²) – filled with water with filling ratios between 40% and 70%, and orientations between horizontal and vertical BHM. The authors showed that inclination has a lower impact on the thermal performances of "non-uniform" FPPHPs than on uniform ones [Chien,12]. Similarly, Yang *et al.* [Yang,15a-b] tested two silicon-based micro-FPPHPs (both of them "non-uniform", (0.3-0.5)x0.25 mm²) filled with pure water (70%) and pure methanol (80%) in vertical BHM. The micro-FPPHP filled with water failed to operate, but with methanol, pulsating two-phase flow was achieved, accompanied by decreasing thermal resistance of the micro-FPPHP with increasing input heat power, without encountering dry-out due to the high *FR*. Shi and Pan [Shi,16] found that their FPPHP with alternated channel widths ((1-1.5)x1 mm², N = 17) had better performances than an FPPHP with uniform channels (1x1 mm², N = 40), whatever the filling ratio and the fluid (acetone, ethanol). Markal and Varol [Markal,20] also tested an alternated-channels FPPHP ((1-2)x2 mm²) to evaluate the performances of binary mixtures (see section 4.2).

On this basis, Jang *et al.* [Jang,19] conducted an optimization study comparing five different channel configurations (3 uniform: 0.82x0.3 mm² to 3.25x0.3 mm²; and 2 non-uniform: (0.82-3.25)x0.3 mm² and (1.55-3.25)x0.3 mm²; figure 23a-c) in the aim of developing a model for mobile electronic applications (see section 5.1). Based on the observation that FPPHP with non-uniform channels ((1.55-3.25)x0.3 mm²) clearly yielded the lowest thermal resistance, owing to the increased driving force with optimized channel geometries and asymmetric structure, they designed a "finished" ultrathin graphite/Mg FPPHP with the same channel dimensions (0.5 mm overall thickness and FC-72 as working fluid): the thermal resistances were, in vertical BHM and horizontal orientations, 63%, and 56% lower, respectively, than those of an equivalent graphite sheet.

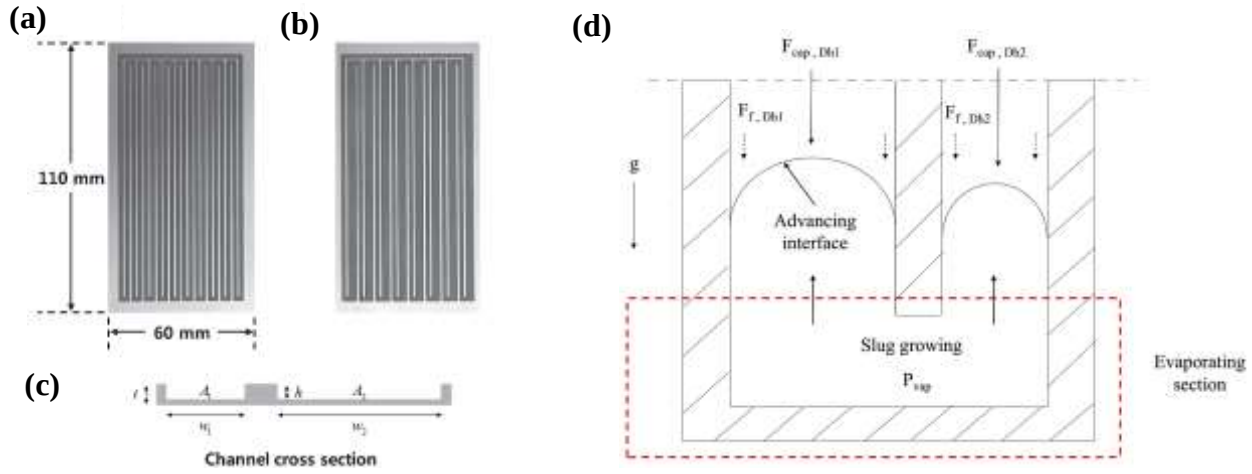

Figure 23: Schematic of FPPHPs with (a) symmetric channels and (b,c) asymmetric channels [Jang,19]; and (d) representation of various forces on a growing and collapsing vapor slug in the evaporation section [Yang,15b]

4.1.2 Non-uniform heating

To go further, on the basis of alternated channel dimensions (non-uniform: (0.5-1.5)x0.5 mm²), Lim and Kim [Lim,19a-b] imagined different specific channel layout configurations compared to classical straight channels in the evaporator zone. The channel layout configurations can be seen on figure 24a; the first objective is to rearrange the channels so that they all partially overlap with a "spot" heating section (small heating area, as in electronics); the second objective, studied via the different channel configurations, is to promote non-uniform channel heating conditions, providing better thermal performance than uniform heating patterns. The proposed concept of effective dissimilarities was previously validated by Mangini *et al.* [Mangini,17] by applying non-uniform heating patterns in a tubular PHP. By distinguishing 5 different heating sources at the top of the five U-turns of the evaporator zone, the authors showed that heating up the tubes non-uniformly at the evaporator leads to preferential direction fluid circulation, improving thermal performances, especially for the lower heat powers tested. Moreover, non-uniform heating configuration has a beneficial impact. In one case [Lim,18][Lim,19], the difference in heating power was transformed into a difference in heated lengths of the channels in the evaporator section. Figure 24b shows the thermal

resistances of the FPPHPs, filled with HFE-7000 and tested in horizontal orientation, as functions of input heat power; it was found that the evaporator temperature and the thermal resistance of the micro-PHP with uniform channel layout (case 1, figure 24a) were much higher than those of all other randomly-arranged configurations (cases 2-6). Case 5 has the lowest thermal resistance, 32% lower than that of the uniformly-arranged FPPHP. Not only the thermal performances but also the operating range is greatly extended (from 7 W -case 1- up to 12 W -cases 3, 5 and 6- maximum input power). Another FPPHP heat spreader with complex channel layout was tested by Laun *et al.* [Laun,15] and can be viewed in section 5.1 (figure 32a).

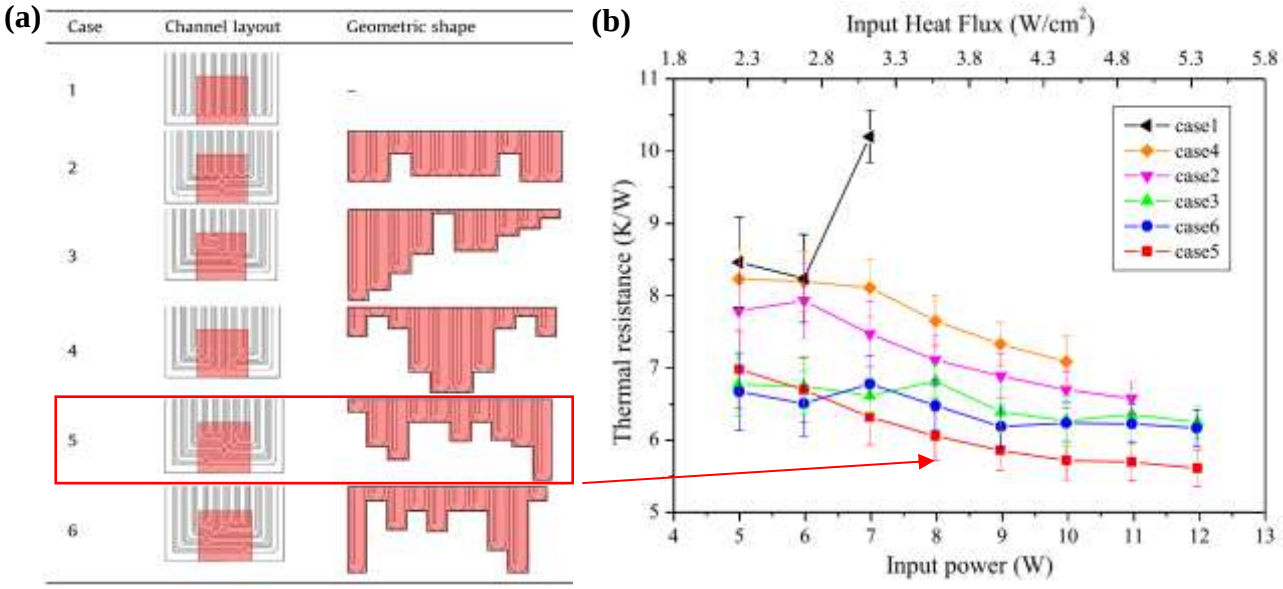

Figure 24: (a) Channel layout configurations; (b) corresponding thermal performances of the MPHPs tested in horizontal orientation [Lim,19]

4.1.3 3D configurations

In order to increase the channel-to-heating/cooling surface ratio (maximizing the number of channels per unit area and minimizing the overall dimensions of the device), several authors have designed 3-dimensional multi-layered flat plate PHPs [Thompson,09][Thompson,11a][Ibrahim,17][Natsume,13]. Furthermore, the concept of deviating from the traditional planar PHP design to a 3-D (non-planar) PHP would increase gravity participation, thereby enhancing the PHP restoration/instability forces regardless of operating orientation [Charoensawan,10]. Thompson *et al.* [Thompson,09] proposed a 3-D FPPHP with two layers of channels (square, 0.762x0.762 mm²), all of them interconnected with one other, including 15 U-turns per layer; at the end of each layer, a circular channel allows the fluid to flow within another channel. While they did not test the device in horizontal orientation, they found comparable performances in vertical BHM and horizontal edge orientations and filled with acetone. The different temperature oscillation modes between two orientations indicate that the device remains partially influenced by gravity. Furthermore, the high-channel density design has proven to be suitable for high heat flux applications, up to 20 Wcm^{-2}. Thompson *et al.*

[Thompson,11a] tested another device with 8 U-turns distributed over two layers of 1.175x1.7 mm² rectangular channels (figure 25a-c). Filled with water and acetone (*FR* = 73%) and taking into account two heating areas (11.49 cm² and 1 cm²), the 3-D FPPHP operated successfully during all investigated experimental conditions (horizontal and vertical BHM). The small heating area showed that the device could efficiently manage heat fluxes as high as 300 Wcm^{-2}. Ibrahim *et al.* [Ibrahim,17] designed a 4 layer 3-D FPPHP made of titanium alloy (Ti-6Al-4V, figure 25d; see manufacturing in section 5.3), with the particularity of circular channels (1.52 mm diameter, four U–turns per layer, see figure 25d). Filled with water, Novec® 7200, acetone or n-pentane, the device operated efficiently, almost independently of orientation (vertical BHM, horizontal, vertical THM). However, they also concluded that there existed an optimum number of layers within the FPPHP of which the total depth should not exceed the "thermal penetration depth". As a result of the heat source and the diffusivity of the solid, this depth can be defined as the depth above which the temperature remains unchanged, thereby rendering the inner layers unnecessary for heat transfer. Depending primarily on the internal fluid heat transfer coefficient and external cooling rates, the thermal spreading resistance of the evaporator/condenser material should be taken into consideration during design.

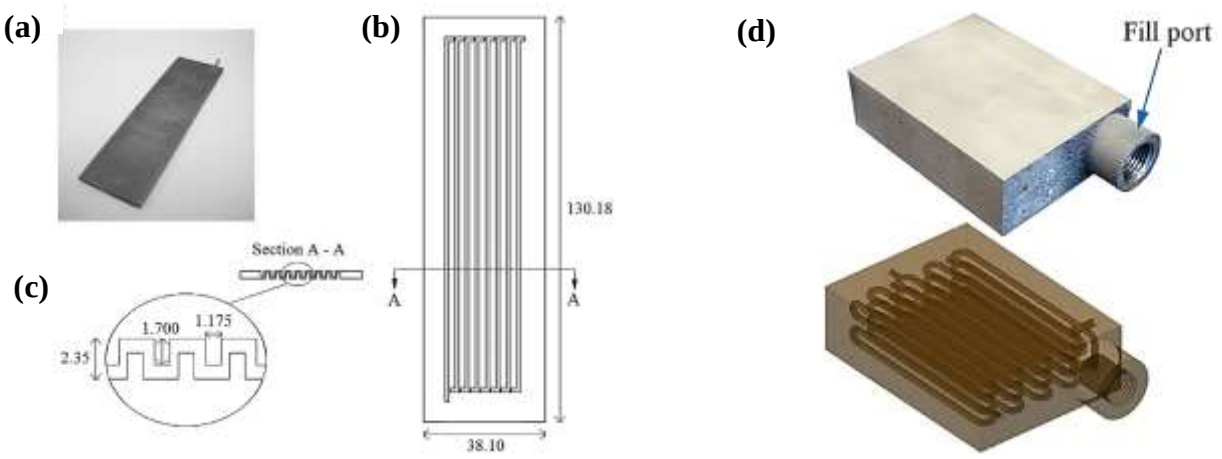

Figure 25: 3D multi layered FPPHPs: (a) photograph, (b) scheme and (c) inter-channel configuration [Thompson,11a]; (d) Ti-6Al-4V additively manufactured multi-layered FPPHP [Ibrahim,17]

4.1.4 Tesla valves

Following the concept of ball check-valves within the adiabatic section in tubular PHPs [Rittidech,07], Thompson *et al.* [Thompson,11b] [Thompson,11c] and, more recently, Wits *et al.* [Wits,18] installed Tesla-type check valves within FPPHPs for fluid flow rectification; Tesla valves (TVs) are non-moving-parts valves that connect in-parallel to a channel containing circulating fluid, and they are capable of promoting net circulation flow by creating a higher pressure drop in the backward direction, mainly by jet flow interaction at the valve exit [Thompson,11b]. One example of FPPHP rectified with Tesla-valves on surrounding channels can be seen in figure 26b. The two authors compared their device to a similar "regular" one, without TV. If Thompson *et al.* found that the presence of TV promoted a circulatory flow direction absent in the regular

device, and also found that TV-FPPHP thermal resistance was reduced by approximately 15-25% when filled with water (for a 6 TV / 6 turn copper FPPHP) [Thompson,11b][Thompson,11c], one can see on figure 26c that the effect is largely mitigated in [Wits,18]. Indeed, their device (2 TV / 6 turn stainless-steel FPPHP) did not operate properly in horizontal orientation (except for ammonia at low input heat powers) and, tested in vertical BHM, the TVs did not provide the performance improvement expected from one-directional circulation. This is particularly true in the case of ammonia, for which the heat transfer performances are so high that the effect of the TVs appears to be non-existent (on figure 26c, only FPPHP filled with methanol seems to be slightly promoted by TVs, but the effect is much less effective than that of the working fluid using ammonia): in that case, the thermal performances are much more affected by the fluid change than by the presence of TVs. As a result, use of such valves to improve performances of FPPHP remains questionable, and the number of valves must be considered when designing FPPHPs.

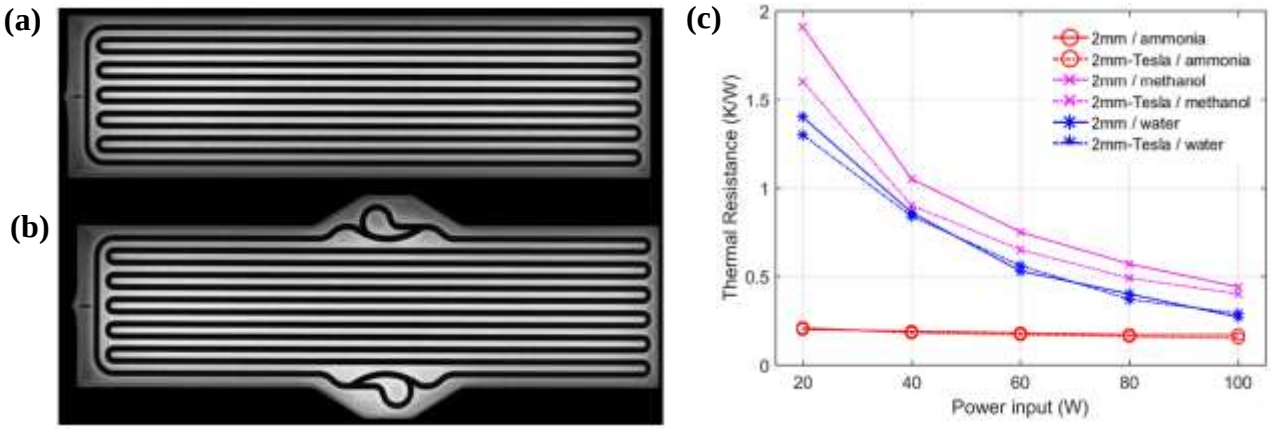

Figure 26: (a) Regular and (b) tesla-type check valves FPPHPs; and (c) overall thermal resistances in vertical BHM for three working fluids [Wits,18]

4.1.5 Liquid supply to the evaporator

Finally, other techniques have been used by authors searching to increase heat transfer rate by different ways. Among them, let quote the study of Sedighi *et al.* [Sedighi,18] who placed additional dead branches (AB) below the evaporator section (figure 27a). Since one end of the branch was closed, generation and expansion of bubbles push up liquid slugs and drew the circulated cold fluid into the branch, on the basis of the bubble pump effect (successive discharging and suction –mixing and filling- phases of liquid slugs in the dead branches). Experimental comparison with a conventional FPPHP (without AB) demonstrated better performances for the device with AB (around 18% lower average resistance at a 50% filling ratio), particularly in the low input power ranges. In order to improve PHP dry-out limitations, Chauris *et al.* [Chauris,18] proposed a remote electro-hydro-dynamic pump ("EHD", without mechanical parts), between two branches of the evaporator and the condenser sections (figure 27b). By bringing liquid from cooled to heated zones, this EHD allows a restart of the oscillations due to local evaporation, but at the cost of an

additional source of energy (a few milli-watts). The authors showed that the EHD pump can enhance FPPHP start-up and control the temperature of the evaporator zone. Finally, Smoot and Ba [Smoot,11] presented a hybrid FPPHP in which the channel is formed by a wick structure (50 μm sintered copper powder) rather than a typical solid wall. When heat is applied, evaporation from the wick takes place and builds vapor pressure between the liquid plugs located near the evaporator, causing motion similar to that occurring in conventional PHPs. They highlighted a significantly decreased start-up heat power requirement compared to typical PHPs, with the highest peak performances found for acetone, and a wider usable heat power input range for water as working fluids. However, compared to the first technique, the last two techniques are effective, but work to the detriment of the simplicity of FPPHP development, and shall be considered only once the limits of the first technique have been reached.

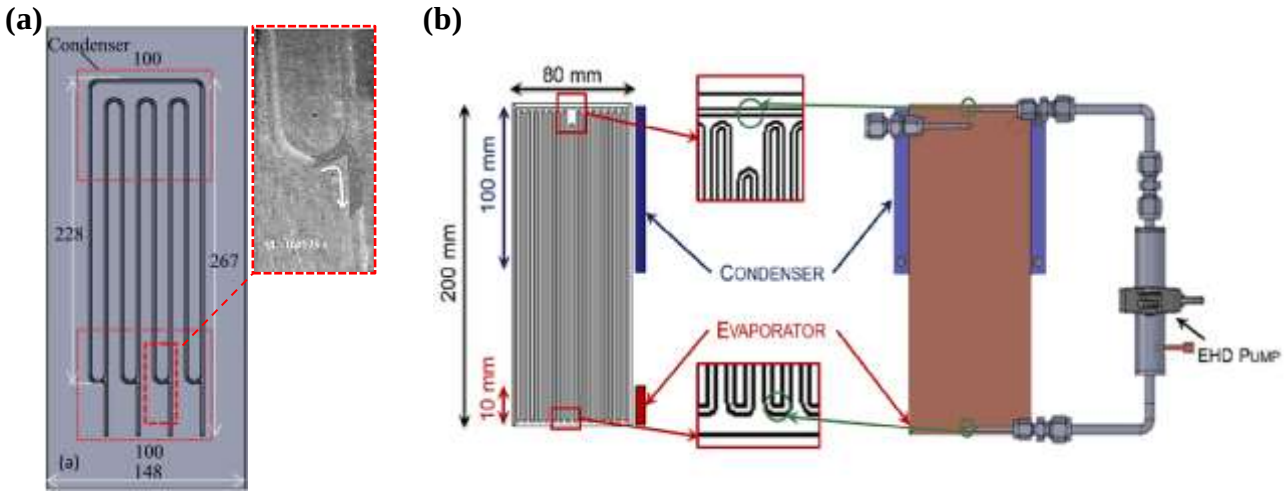

Figure 27: (a) FPPHP with additional branches in the evaporator section [Sedighi,18]; and (b) FPPHP with remote EHD pump [Chauris,18]

4.2 Modification of fluid and fluid/solid properties

4.2.1 Effect of the internal channel surface wettability

Several authors have attempted to modify the internal surface of tubes or channels with hydrophilic or hydrophobic coatings in order to influence the wettability of fluid/solid couples, thereby influencing the thermal performances of PHPs. Water has been particularly targeted for its good thermophysical properties, but is often ineffective, particularly at low input heat powers, due to its low wettability with many surfaces. On the one hand, Hao *et al.* [Hao,14a] investigated heat transfer and slug motion for hydrophilic and pure copper channels of FPPHPs, and found that the thin liquid film at the end of a receding liquid slug increased with surface wettability (*i.e.* with an hydrophilic surface coating). On the other hand, Khandekar *et al.* [Khandekar,02] maintained that a surface with negligible dynamic contact angle hysteresis should be preferred in PHPs, the objective being to reduce capillary resistance under slug flow conditions. Using

superhydrophobic coatings to produce drag reduction (with negligible contact angle hysteresis) in both laminar and turbulent flows [Rothstein,10], Hao *et al.* [Hao,14b] carried out their study by comparing three similar copper FPPHPs filled with water: one with pure copper surface (I), one with superhydrophilic (CuO coating layer) evaporation zone and superhydrophobic ($C_{18}H_{38}S$ coating layer) condensation zone (II), and the last with uniform superhydrophobic surface (III). It appeared that the device with both hydrophilic and hydrophobic coatings (II) presented a stronger oscillating motion and lower thermal resistance, (about 5-20%), in comparison with that of copper FPPHP (I). However, heat transfer performance was significantly decreased in the uniform superhydrophobic device (III).

4.2.2 Self-rewetting fluids

More recently, several authors have demonstrated the benefits of self-rewetting fluids (SRWF) instead of pure water, particularly in pulsating heat pipes: SRWFs are mixtures of which the surface tension increases with temperature above a certain threshold value (see figure 28a). As regards SRWFs on heated surfaces, liquid/vapor interfaces and temperature gradients should lead to surface tension-driven convection, preventing dry-out of the heated surface. Figure 28b-e shows a comparison between the flow structures of water and a water / 5% butanol SRWF mixture, near the contact line of evaporating menisci in a capillary heated tube (1 mm inner diameter) under the same operating conditions [Sefiane,20]. For water (b,c), there is only a slight liquid supply flow from the central part to the meniscus corner, whereas for SRWFs (d,e), convection appears more effective; the temperature-induced thermo-capillary flow, or reversed Marangoni flow, leads cool liquid at the center of the meniscus to move towards the hot region of the tube. The evaporation rate appeared higher for SRWF than for pure fluids. The Marangoni effect becomes more pronounced when fluid temperature exceeds critical temperature. However, due to the overall fluid motion during normal operation, questions can be raised on the effective performances of SRWFs in PHPs compared to the enhancement brought to static evaporative meniscus in capillary structures.

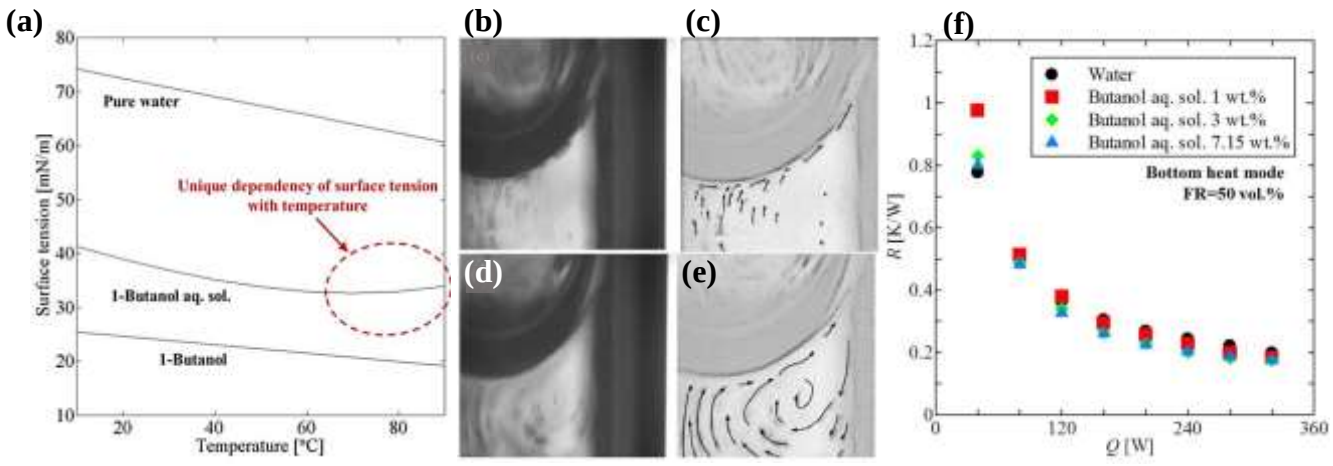

Figure 28: (a) Temperature-dependence of the surface tension of a SRWF mixture compared to both mixture constituents; flow structure (liquid side) near the meniscus during evaporation in a tube: (b,c)

water, T_w = 75°C and (d,e) water / 5% butanol mixture, T_w = 75°C [Sefiane,20] and (f) thermal resistance as function of heat power for 4 SRWF concentrations [Yamagani,16]

Fumoto and Kajawi [Fumoto,09] and Yamagami *et al.* [Yamagami,16] tested mixtures of water with different concentrations of butan-1-ol as working fluids in FPPHPs. The first results showed that, tested in vertical BHM, the effect of butan-1-ol concentration on the operation of the FPPHP is quite low, but that better thermal performances are obtained for the highest concentrations (up to 1% in weight) [Fumoto,09]. Furthermore, the maximum input heat power before dry-out was significantly increased with higher butan-1-ol concentrations. Yamagami *et al.* [Yamagami,16] also observed that performance is only modestly enhanced when a given concentration of butan-1-ol is exceeded in BHM (figure 28f). Nevertheless, Cecere *et al.* [Cecere,18] tested a FPPHP filled with a SRWF mixture composed of water and 4 wt.% of butan-2-ol during the 65th parabolic flight campaign of ESA. They found that, tested in vertical BHM, the FPPHP had poorer thermal performances with SRWF than with water under normal gravity conditions, but that under microgravity, it appeared to operate with much better performances than with water. Visualizations showed that for water, during microgravity conditions the fluctuations are stopped and that liquid accumulates at the condenser section, while in only one or two channels, liquid plugs move towards the evaporator.

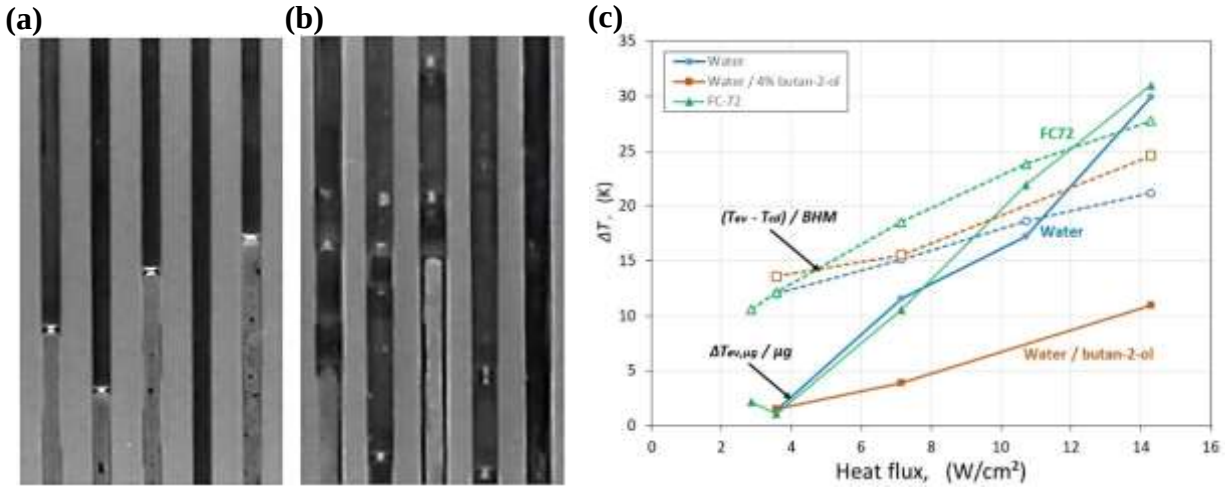

Figure 29: Flow regime for: (a) water, and (b) SRWF, under vertical BHM in a copper FPPHP [Cecere,18]; and (c) resulting temperature differences under normal ($(T_{ev} - T_{cd})$, dotted lines) and microgravity ($\Delta T_{ev,\mu g}$, continuous lines) conditions

Figure 29a-b shows the liquid slug flow patterns for water and SRWF [Cecere,18]; on the one hand, the contact angle of water/copper is high and water does not properly wet the wall; on the other hand, with butan-2-ol the contact angle is strongly reduced and thin liquid films are clearly visible along the corners of the walls. During operation in microgravity phases, the liquid re-wet several times the evaporator zone triggering the oscillating regime. Plotting the difference of temperatures between averaged evaporator zone and averaged condenser one in vertical BHM and normal gravity ($(T_{ev} - T_{cd})$, dotted lines, figure 29c), the relative evaporator temperature appears to be the lowest for water, even when compared to FC-72 tested during a

previous parabolic flight campaign in the same device [Ayel,19]. That said, the mean evaporator temperature increases during the transient periods of 22 s of microgravity ($\Delta T_{ev,\mu g}$, figure 29c) are apparently much lower with SRWF than with water, showing clear improvement in thermal performances using SRWF with butan-2-ol under the relevant operating conditions (also in horizontal orientation).

4.2.3 Binary mixtures

However, not only SRWF mixtures but also binary mixtures, without self-rewetting effect, enhanced thermal performances of FPPHPs compared to pure fluid performances. Markal and Varol [Markal,20b] tested mixtures of ethanol and n-pentane with different concentrations (volume mixing ratios V_{eth}/V_{pent} of 1:1, 1:3 and 3:1) in an alternated channel width FPPHP ((1-2)x2 mm²). The mixture with volume ratio of 1:3 appeared to yield the best thermal performances compared to other mixing ratios (3:1 ratio being the worst), both in both vertical and horizontal orientations, and they did so for two filling ratios (30% and 60%). For the authors, boiling point, latent heat, surface tension and dynamic liquid viscosity values were significantly lower for n-pentane compared to ethanol. On the other hand, saturation pressure variation with temperature $(dP/dT)_{sat}$ is far greater for n-pentane than for ethanol, better promoting the flow motion. These analyses remain to be validated due to the difficulty of differencing phenomena in such complex systems. By the same token, a question is raised in the study by Slobodeniuk *et al.* [Slobodeniuk,20] on the actual origin of the FPPHP performance improvements using SRWFs [Fumoto,09], [Yamagami,16] and [Cecere,18]: Do the observed enhancements come from the self-rewetting effect, or simply from better wettability using such mixtures rather than pure water, or do they come from other factors associated with thermophysical properties as described above in [Markal,20b] (increasing $(dP/dT)_{sat}$, etc.). Comparisons of aqueous mixtures of water with 5 wt. % of butan-2-ol and with 20 wt. % of ethanol (both mixtures having approximately the same surface tensions at 40-50°C), tested in a copper FPPHP at 50% filling ratio showed very similar performances for the two fluids, and much better performances than with pure fluids when tested in horizontal inclination; due to the gravity forces that help the liquid to flow back to the evaporator, becoming less influenced by surface tension forces, the vertical BHM does not yield similarly conclusive results.

To sum up, improving the thermal performances of FPPHPs by combining different fluid mixtures according to their properties seems quite promising, especially in terms of ease of implementation.

4.2.4 Nanofluids

Several authors have tested the influence of nanofluids inside tubular PHPs, but very few have provided comparable testing inside FPPHPs. Wu *et al.* [Wu,16] tested an FPPHP using ethanol mixed with fullerene C60 nanoparticles with concentrations between 0.1 and 0.3 wt. %. They observed real improvement of thermal performances with increasing concentrations (*R*, figure 30a), a finding that can be explained by an intensification of boiling and condensing processes, particularly at low heat loads (up to 35% lower thermal resistance compared to pure ethanol for 0.3 wt. % concentration, at 20 W). On the other hand and against all

odds, notwithstanding the better performances the maximal heat power attained before dry-out was severely decreased, with increasing concentration of nanoparticles (Q_{cr}, figure 30b). They explain this phenomenon by an increase of active nucleation sites resulting in sharper liquid boiling, rendering the FPPHP easier to dry out. This point becomes critical and needs to be analyzed if the use of nanoparticles is to be considered.

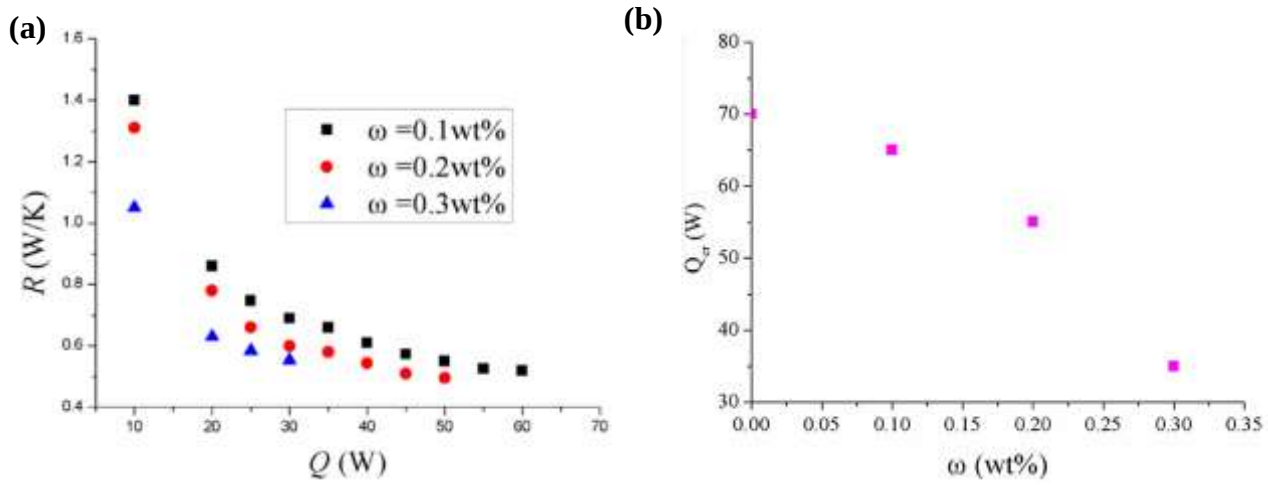

Figure 30: (a) Thermal resistance as function of input heat power for different nanoparticles concentrations, and (b) critical heat power *vs.* nanoparticles concentrations (2x2 mm², ethanol, *FR* = 50%, orientation: 50°) [Wu,16]

5 Applications and manufacturing

Due to their specific shape and manufacturing process, flat plate pulsating heat pipes should be considered differently from tubular PHPs with regard to applications. By allowing good contact between the two surfaces, their external flat shape makes them suitable for removing heat from flat hot sources such as dissipative electronic components. They can also be used as efficient thermal spreaders. Conversely, their disadvantages lie in lower capability of integration flexibility compared to tubular PHPs, and probably higher mass due to continuity of solid material between the channels in the massive plates. Moreover, they can generally not be considered as enhanced heat exchangers between two fluids such as TPHPs.

5.1 Electronic cooling

As mentioned above, one of the most promising fields of application for FPPHP is in dissipative electronic component cooling. Mehta and Mehta [Mehta,16] proposed a short review of the development of FPPHP products with emphasis on its applications in heat spreading, heat sinking and electronic cooling over the coming years. Li and Jia [Li,13] experimented with aluminum flat plate PHPs combined with natural convection fins for cooling high-power LED (up to 100 W). They showed that a high-power LED could be cooled by an FPPHP with a finned area through natural air convection, with pronounced influence of the fins area. Boswell *et al.* [Boswell,15] investigated light weight heat sink embedded with an FPPHP for thermal management of circuit credit card assembly. Mehta [Mehta,20] tested an FPPHP embedded in a massive aluminum heat sink for MOSFET (Metal Oxide Semiconductor Field Effect Transistor) cooling (Fig. 31a). It

was shown that the device was able to transfer heat with acetone as working fluid in vertical orientation through natural convection. Of course, FPPHP can be mixed with other solutions such as a vertical radiator with plane evaporator end and multi-pulse condenser ends for CPU cooling applications [Guowei,19]. And Laun *et al.* [Laun,15] developed a radial FPPHP, with very complex channel configuration, to study the effect of central heating of a 30x30 mm² heat source on the 100x100 mm² heat spreader (figure 32a). Heat power reached 525 W, corresponding to a heat flux of 58 W/cm².

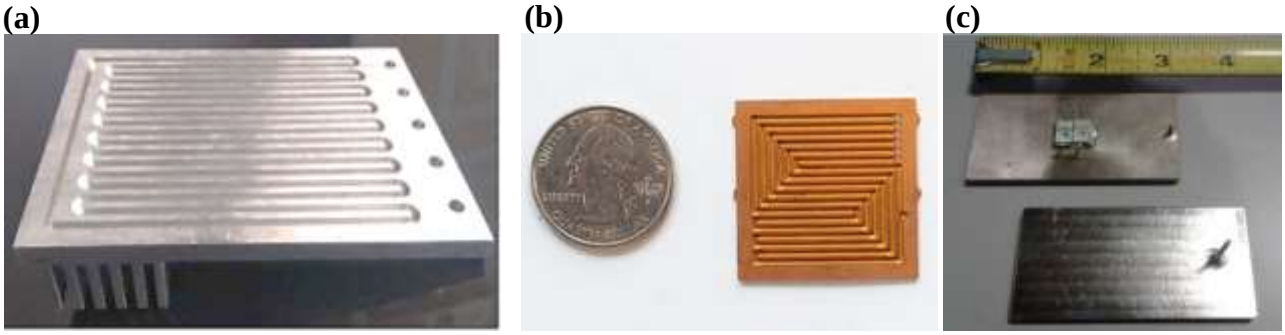

Figure 31: (a) FPPHP embedded in heat sink for MOSFET cooling [Mehta,20]; (b) spreader FPPHP for power electronics and (c) laser diode in communication and defense systems (Courtesy of ThermAvant Technologies, LLC)

Concerning micro-electronic cooling, miniature flat plate PHPs are presented on figure 31b-c [Thermavant,21]. Jang *et al.* [Jang,19] showed thermal performance improvement of an ultrathin FPPHP (0.4 mm thick) against an equivalent graphite sheet for use in mobile electronic devices (see section 4.1 and figure 23a). They designed an optimized prototype made of magnesium covered by a thin graphite sheet, which, filled with FC-72, displayed thermal resistance lower than that of the pure graphite sheet. They concluded that flat plate pulsating heat pipes are highly recommended for the cooling of mobile electronic devices owing to their higher thermal performances at all inclination angles.

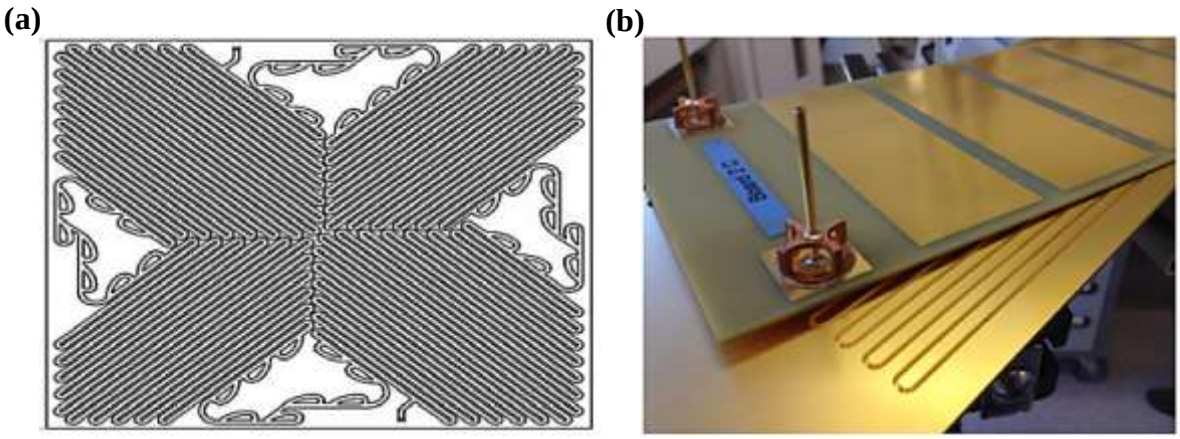

Figure 32: (a) Radial heat spreader FPPHP [Laun,15]; and (b) two PCBs with an exposed embedded meandering mini-channel [Kearney,16]

Kearney *et al.* [Kearney,14] and [Kearney,16] tested an embedded FPPHP for integrated electronic cooling applications (figure 32b). The device was directly machined in the FR4 substrate of a PCB (Printed Circuit Board) for direct integrated cooling, and the inner walls were coated with a nickel-based layer of several microns, ensuring impermeability and low surface roughness. While their experiments with ethanol, Novec 649 and Novec 774 clearly demonstrated the potential of such prototype as a heat spreading device, the authors concluded that further investigations were necessary in order to achieve greater heat flux (up to 50 $W.cm^{-2}$) in integrated power cooling electronic applications.

5.2 Other fields of applications

5.2.1 Space and transport applications

Flat plate pulsating heat pipes have been considered for space applications, using the same kinds of electronic component cooling as in the previous section, but with a microgravity environment [Gu,05][Taft,15][Belfi,18]: Taft and Irick [Taft,19] present the feedback of six months of space flight experiments with their ASETS-II (Advanced Structurally Embedded Thermal Spreader) aluminum Pulsating Heat Pipes. The extensive data set comparison between three devices, filled with butane and R134a and tested in microgravity aboard the X-37B reusable space plane, showed expected heat transfer performances compared to ground tests. More specifically, the FPPHPs experienced no significant hysteresis effects and performed steadily and successfully during a continuous six-week-long operation. Similarly, Ayel *et al.* [Ayel,15a] tested a copper flat plate PHP filled with FC-72 (with 1.6x1.7 mm^2 channel dimensions) on ground and in hyper –and micro-gravity conditions during the 60^{th} parabolic flight campaign of the ESA. They showed that tested in horizontal inclination, the FPPHP was not influenced by changes of gravity levels, particularly during the 22 s of microgravity, confirming that such a system can be an efficient candidate for thermal control in different space applications, once a greater channel size will has been combined with a sufficient number of turns. Further investigations have been conducted by the same authors [Ayel,18][Ayel,19], performing visualizations of flow patterns in copper/borosilicate glass FPPHPs filled with FC-72 (during ESA 62^{nd} and 64^{th} parabolic flight campaigns), and showed that heat transfer performances seem to increase with increasing channel hydraulic diameter under microgravity conditions, up to a certain limit associated with the fluid and its corresponding critical diameter, taking inertial and viscous forces into consideration. According to Taft *et al.* [Taft,15], when a PHP is not terrestrially independent, it is likely to perform better in a microgravity environment.

FPPHPs should also be seriously considered for transport applications. For example, Manno *et al.* [Manno,15] tested a flat plate copper PHP in specific operating conditions to evaluate its thermal performance and behavior in accordance with possible application in automotive engineering for thermal management of hybrid electric vehicles' crucial components (electronics, batteries, etc.). They tested their device filled with ethanol under different orientations, particularly during transient tests simulating the variations of vehicle

stability by dynamically varying the pitch (±22.5°, along the longitudinal axis of the device) and roll (±22.5°, around the median longitudinal axis) angles. The results show that FPPHP thermal response is positive when pitched up in favorable gravity conditions, and vice versa. Variations of roll angle lead to acceptable variations of the temperature of the device.

5.2.2 Various applications and heat recovery

Several industrial manufacturers now offer FPPHPs for different cooling applications: heat sinks, including air or liquid cooling, heat spreaders, including power electronics and amplifiers, and laser diodes in industrial communication and defense systems and thermal straps, for high-power, temperature-sensitive devices, including long-distance to flexible 3-D structures [Thermavant,21]. Among less likely applications, Chao *et al.* [Chao,13] successfully adopted a specific design of defrosting plates using FPPHPs to substitute for the design using traditional heat pipes, and Natsume *et al.* [Natsume,13] tested a flat-plate cryogenic PHP filled with H_2, Ne and N_2 to improve HTS ("High Temperature -20-77 K- Superconductors") magnet cooling. The very good performances of these fluids at such low temperatures (from 18 K to 84 K) has prompted consideration of PHPs and FPPHPs for cryogenic applications.

Finally, another important field of applications in the current context of sustainable development lies in thermal management of renewable and conversion energy systems, often involving electric dissipative components. Alizadeh *et al.* [Alizadeh,20] proposed a flat plate PHP to reduce the rear surface temperature of a photovoltaic solar panel by comparing different architecture scenarios using air convection or water flow channels to cool the condenser. Another approach was proposed by Zabek *et al.* [Zabek,16], using outer wall driven temperature fluctuations from FPPHPs for waste heat recovery and thermal energy harvesting, by means of pyroelectric generators that can effectively charge a storage capacitor to convert thermal energy from high frequency temperature oscillations, thereby generating electrical energy that would be available for discharge. While the amount of electrical energy would be very low, the couple has the potential to cover ranges from watts to kilowatts of heat power, and is capable of replacing conventional blower fans and large sized heat sinks and providing electrical power from μW to mW, for wireless sensor nodes, internet of things devices, and battery-less technologies. Of course, the list of potential applications is very long and virtually any system can be imagined as soon as energy production/conversion systems can ensure thermal management.

5.3 Process manufacturing

5.3.1 Milled/engraved substrates bonding

FPPHPs can be easily obtained from a base plate machined with a single channel wound in a serpentine between two ends, and covered with a second plate of the same dimensions (except thickness). Both plates have to be brazed on the edges and between channels to guarantee perfect sealing from outside and from

adjacent channels relative to one another. While this is the most common way, some authors propose other fabrication processes to be described hereinafter. Facin *et al.* [Facin,18] and Betancur *et al.* [Betancur,20] fabricated copper FPPHPs using diffusion bonding process; the two flat plates are mechanically pressed and subjected to thermal cycle at temperatures closed/below the melting point (about $0.7T_{melt}$), under a high vacuum environment (< 10^{-6} Torr). The advantages reside in solid state union of the plates at microscopical level, so that the united surfaces present the properties of the bulk material, thereby avoiding the use of filler material as in conventional soldering/brazing. Taft *et al.* [Taft,15] used ultrasonic consolidation (UC) to manufacture their FPPHP; UC is an additive/subtractive manufacture technique that allows for the creation of high-strength materials with internal features that significantly exceed the strength-to-weight ratio of many current aerospace materials. In the FR4-FPPHP of Kearney *et al.* [Kearney,16], low thickness nickel-based layers are diffusion-bonded together, forming a monolithic substrate encapsulating the PHP.

Another method presented by Lin *et al.* consists in molding Polydimethylsiloxane (PDMS, the most widely used silicon-based organic polymer) [Lin,08], and PDMS with copper powder in order to increase thermal conductivity, PDMS being a heat insulation material [Lin,09]. The original mold was obtained from milling an aluminum plate. The device facilitated (a) visualizations of flow pattern using methanol and ethanol as working fluids and (b) parametric investigation of its performances.

5.3.2 Additive manufacturing

Belfi *et al* [Belfi,18] describe an embedded FPPHP built by additive manufacturing technology, on the basis of 3D objects made from adding layer-upon-layer of material. According to them, the most suitable techniques are direct metal laser sintering and direct metal laser melting, both of which use lasers to completely or partially melt an ultra-thin layer of metal powder on a print bed. In their paper, the powder material chosen is CL 31AL, and they tested two levels of printing layer definition: 25 μm (high) and 50 μm (standard), highlighting the capability and the limits of such technique. By the same token, Ibrahim *et al.* [Ibrahim,17] employed the laser powder bed fusion additive manufacturing method to fabricate a multi-layered titanium alloy (Ti-6Al-4V) 3D pulsating heat pipe including four layers of circular channels (see figure 25d, section 4.1), using gas atomized spherical particles with a diameter range of 15-45 μm. Additive manufacturing provides a unique opportunity to build heat transfer devices with better matching coefficients of thermal expansion, “CTE” (the CTE of titanium being much closer to silicon than the CTE of copper or aluminum in direct cooling of electronic components) and higher melting temperatures, but also with low thermal conductivity (6.7 $Wm^{-1}K^{-1}$), which can be damaging according to the heat flux level. In parallel, Hideyama *et al.* [Hideyama,18] manufactured a transparent FPPHP using 3D printing technology and Acrylonitrile Butadiene Styrene (ABS) filament as a material. Tests with HFE-7000 confirmed the pulsating behavior of the device, but heat transfer performances required additional experiments to optimize the thermal design.

5.3.3 Flexible FPPHPs

Lastly, Der *et al.* [Der,18] presented a new kind of FPPHP, the "pulsating heat stripes", having no equivalent among state-of-art commercial or research-based heat transfer devices; a thin, low-cost flexible and lightweight FPPHP was obtained by assembling three layers of composite polypropylene sheets joined together by selective laser welding (figure 33a). Tests performed with FC-27 as working fluid showed a six-fold increase of equivalent thermal conductance in comparison with a single polymer plate of same dimension, thereby suggesting a promising way to address the demand for heat transfer devices characterized by low weight, small thickness, low cost and high mechanical flexibility. More recently, Jung *et al*. [Jung,20] developed another kind of flexible FPPHP composed of a 0.5 mm thick polycarbonate plate ("PC", figure 33b), engraved with 15-turn alternated micro-channels, and wrapped in flexible 70 μm copper-clad-laminates ("FCCL"). This packaging prevents the permeation of non-condensable gases from the ambient while remaining flexible (figure 33c). Once filled with HFE-7000, the device has a maximum thermal conductivity approximately 2.7 times higher than that of copper at a heat flux of 2.8 $W.cm^{-2}$.

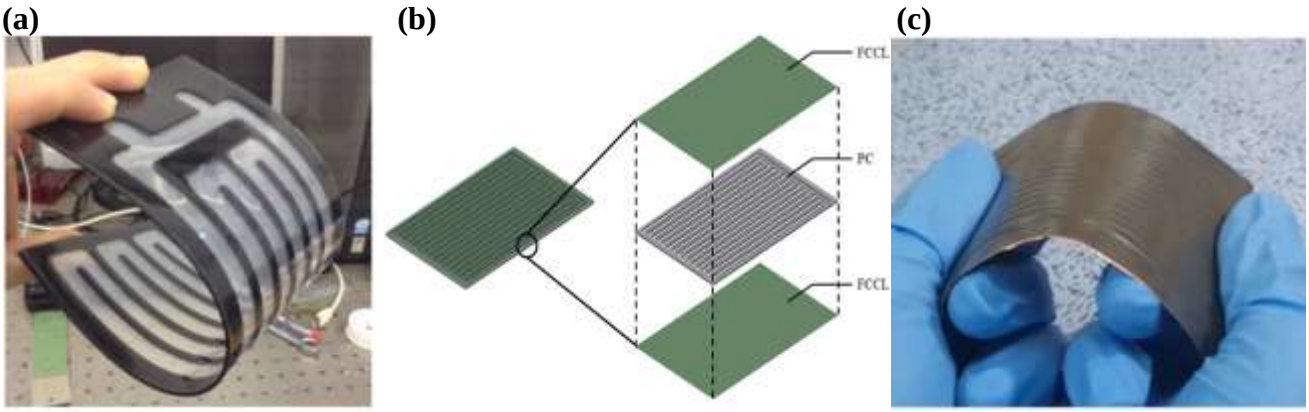

Figure 33: (a) flexible polymer FP pulsating heat stripe [Der,18]; (b) schematic and (c) photograph of bent flexible FPPHP (right) [Jung,20]

6 Conclusions

In this paper, an exhaustive review of numerous recent scientific experimental and some theoretical studies on thermal and flow behaviors of flat plate pulsating heat pipes, as well as two-phase flows in rectangular mini- and microchannels, has been presented, the objective being to improve understanding of thermofluidic working principles of rectangular-channel FPPHPs.

The reviewed papers mainly dealt with the complicated two-phase flow mechanism in the channels of the flat plate pulsating heat pipe. As mentioned above, one of the great advantages of FPPHP is the possibility of providing complex visual investigations of flow with simultaneous measurements of pressure and temperature fluctuations, via both temperature sensors and infrared approaches. A visualization approach has been used by authors to determine the flow regime patterns, flow regime transition parameters or/and to understand the

influence of liquid slug on heat transfer parameters. Few researchers have investigated the influence of capillary rewetting in the channel corners on the start-up mechanism and dry-out phenomena.

Although it is very difficult to provide an overall synthesis on the influence of all the parameters acting on their operation, as they are interconnected to each other, the main trends are summarized here:

- The physical equations that describe the physics of FPPHPs remain similar to classical tubular PHPs. But specific supplementary effects (capillary forces in the corners and transverse heat conduction) brings new phenomena necessary to take into account.
- Thin film evaporation is of major importance when considering heat transfer in pulsating heat pipes. Authors have shown that the exchanged latent heat was preponderant relative to sensible heat.
- The square or rectangular shape of the channels leads to capillary pumping in the corners that improve the wetting of the evaporation zone and enhances evaporation in comparison with round channels. This has been experimentally demonstrated both in single channels and in complete FPPHPs. Furthermore, considering equivalent hydraulic diameter, thermal performances of triangular channels prove to be better than square channels, and the latter better than circular channels.
- Visualizations of flow patterns in the overall channels of the devices highlighted mixed flows from slug flow to annular flow patterns in vertical bottom heated mode. Nucleate boiling was sometimes observed in the evaporator zone, it was accompanied by intense film evaporation, specific to intense heat transfer in these zones. In horizontal orientation, dry-out of the evaporator zone has often been observed and was attributed to the transverse conduction between channels, resulting in a decrease in pressure instabilities and being the motor of the liquid slug motion.
- Thermal performances depend on many parameters, the first one being heat flux or heat input at the evaporator zone: the bigger the heat flux, the better the thermal performances. Like in tubular PHPs, other parameters like the working fluid, the filling ratio or the orientation have also an important influence on operations. Generally speaking, the more U-turns, the less the FPPHPs are influenced by these parameters.
- Channel hydraulic diameter is also of primary importance and a higher diameter leads to better performances while a critical value depending on the working fluid and the operating conditions, is not exceeded.
- The thermophysical properties of the working fluids directly impacts performances. Vapor thermodynamic state, although difficult to evaluate between saturated and superheated states, is of primary importance for fluid heat and mass transfer modeling. Some authors have proposed some Figures of Merit which are relatively well correlated with their experimental results. But an extension to other studies has shown that these numbers are not adapted to all situations.
- Improved thermal FPPHP performances will necessitate attempts to reach unidirectional flow using asymmetric channels (different diameters of the neighboring channels), check-valves, pumping

systems or additional closed-ended branches in the evaporation zone; an increased number of channels in the evaporation zone simulating hot-spot cooling; fluid modification using self-rewetting fluids, surfactant and nanoparticle addition evaluating the expected effect of channel wall rewetting, wettability increase etc.; and, finally, hydrophobic or hydrophilic coating deposition on the channel wall surface in order to modify liquid/solid pair iterations.

- Due to their design features, flat plate pulsating heat pipes have been developed for electronic cooling application. In microelectronic and portable electronic applications, however, FPPHPs with micro-channels are preferable due to their small dimensions, whereas aerospace and high-power applications require more efficient thermal rejection systems capable of rejecting heat to longer distances.

There have been many disagreements between the works authored by different teams, and even though numerical modeling has begun to be efficient, reliable predictive tools are lacking, and there exist virtually no correct practical recommendations for FPPHP design. Hence, more studies will be required, primarily visualization studies needed to understand the coupling of different phenomena influencing on two-phase flow behavior.

Nomenclature

a,b	Channel cross-section dimensions (m)
A	Cross-section (m^2)
AB	Additional Branches
ABS	Acrylonitrile Butadiene Styrene
BHM	Bottom Heated Mode
Bo	Bond number
Ca	Capillary number
c_p,c_v	Specific heat capacities ($J.kg^{-1}K^{-1}$)
CTE	Coefficient of Thermal Expansion
D	Diameter, dimension (m)
E	Edge orientation
EHD	Electro-Hydro-Dynamic
ESA	European Space Agency
F	Force (N)
FCCL	Flexible Copper-Clad-Laminates

FPPHP	Flat Plate Pulsating Heat Pipe
FR	Feeling ratio (%)
Ga	Garimella number
g	gravity acceleration ($m.s^{-2}$)
h	Heat transfer coefficient ($W.m^{-2}K^{-1}$)
h	Latent heat ($J.kg^{-1}$)
h	height, thickness (m)
H	Horizontal
HTC	Heat transfer coefficient
J	Mass flux ($kg.s^{-1}m^{-2}$)
L	Length, dimension (m)
m	mass (kg)
M	Figure of Merit
N	Number of U-turns
P	Pressure (Pa)
PDMS	Polydimenthylsiloxane
PHP	Pulsating Heat Pipe
PIV	Particle Image Velocimetry
$\dot{q}$	Heat flux density (Wm^{-2})
$\dot{Q}$	Heat power (W)
r	Radius, radial coordinate (m)
R	Radius (m)
R	Thermal resistance ($K.W^{-1}$)
R	Specific gas constant ($J.K^{-1}kg^{-1}$)
Re	Reynolds number
S	Surface (m^2)
SRWF	Self-Rewetting Fluid
t	Thickness (m)

T	Temperature (°C)
THM	Top Heat Mode
TPHP	Tubular Pulsating Heat Pipe
TV	Tesla Valve
u,v,w	Velocities along x, y and z-axes, respectively (m s^{-1})
u,U	Velocity (m s^{-1})
UC	Ultrasonic consolidation
V	Volume (m^3)
w	Width (m)
We	Weber number
x,y,z	Cartesian coordinates (m)
Z	Compressibility factor

Greek symbols

γ	Ratio
δ	Liquid film thickness (m)
θ	Contact angle (°)
λ	Thermal conductivity ($W.m^{-1}K^{-1}$)
Λ	Poiseuille number
μ	Dynamic viscosity (Pa.s)
ρ	Density ($kg.m^{-3}$)
σ	Surface tension ($N.m^{-1}$)
τ	Shear stress (Pa)

Subscripts

II°	secondary cooling fluid
a	advancing
avg	average
c,cap	capillary
c	center /cavity/covering (plate)

cd	condenser
crit	critical
cryo	cryothermostat
d	diagonal
eff	effective
ev	evaporator
f	friction
H	heater
h	hydraulic
i	interface
l	liquid
l-s	liquid slug heat transfer
m	machined (plate)
min	minimum
n	nucleus
r	receding
ref	reference
res	residual
sat	saturation
sens	sensible (heat)
t	transverse
v	vapor
s	solid
th	thermal
theo	theoretical
turns	U-turns
w	wall
µg	microgravity

τ shear stress

References

[Abdollahi,20] A. Abdollahi, S-E. Norris, R-N. Sharma, Pressure drop and film thickness of liquid-liquid Taylor flow in square microchannels, *Int. J. heat Mass Tr.* 156 (2020) 119802.

[Alizadeh,20] H. Alizadeh, M-A. Nazari, R. Ghasempour, M-B. Shafii, A. Akbarzadeh, Numerical analysis of photovoltaic solar panel cooling by a Flat Plate closed-loop Pulsating Heat Pipe, *Solar En.* 206 (2020) 455-463.

[Ayel,14] V. Ayel, C. Romestant, Y. Bertin, V. Manno, S. Filippeschi, Visualization of flow patterns in flat plate Pulsating Heat Pipe: influence of hydraulic behavior on thermal performances, *Heat Pipe Sc. Tech.: an Int. J.* 5 (2014) 377-384.

[Ayel,15a] V. Ayel, L. Araneo, A. Scalambra, M. Mameli, C. Romestant, A. Piteau, M. Marengo, S. Filipeschi, Y. Bertin, Experimental study of a closed loop flat plate pulsating heat pipe under a varying gravity force, *Int. J. Th. Sc.* 96 (2015) 23-34.

[Ayel,15b] V. Ayel, R. Bertossi, B. Mehta, N. Chauris, C. Romestant, Y. Bertin, Evaporation of a thin liquid film in a heated capillary tube: experimental results and discussion on the related physical phenomena, *IX Minsk International Seminar "Heat Pipes, Heat Pumps, Refrigerators, Power Sources"*, Minsk, Belarus, Sept. 07-10, 2015, 8 p.

[Ayel,18] V. Ayel, L. Araneo, P. Marzorati, C. Romestant, Y. Bertin, M. Marengo, Visualization of flow patterns in closed loop flat plate pulsating heat pipe acting as hybrid thermosyphons under various gravity levels, *H. Tr. Eng.* 40 (2018) 1-10.

[Ayel,19] V. Ayel, L. Pietrasanta, G. Lalizel, C. Romestant, Y. Bertin, M. Marengo, Thermo-hydraulic analysis of semi-transparent flat plate Pulsating Heat Pipes tested in 1g and Microgravity conditions, *Micrograv. Sc. Tech.* 31 (2019) 403-415.

[Bae,17] J. Bae, S-Y. Lee, S-J. Kim, Numerical investigation of effect of film dynamics on fluid motion and thermal performances in Pulsating Heat Pipes, *En. Conv. Manag.* 151 (2017) 296-310.

[Bastakoti,18] D. Bastakoti, H. Zhang, D. Li, W. Cai, F. Li, An overview on the developing trend of Pulsating Heat Pipe and its performance, *Appl. Th. Eng.* 141 (2018) 305-332.

[Belfi,18] F. Belfi, F. Iorizzo, C. Galbiati, F. Lepore, Space structures with embedded Flate Plate Pulsating Heat Pipe built by Additive Manufacturing technology: development, test and performance analysis, *Joint 19th IHPC and 13th IHPS*, Pisa, Italy, June 10-14, 2018, 9 p.

[Betancur,20] L-A. Betancur-Arboleda, J-P. Florez-Mera, M. Mantelli, Experimental study of channel roughness effect in diffusion bonded Pulsating Heat Pipe, *Appl. Th. Eng.* 166 (2020) 114734.

[Borgmeyer,07]B. Borgmeyer, H-B. Ma, Experimental investigation of oscillating motions in a flat plate Pulsating Heat Pipe, *J. Thermophys. Heat Tr.* 21 (2007) 405-409.

[Boswell,15] J. Boswell, C. Smoot, E. Short, N. Francis, Circuit credit card assembly heat sinks embedded with oscillating Heat Pipes, *Elec. Cool.* (2015).

[Bretherton,61] F. Bretherton, The motion of long bubbles in tubes, *J. Fl. Mech.* 10 (1961) 166-188.

[Cecere,18] A. Cecere, D. De Cristofaro, R. Savino, V. Ayel, T. Solé-Agostinelli, M. Marengo, C. Romestant, Y. Bertin, *Acta Astronautica* 147 (2018) 454-461.

[Chao,13] C. Chao, W-K. Lin, T-Y. Hsiung, K-C. Liaw, M. Wang, Y-C. Yeh, H-C. Sheng, S-I. Chen, S-W. Chen, Performance tests of defrosting plates designed with a Pulsating Heat Pipe (PHP) as the heat carrier, *J. Enhanced Heat Tr.* 20 (2013) 527-541.

[Charoensawan,03] P. Chroensawan, S. Khandekar, M. Groll, P. Terdtoon, Closed loop Pulsating Heat Pipes – part A: parametric experimental investigations, *Appl. Th. Eng.* 23 (2003) 2009-2020.

[Chauris,15] N. Chauris, V. Ayel, Y. Bertin, C. Romestant, Evaporation of a liquid film deposited on a capillary heated tube: experimental analisis by infrared thermography of its thermal footprint, *Int. J. Heat Mass Tr.* 86 (2015) 492-507.

[Chauris,18] N. Chauris, V. Ayel, C. Louste, C. Romestant, Y. Bertin, Influence of Electrohydrodynamic pump on a Pulsating Heat Pipe, *Joint 19th IHPC and 13th IHPS*, Pisa, Italy, June 10-14, 2018, 9 p.

[Chauvet,10] F. Chauvet, S. Cazin, P. Duru, M. Prat, Use of infrared thermography for the study of evaporation in a square capillary tube, *Int. J. Heat Mass tr.* 53 (2010) 1808-1818.

[Chien,12] K-H. Chien, Y-T. Lin, Y-R. Chen, K-S. Yang, C-C. Wang, A novel design of pulsating heat pipe with fewer turns applicable to all orientations, *Int. J. Heat Mass Tr.* 55 (2012) 5722-5728.

[Der,18] O. Der, M. Marengo, V. Bertola, Thermal performances of Pulsating Heat Stripes (PHS) built with plastic materials, *Joint 19th IHPC and 13th IHPS*, Pisa, Italy, June 10-14, 2018, 7 p.

[Facin,18] A. Facin, L. Betancur, M. Mantelli, J-P. Florez, B-H. Coutinho, Influence of channel geometry on diffusion bonded flat plate Pulsating Heat Pipes, *Joint 19th IHPC and 13th IHPS*, Pisa, Italy, June 10-14, 2018, 9 p.

[Fumoto,09] K. Fumoto, M. kawaji, Performance improvement in Pulsating Heat Pipes using a self-rewetting fluid, *Heat Tr. Summer Conf.*, San Francisco, California, USA, July 19-23, 2009, 7 p.

[Gatapova,19] E-Ya Gatapova, S. Khandekar, Spatial temperature distribution of an open square capillary tube wall during passage of a Taylor liquid plug, J. Phys.: Conf. Series 1369 (2019) 5 p.

[Gu,04] J. Gu, M. Kawaji, R. Futamata, Effects of gravity on the performances of Pulsating Heat Pipes, *J. Thermophys. Heat Tr.* 18 (2004) 370-378.

[Gu,05] J. Gu, M. Kawaji, R. Futamata, Microgravity performance of micro Pulsating Heat Pipes, *Microg. Sc. Tech.* 16 (2005) 181-185.

[Gully,15] P. Gully, F. Bonnet, V. Nikolayev, N. Luchier, T-Q. Tran, Evaluation of the vapor thermodynamic state in PHP, *17th Int. Heat Pipe Conf. (IHPC)*, Kanpur, India, Oct. 13-17, 2013, 369-376.

[Guowei,10] Novel heat pipe radiator for vertical CPU cooling and its experimental study, *Int. J. Heat Mass Tr.* 130 (2019) 912-922.

[Gurumurthy,18] V-T. Gurumurthy, D. Rettenmaier, I-V. Roisman, C. Tropea, Computations of spontaneous rise of a rivulet in a corner of a vertical square, *Coll. Surf. A* 544 (2018) 118-126.

[Han,09] Y. Han, N. Shikazono, Measurement of liquid film thickness in micro square channel, *Int. J. Multiph. Flow* 35 (2009) 896-903.

[Hao,14a] T. Hao, X. Ma, Z. Lan, N. Li, Y. Zhao, Effect of hydrophilic surface on heat transfer performance and oscillating motion of an Oscillating Heat Pipe, *Int. J. Heat Mass Tr.* 72 (2010) 50-65.

[Hao,14b] T. Hao, X. Ma, Z. Lan, N. Li, Y. Zhao, Effects of superhydrophobic and superhydrophilic surfaces on heat transfer and oscillating motion of an Oscillating Heat Pipe, *J. Heat Tr.* 136 (2014) 1-13.

[Harichian,10] T. Harichian, S. Garimella, A comprehensive flow regime map for micro- channel flow boiling with quantitative transition criteria, *Int. J. Heat Mass Transf.* 53 (2010) 694-702.

[Hideyama,18] F. Hideyama, M. Kawaji, Y. Koito, T. Tomimura, Experimental investigation of a Pulsating Heat Pipe fabricated by a 3-D printer, *Joint 19th IHPC and 13th IHPS*, Pisa, Italy, June 10-14, 2018, 5 p.

[Howel,67] J-R. Howel, R. Siegel, Activation, growth, and detachment of boiling bubbles in water from artificial nucleation sites of known geometry and size, NASA-TN-D-4101. NASA, 1967.

[Ibrahim,17] O-M. Ibrahim, J.G. Monroe, S-M. Thompson, N. Shamsaei, H. Bilheux, A. Elwany, L. Bian, An investigation of a multi-layered Oscillating Heat Pipe additively manufactured from Ti-6Al-4V powder, *Int. J. Heat Mass Tr.* 108 (2017) 1063-1047.

[Jang,19] D-S. Jang, D. Kim, S-H. Hong, Y. Kim, Comparative thermal performance evaluation between ultrathin flat plate pulsating heat pipe and graphite sheet for mobile electronic devices at various operating conditions, *Appl. Th. Eng.* 149 (2019) 1427-1434.

[Jo,19] J. Jo, J. Kim, S-J. Kim, Experimental investigations of heat transfer mechanisms of a Pulsating Heat Pipe, *En. Conv. Manag.* 181 (2019) 331-341.

[Jun,16] S. Jun, S-J. Kim, Comparison of the thermal performances and flow characteristics between closed-loop and closed-end micro Pulsating Heat Pipes, *Int. J. Heat Mass Tr.* 95 (2016) 890-901.

[Jun,18] S. Jun, S-J. Kim, Experimental study on thermal characteristics of Pulsating Heat Pipes, *Joint 19th IHPC*

and 13th IHPS, Pisa, Italy, June 10-14, 2018, 6 p.

[Jung,20] C. Jung, J. Lim, S-J. Kim, Fabrication and evaluation of a high-performance flexible Pulsating Heat Pipe hermetically sealed with metal, *Int. J. Heat Mass Tr.* 149 (2020) 119180.

[Jung,21] C. Jung, S-J. Kim, Effects of oscillation amplitudes on heat transfer mechanisms of Pulsating Heat Pipes, *Int. J. Heat Mass Tr.* 165 (2021) 120642.

[Kamijima,20] C. Kamijima, Y. Yoshimoto, Y. Abe, S. Takagi, I. Kinefuchi, Relating the thermal properties of a micro Pulsating Heat Pipe to the internal flow characteristics via experiments, image recognition of flow patterns and heat transfer simulation, *Int. J. Heat Mass Tr.* 163 (2020) 120415.

[Kandlikar,02] S-G. Kandlikar, Fundamental issues related to flow boiling in minichannels and microchannels, *Exp. Th. Fl. Sc.* 26 (2002) 389-407.

[Kearney,14] D. Kearney, J. Griffin, An open loop Pulsating Heat Pipe for integrated electronic cooling applications, *J. Heat Tr.* 136 (2014) 1-7.

[Kearney,16] D. Kearney, O. Suleman, J. Griffin, G. Mavrakis, Thermal performances of a PCB embedded Pulsating Heat Pipe for power electronics applications, *Appl. Th. Eng.* 98 (2016) 798-809.

[Khandekar,02] S. Khandekar, M. Schneider, P. Schäfer, R. Kulenovic, M. Groll, Thermofluid dynamic study of flat-plate cosed-loop Pulsating Heat Pipes, *Microsc. Thermophys. Eng.* 6 (2002) 303-317.

[Khandekar,04] S. Khandekar, M. Groll, P. Chaorensawan, S. Rittidech, P. Terdtoon, Closed and open loop Pulsating Heat Pipes, *13th Int. Heat Pipe Conf. (IHPC)*, Shangai, China, 2004, 36-49.

[Khandekar,10] S. Khandekar, P-K. Panighahi, F. Lefèvre, J. Bonjour, Local hydrodynamic of flow in a Pulsating Heat Pipe: a review, *Fr. Heat Pipes* 1 (2010) 1-20.

[Khodaparast,18] S. Khodaparast, O. Atasi, A. Deblais, B. Scheid, H-A. Stone, Dewetting of thin liquid films surrounding long bubbles in microchannels, *Langmuir* 34 (2018) 1363-1370.

[Kim,03a] J-S. Kim, N-H Bui, J-W. Kim, H. Jung, Flow visualization of oscillation characteristics of liquid and vapor flow in the oscillating capillary tube heat pipe, *KSME Int. J.*. 17 (2003) 1507-1519.

[Kim,03b] J-S. Kim, N-H Bui, H-S. Jung, W-H. Lee, The study on pressure oscillation and heat transfer characteristics of oscillating capillary tube heat pipe, *KSME Int. J.*. 17 (2003) 1533-1542.

[Kim,20] J. Kim, S.J. Kim, Experimental investigation on working fluid selection in a micro Pulsating Heat Pipe, *En. Conv. Man.* 205 (2020) 112462.

[Laun,14] F-F. Laun, B-S. Taft, Experimental investigation of in situ pressure measurement of an oscillating heat pipe, Fr. Heat Pipes 5 (2014) 5 p.

[Laun,15] F-F. Laun, H. Lu, H-B. Ma, An experimental investigation of an Oscillating Heat Pipe heat spreader, *J. Therm. Sci. Eng. Appl.* 7 (2015) 1-5.

[Lee,16] J. Lee, S-J. Kim, Experimental investigation on silicon-based Pulsating Heat Pipes with different channel geometries, *Joint 18th IHPC and 12th IHPS*, Jeju, Korea, June 12-16, 2018, 501-506.

[Lee,17] J. Lee, S-J. Kim, Effect of channel geometry on the operating limit of micro Pulsating Heat Pipes, *Int. J. Heat Mass Tr.* 107 (2017) 201-212.

[Lee,18] J. Lee, Y. Joo, S-J. Kim, Effects of the number of turns and the inclination angle no the operating limit of micro Pulsating Heat Pipes, *Int. J. Heat Mass Tr.* 124 (2018) 1172-1180.

[Li,13] Z. Li, L. Jia, Experimental study on natural convection cooling of LED using a flat-plate Pulsating Heat Pipe, *Heat Tr. Res.* 44 (2013) 133-144.

[Lim,18] J. Lim, S-Y. Kim, Effect of a channel layout on the thermal performance of Pulsating Heat Pipe under local heating condition, *Int. Heat Transf. Conf. 16*, Beijing, China, August 10-15, 2018, p. 4905-4910.

[Lim,19] J. Lim, S-Y. Kim, Effect of a channel layout on the thermal performance of a Flat Plate Micro Pulsating Heat Pipe under the local heating condition, *Int. J. Heat Mass Tr.* 137 (2019) 1232-1240.

[Lin,08] Y-H Lin, K-T Chen, P-H Cheng, S-W Kang, Fabrication of PCP Pulsating Heat Pipe, *9th Int. Heat Pipe Symp.*, Kuala Lumpur, Malaysia, 2008, 5 p.

[Lin,09] Y-H Lin, S-W Kang, T-Y Wu, Fabrication of polymethylsiloxane (PDMS) Pulsating Heat Pipe, *Appl. Th. Eng.* 29 (2009) 573-580.

[Ma,15] H. Ma, Oscillating heat pipes, Springer-Verlag, New York, 2015, 427 p.

[Magnini,20] M. Magnini, O-K. Matar, Morphology of long gas bubbles propagating in square capillaries, *Int. J. Multiph. Flow* 129 (2010) 103353.

[Majumber,13] A. Majumber, B. Mehta, S. Khandekar, Local Nusselt number enhancement during gas-liquid bubble flow in a square mini-channel: an experimental study, *Int. J. Th. Sc.* 66 (2013) 8-18. 17Esamés?24

[Mameli,19] M. Mameli, A. Catarsi, D. Mangini, L. Pietrasanta, N. Miché, M. Marengo, P. Di Marco, S. Filippeschi, Start-up in microgravity and local thermodynamic states of a hybrid loop thermosyphon/Pulsatin Heat Pipe, *Appl. Th. Eng.* 158 (2019) 113771.

[Mangini,15] D. Mangini, M. Mameli, A. Georgoulas, L. Araneo, S. Filippeschi, M. Marengo, A Pulsating Heat Pipe for space applications: Ground and microgravity experiments, *Int. J. Th. Sc.* 95 (2015) 53-63.

[Mangini,17] D. Mangini, M. Mameli, D. Fioriti, S. Filippeschi, L. Araneo, M. Marengo, Hybrid Pulsating Heat Pipe for space applications with non-uniform heating patterns: Ground and microgravity experiments, *Appl. Th. Eng.* 126 (2017) 1029-1043.

[Manno,15] V. Manno, S. Filippeschi, M. Mameli, C. Romestant, V. Ayel, Y. Bertin, Thermal-hydraulic characterization of a Flat Plate Pulsating Heat Pipe for automotive applications, *Interfac. Phen. H. Tr.* 3 (2015) 413-425.

[Marengo,18] M. Marengo, V. Nikolayev, Pulsating Heat Pipes: Experimental Analysis, Design and Applications, In: *Encyclopedia of Two-Phase Heat Transfer and Flow IV*, Thome, J. R. (ed.), vol. 1: Modeling of Two-Phase Flows and Heat Transfer, World Scientific, 2018, 1-62.

[Markal,20a] B. Markal, K. Aksoy, The combined effects of filling ratio and inclination angle on thermal performance of a closed loop pulsating heat pipe, *Heat Mass Tr.* 114 (2020) 1-13.

[Markal,20b] B. Markal, R. Varol, Thermal investigation and flow pattern analysis of a closed-loop pulsating heat pipe with binary mixtures, *J. Braz. Soc. Mech. Sc. Eng.* 42 (2020) 1-18.

[Mehta,14] B. Mehta, S. Khandekar, Taylor bubble-train flows and heat transfer in the context of Pulsating Heat Pipes, *Int. J. Heat Mass Tr.* 79 (2014) 279-290.

[Mehta,16] K. Mehta, S. Mehta, Development of Flat Plate Oscillating Heat Pipe as a heat transfer device, *Fr. Heat Pipes* 7 (2016) 1-7.

[Mehta,20] K. Mehta, Experimental investigations of Flat Plate Oscillating Heat Pipe, PhD thesis, Gujarat Technological University Ahmedabad, Nov. 2020, 180 p.

[Miyazaki,99] Y. Miyazaki, M. Arikawa, Oscillatory flow in the Oscillating Heat Pipe, *11th Int. Heat Pipe Conf. (IHPC)*, Tokyo, Japan, 1999, 367-372.

[Natsume,13] K. Natsume, T. Mito, N. Yagani, H. Tamura, Development of a flat-plate cryogenic oscillating heat pipe for improving HTS magnet cooling, *Phys. Proc.* 45 (2013) 233-236.

[Nikolayev,18] V. Nikolayev, M. Marengo, Pulsating Heat Pipes: Basics of Functioning and Numerical Modeling, In: *Encyclopedia of Two-Phase Heat Transfer and Flow IV*, Thome, J. R. (ed.), vol. 1: Modeling of Two-Phase Flows and Heat Transfer, World Scientific, 2018, 63-139.

[Noh,20] H-Y. Noh, S-J. Kim, Numerical simulation of Pulsating Heat Pipes: Parametric investigation and thermal optimization, *En. Conv. Manag.* 203 (2020) 112237.

[Pagnoni,18a] F. Pagnoni, V. Ayel, E. Scoletta, Y. Bertin, Effects of the hydrostatic pressure gradient no thermohydraulic behavior of flat plate Pulsating Heat Pipe: experimental and numerical analyses, *16th Int. Heat Tr. Conf., IHTC-16*, Beijing, China, August 10-15, 2018, 8 p.

[Pagnoni,18b] F. Pagnoni, V. Ayel, C. Romestant, Y. Bertin, Experimental Behaviors of Closed Loop Flat Plate Pulsating Heat Pipes: a Parametric Study, *Joint 19th IHPC and 13th IHPS*, Pisa, Italy, June 10-14, 2018, 8 p.

[Qu,07a] W. Qu, H-B. Ma, Theoretical analysis of startup of a Pulsating Heat Pipe, *Int. J. Heat Mass. Tr.* 50 (2007) 2309-2316.

[Qu,07b] W. Qu, Y. Zhou, Y. Li, T. Ma, Experimental study on mini Pulsating Heat Pipe with square and regular

triangle capillaries, *14th Int. Heat Pipe Conf. (IHPC)*, Florianopolis, Brazil, April 22-27, 2007.

[Qu,10] J. Qu, H. Wu, Flow visualization of silicon-based micro Pulsating Heat Pipes, Sc. China Tech. Sc. 52 (2010) 984-990.

[Qu,12] J. Qu, H. Wu, P. Cheng, Start-up, heat transfer and flow characteristics of silicon-based micro Pulsating Heat Pipes, *Int. J. Heat Mass Tr.* 55 (2012) 6109-6120.

[Rahatgahonkar,18] A-M. Rahatgahonkar, V. Srivasan, S. Khandekar, Ocillations of a completely wetting isolated liquid plug in a square capillary tube, *Joint 19th IHPC and 13th IHPS*, Pisa, Italy, June 10-14, 2018, 7 p.

[Rana,14] G-R. Rana, B-S. Sikarwar, S. Khandekar, P-K. Panigrahi, Hydrodynamics of a confined meniscus in a square capillary tube at low capillary numbers, *Fr. Heat Pipes* 7 (2014) 1-12.

[Rittidech,07] S. Rittidech, N. Pipatpaiboon, P. Terdtoon, Heat-transfer characteristics of closed-loop Oscillating Heat Pipe with check valves, *Appl. En.* 84 (2007) 565-577.

[Rothstein,10] J-P. Rothstein, Slip on superhydrophobic surfaces, *Ann. Rev. Fl. Mech.* 42 (2010) 89-109.

[Sedighi,18] E. Sedighi, A. Amarloo, B. Shafii, Numerical and experimental investigation of flat-plate Pulsating Heat Pipe with extra branches in the evaporator section, *Int. J. Heat Mass Tr.* 126 (2018) 431-441.

[Sefiane,20] K. Sefiane, X. Yu, G. Duursma, J. Xu, On heat and mass transfer using evaporating self-rewetting mixtures in microchannels, *Appl. Th. Eng.* 179 (2020) 115662.

[Senjaya,13] R. Senjaya, T. Inoue, Oscillating heat pipe simulation considering bubble generation Part I: Presentation of the model and effects of a bubble generation, *Int. J. Heat Mass Tr.* 60 (2013) 816-824.

[Shafii,01] M-B. Shafii, A. Faghri, Y-W. Zhang, thermal modeling of unlooped and looped Pulsating Heat Pipes, *J. Heat Tr.* 123 (2001) 1159-1172.

[Shi,16] W-X. Shi, L-S. Pan, Experiment investigation on visualization and operating characteristics of closed loop plate Oscillating Heat Pipe with parallel channels, *J. Cent. South Univ.* 23 (2016) 2410-2418.

[Shi,17] W-X. Shi, L-S. Pan, Influence of filling ratio and working fluid thermal properties on starting up and heat transferring performance of closed loop plate Oscillating Heat Pipe with parallel channels, *J. Th. Sc.* 26 (2017) 73-81.

[Slobodeniuk,20] M. Slobodeniuk, F. Martineau, V. Ayel, R. Bertossi, C. Romestant, Y. Bertin, Thermal performance of flat plate Pulsating Heat Pipe using aqueous alcohol solutions, 28th *Conf. Soc. Fr. Therm. (SFT)*, Belfort, France, June 9-12, 2020, 8 p.

[Smoot,11] C-D. Smoot, H-B. Ma, An experimental investigation of hybrid Oscillating Heat Pipe, *Fr. Heat Pipes* 2 (2011) 1-6.

[Srinivasan,17] V. Srinivasan, S. Kumar, M. Asfer, S. Khandekar, Oscillation of an isolated liquid plug inside a dry capillary, *Heat Mass Tr.* 53 (20177) 3353-3362.

[Taft,15] B. Taft, F. Laun, S. Smith, Microgravity performance of a structurally embedded Oscillating Heat Pipe, *J. Thermophysics Heat Tr.* 29 (2015) 329-337.

[Taft,19] B. Taft, K. Irick, ASETS-II Oscillating Heat Pipe space flight experiment: the first six months on orbit, *Fr. Heat Mass Tr.* 12 (2019) 1-7.

[Taha,06] T. Taha, Z-F. Cui, CFD modelling of slug flow inside square capillaries, *Chem. Eng. Sc.* 61 (2006) 665-576.

[Takawale,19] A. Takawale, S. Abraham, A. Sielaff, P-S. Mahapatra, A. Pattamatta, P. Stephan, A comparative study of flow regimes and thermal performance between flat plate Pulsating Heat Pipe and capillary tube Pulsating Heat Pipe, *Appl. Th. Eng.* 149 (2019) 613-624.

[Thermavant,21] https://www.thermavant.com/oscillating-heat-pipes

[Thompson,09] S-M. Thompson, H-B. Ma, R-A. Winholtz, C. Wilson, Experimental investigation of miniature three-dimensional Flat-Plate Oscillating Heat Pipe, *J. Heat Tr.* 131 (2009) 1-9.

[Thompson,11a] S-M. Thompson, P. Cheng, H-B. Ma, An experimental investigation of a three-dimensional Flat-Plate Pulsating Heat Pipe with staggered microchannels, *Int. J. Heat Mass Tr.* 54 (2011) 3951-3959.

[Thompson,11b] S-M. Thompson, H-B. Ma, C. Wilson, Investigation of a flat-plate Oscillating Heat Pipe with Tesla-type check valves, *Exp. Th. Fl. Sc.* 35 (2011) 1265-1273.

[Thompson,11c] S-M. Thompson, H-B. Ma, A statistical analysis of temperature oscillations on a flat-plate Oscillating Heat Pipe with Tesla-type check valves, *Fr. Heat Pipes* 2 (2011) 1-8.

[Winkler,20] M. Winkler, D. Rapp, A. Mahlke, F. Zunftmeister, M. Vergez, E. Wischerhoff, J. Clade, K. Bartholomé, O. Schafer-Welsen, Small-sized Pulsating Heat Pipes/Oscillating Heat Pipes with low thermal resistance and high heat transport capability, Energies 13 (2020) 1713.

[Wits,18] W-W. Wits, G. Groeneveld, H-J. Van Gerner, Experimental investigation of a flat-plate closed-loop Pulsating Heat Pipe, *Joint 19th IHPC and 13th IHPS*, Pisa, Italy, June 10-14, 2018, 7 p.

[Wu,16] Q. Wu, R. Xu, R. Wang, Y. Li, Effect of C60 nanofluid on the thermal performance of a flat-plate Pulsating Heat Pipe, *Int. J. Heat Mass. Tr.* 100 (2016) 892-989.

[Wu,19] Z. Wu, Z. Cao, B. Sunden, Flow patterns and slug scaling of liquid-liquid flow in square microchannels, *Int. J. Multiph. Fl.* 112 (2019) 27-39.

[Yamagami,16] K. Yamagami, K. Fumoto, R. Savino, T. Kawanami, T. Inamura, Heat transfer characteristics of flat plate Pulsating Heat Pipe using self-rewetting fluids, *Joint 19th IHPC and 13th IHPS*, Pisa, Italy, June 10-14, 2018, 8 p.

[Yang,09] H. Yang, S. Khandekar, M. Groll, Performance characteristics of Pulsating Heat Pipes as integral thermal spreaders, *Int. J. Th. Sc.* 48 (2009) 815–824.

[Yang,15a] K-S. Yang, Y-C. Cheng, M-S. Jeng, K-H. Chien, J-C. Shyu, Fabrication and visualization of a micro Pulsating Heat Pipe, *Int. Heat Transf. Conf. 15*, Kyoto, Japan, August 10-15, 2014, p. 5665-5676.

[Yang,15b] K-S. Yang, Y-C. Cheng, M-C. Liu, J-C. Shyu, Micro Pulsating Heat Pipe with alternate microchannels widths, *Appl. Th. Eng.* 83 (2015) 131-138.

[Yoon,17] A. Yoon, S-J. Kim, Characteristics of oscillating flow in a micro Pulsating Heat Pipe: Fundamental-mode oscillation, *Int. J. Heat Mass Tr.* 109 (2017) 242-253.

[Yoon,18] A. Yoon, S-J. Kim, Understanding of the therms-hydrodynamic coupling in a micro Pulsating Heat Pipe, *Int. J. Heat Mass Tr.* 127 (2018) 1004-1013.

[Youn,18] Y-J. Youn, Y. Han, N. Shikazono, Liquid film thickness of oscillating slug flows in a capillary tube, *Int. J. Heat Mass Tr.* 124 (2018) 542-551.

[Zabek,16] D. Zabek, J. Taylor, V. Ayel, Y. Bertin, C. Romestant, C-R. Bowen, A novel pyroelectric generator utilizing naturally driven temperature fluctuations from oscillating heat pipes for waste heat recovery and thermal energy harvesting, *J. Appl. Phys.* 120 (2016) 1-8.

[Zhang,04] X. Zhang, Experimental study of a Pulsating Heat Pipe using FC-72, ethanol and water as working fluids, *Exp. H. Tr.: a J. of Th. En. Gen.* 17 (2004) 47-67.

[Zhang,08] Y. Zhang, A. Faghri, Advances and unsolved issues in Pulsating Heat Pipes, *Heat Tr. Eng.* 29 (2008) 20-44.

Appendices

A.1 Quantitative comparison of FPPHPs effective thermal conductivities

In this appendix, a synthesis was carried out on the thermal performances achieved by most authors based on the data available in the literature. It is important to specify that only the papers with complete information on the geometrical features described in figure A.1-1 concerning operating conditions (orientation, heat input or heat power, cooling fluid temperature) and experimental results (effective thermal conductivity, thermal resistance or evaporator and condenser temperatures) were selected. They are indicated in the reference column of table A1 (appendix A.2) by the asterisks*, for the classically sized FPPHPs, and **, for the micro-FPPHPs. Two orientations were chosen: horizontal and vertical BHM, and a selection of three values of thermal conductivities were extrapolated from each paper, for each orientation and for the overall heat power range.

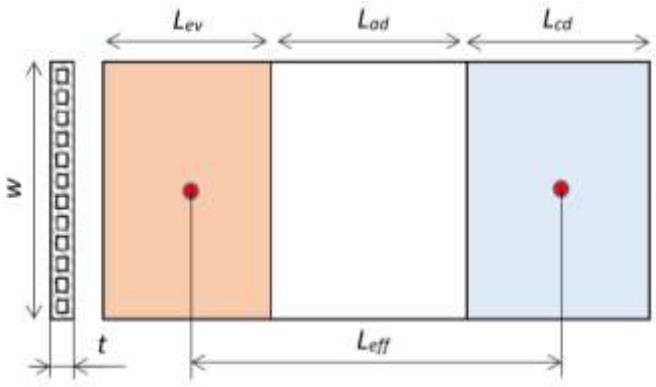

Figure A.1-1: Simplified scheme of FPPHP geometrical parameters used for the comparative analysis

On the basis of the definition of the thermal conductivity λ_{eff} presented in section 3, the same parameters have been used for all papers, the objective being to make the most accurate and fair comparison possible. First, only 1-layer channels FPPHPs, with the evaporator and condenser zones placed at both ends of the device, were considered. In the effective thermal conductivity equation below (A-1), L_{eff} is defined as the effective length of the device, according to the equation widely used for heat pipe systems ($L_{eff} = L_{ad} + (L_{ev} + L_{cd})/2$); $\dot{Q}$ is the heat input; $\overline{T}_{ev}$ and $\overline{T}_{cd}$ are, respectively, the evaporator and condenser outer wall temperatures, averaged in space and time; A_t is the transverse cross-section of the FPPHP, defined as the overall section ($A_t = w.t$), taking into account both solid and fluid channel areas.

$$\lambda_{eff} = \frac{\dot{Q}}{A_t} \frac{L_{eff}}{(\overline{T}_{ev} - \overline{T}_{cd})} = \frac{L_{eff}}{A_t R_{th}} \quad \text{(A-1)}$$

The first curve which may be presented concerns the overall effective thermal conductivities plotted as functions of the heat flux $\dot{q}_{ev}$ ($\dot{q}_{ev} = \dot{Q}/A_{ev}$, with $A_{ev} = L_{ev}.w$). A choice was made for $\dot{q}_{ev}$ to be calculated with regard to the evaporator plate area A_{ev}, instead of the channel walls-to-fluid area. Indeed, it is certain that the

heat flux passes through A_{ev}, whereas the wall-to-fluid area is not precisely defined; longitudinal heat conduction through the solid substrate leads to a greater length of the zone, which cannot be preliminarily defined. The set of values of λ_{eff} as functions of $\dot{q}_{ev}$ is shown in figure A.1-2, distinguishing the orientation and the size of the FPPHP (micro or not), and using a logarithmic scale for the *y*-axis. If the overall trend shows increasing values of λ_{eff} with increasing heat flux, it is clear that the values are pronouncedly dispersed, ranging from around 72 $W.m^{-1}K^{-1}$ for the lowest [Yang,15] (micro-FPPHP, vertical BHM) up to $11x10^3$ $W.m^{-1}K^{-1}$ for the highest [Winkler,20] (vertical BHM). A distinction can be drawn between micro-FPPHPs *vs.* classical ones, and horizontal *vs.* vertical BHM positions. Generally speaking, higher values are obtained in vertical BHM than in horizontal orientation (for both types of FPPHPs), and also the micro-FPPHPs mean effective thermal conductivities (mean value in BHM: 370 $W.m^{-1}K^{-1}$) are about one order of magnitude lower than those of classical devices (mean value in BHM: 2300 $W.m^{-1}K^{-1}$). The difference can be attributed to the effective length of these devices, which is used in the definition of λ_{eff}, is also around one order of magnitude lower than for classical FPPHPs.

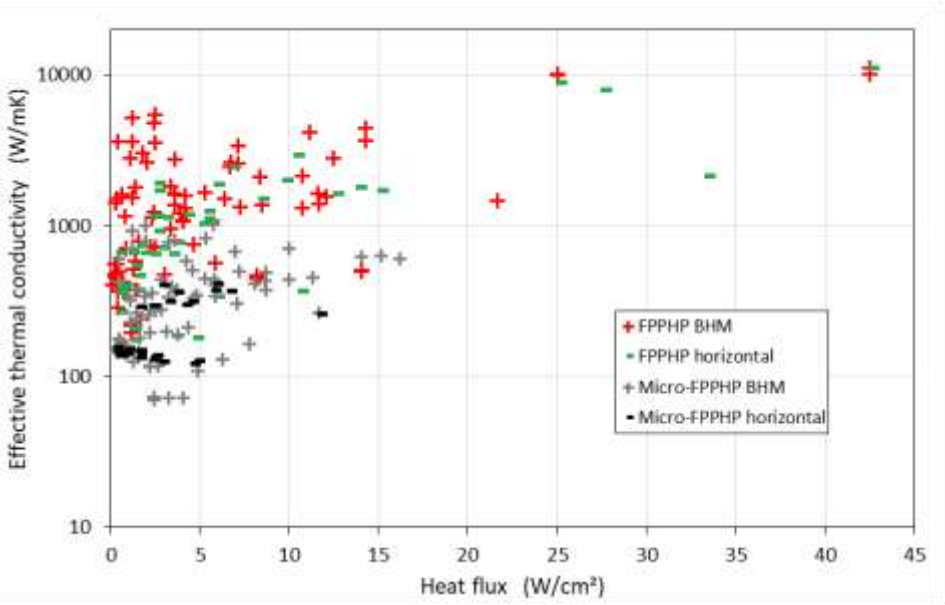

Figure A.1-2: Comparison of effective thermal conductivities *vs.* heat flux from the literature[*,**]

Attempts can be made to plot trends of effective thermal conductivities as functions of Merit numbers from the literature. For example, from the expression of the thermal resistance of Kim and Kim [Kim,20], the right-hand term of Eq. (17) (section 3.3) corresponding to the so-called residual term, depends largely on the FPPHP geometry:

$$R_{th} \approx [\mathrm{M}_{PHP}]^{-1} 16 \gamma_{sens} \left(\frac{L_s}{SD_h^2 (T_{sat,r} - T_{sat,a})} \right) \quad \text{(A-2)}$$

If one considers that the motor term for evaporation in vapor bubbles is directly proportional to the heat flux at the evaporator (replacing $(T_{sat,r} - T_{sat,a})$), that the liquid slug length L_s is of the order of magnitude

of the effective length L_{eff}, and the section S is proportional to D_h^2, another kind of Figure of Merit (named "residual" from the terminology of Kim and Kim [Kim,20] when designating the right hand side of Eq. [A-2]) could be extracted from the operating condition ($\dot{q}_{ev}$) and the geometrical parameters (L_{eff} and D_h):

$$M_{res} = \frac{\dot{q}_{ev} D_h^4}{L_{eff}} \tag{A-3}$$

Finally, from the numerical study of Noh and Kim [Noh,20], the authors found a Merit number for optimum number of turns of a PHP under the constraint of fixed space. Their results indicated that D^2N can be used as the Merit number designing a PHP when other variables except channel diameter and number of turns are fixed. In the literature, all other parameters obviously vary from one case to the other, which makes comparison particularly difficult. Nevertheless, on the basis of the two proposed numbers, Figure A.1-3a shows the evolution of λ_{eff} from the literature as function of M_{res} calculated for all studies (referenced by * and ** in table A1). Because the theoretical analysis leading to Eq. (A-2) and (A-3) is based on pure slug flow pattern, classical FPPHPs tested in vertical BHM have not been plotted insofar as they may operate under annular flow pattern. Except for the horizontal micro-FPPHPs, of which the evolution does not seem linked to this parameter, an overall increase of the values of λ_{eff} from the literature is noticeable, particularly for the largest FPPHPs. On the other hand, figure A.1-3b shows the evolution of λ_{eff} as function of the Merit number D^2N from [Noh,20]. With this number, the results seem more dispersed, and the increasing trend is barely distinguishable. However, it allows for a fairly clear distinction between what have been defined as "micro-FPPHPs" and classical FPPHPs, and seems to justify such a distinction.

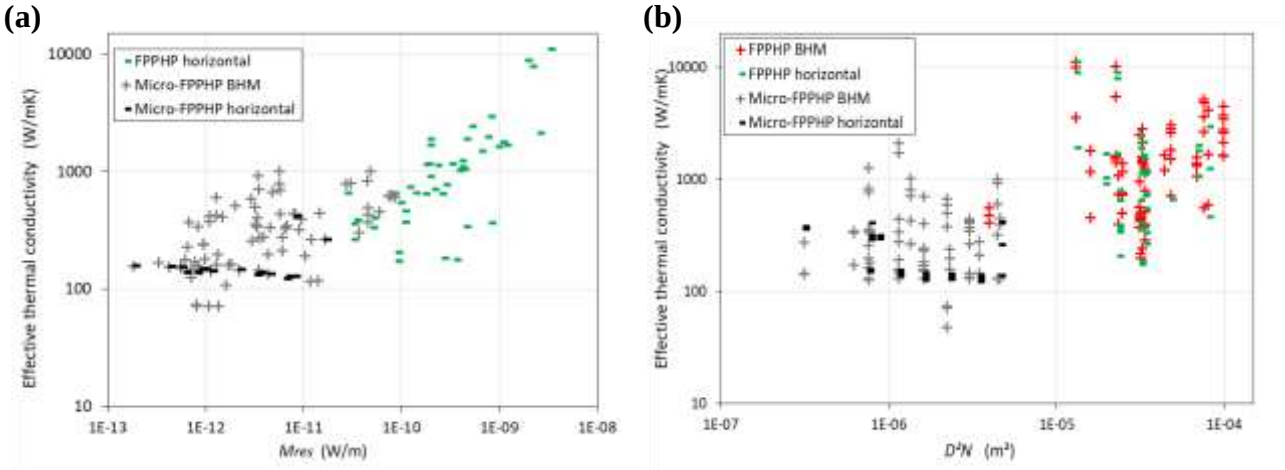

Figure A.1-3: Comparison of effective thermal conductivities from the literature[*,**] as functions of (a) M_{res}; and (b) D^2N.

Lastly, an interesting trend has been highlighted in figure A.1-4: the effective thermal conductivities of micro-FPPHPs have been plotted as functions of the ratio between channel hydraulic diameters D_h and the capillary length, L_{cap}, calculated thanks to the fluid thermophysical properties ($L_{cap} = \sqrt{\sigma/(\rho_l - \rho_v)g}$). Interestingly, this ratio does not exceed unity in the literature range for such kind of FPPHPs. Nevertheless, it

appears that the disparity of effective thermal conductivity values strongly increases with increasing ratio. This confirms the idea that increasing the channel diameter enhances the thermal performances of FPPHPs as soon as this diameter is not above a critical value, not exceeded in the case of micro-FPPHPs.

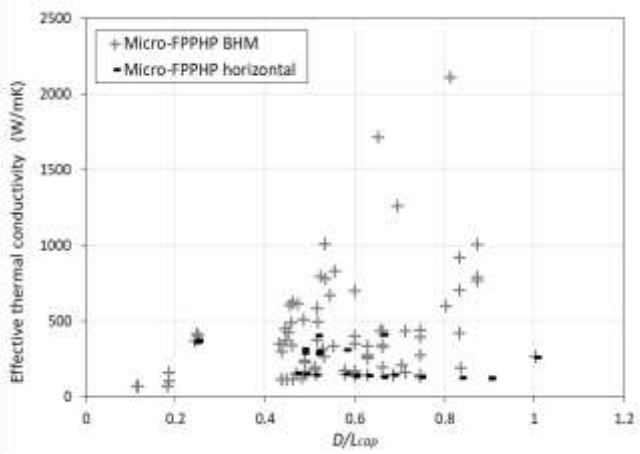

Figure A.1-4: Effective thermal conductivities of Micro-FPPHPs from the literature[*,**] as functions of the ratio D_h/L_{cap}.

A.2 Table A1. FPPHPs material, geometrical characteristics and experimental operating conditions

	Material / geometry				Operating conditions					
	Material	**Overall dimensions**	**Evap. / cond. lengths**	**Channels**	**Fluids**	**Filling ratio**	**Heat power applied**	**Cooling system**	***T sat°***	**Orientation / gravity field**
Reference	machined plate / covering plate	*wxLx(t m+t c)* (mm3) Visu. (Y/N)	*L ev* (mm) *L cd* (mm)	*N* Shape *D (mm) / axb* (mm²)		%	(W) or (W/cm²)	fluid / cooling block		
[Ayel,14]*	copper / borosilicate	125x265x(5+5) Y	45 67	12 square 2x2	ethanol	50	0-100 W	water / copper block	20°C	BHM / H / E
[Ayel,15a]*	copper	120x200x3 N	10 120	12 rectangular 1.6x1.7	FC-72	50	0-180 W	air / aluminum heat sink	≈ 22°C	BHM / H / µg
[Ayel,18]*	copper / borosilicate	124x204x(2.5+5) Y	10 160	11 square 2.5x2.5	FC-72	50	0-150 W	air / aluminum heat sink	≈ 22°C	BHM / H / µg
[Ayel,19]*	copper / borosilicate	(118-140) x204x(2.5+5) Y	10 100	11 square 1.5x1.5-3x3	FC-72	50	0-200 W	water / copper block	≈ 25°C	BHM / µg
[Betancur,20]*	copper	150x208 x(2.5+2.5) N	40 82	5 circular 2.5	water	10-75	20-350 W	water / aluminum block	20°C	BHM / H
[Borgmeyer,07]	copper / glass	76.2x76.2x(2.54+?) Y	15 2x15	2x14 square 1.59x1.59	water ethanol Flutec PP2 fluoroinert	50 80	0-160 W	water / aluminum block	20°C	BHM / H
[Cecere,18]*	copper / borosilicate	140x210x(2.5+5) Y	10 100	11 square 3x3	water water / 4% butan-2-ol	50	0-200 W	water / copper block	≈ 25°C	BHM / µg
[Chauris,18]*	copper	80x200x(1.5+1) N	10 100	16 square 1.1x1.1	HFE-7200	50	20-120 W	water / copper block	30-40°C	H / -5°
[Chien,12]*	copper / glass	57x122x5.5 Y	15 39	8 square/rect 2x2 / 1-2x2	water	40 50 60 70	0-100 W	water / cold plate	?	BHM / 60° / 30° / H
[Der,18]	polymer	98x250x1.5 Y	?	3 Rectangular 9x0.7	FC-72	48	0-32 W	air	?	bended BHM / H
[Facin,18]*	copper	150x210x? N	40 80	5 circ./square 2.5 / 2.5x2.5	water	40 50 60	20-400 W	water / aluminum block	20-40°C	BHM / H
[Fumoto,09]	aluminum	25x145x2 N	50 50	6 square 1.26x1.26	water water / 0.1-1% butan-1-ol	20 30 40 50	0-140 W	air / aluminum heat sink	22-25°C	BHM
[Gu,05]	aluminum	250x60x2 N	28 ?	48 square 1x1	R-134a	50	1.4-5.9 W	air / aluminum heat sink	?	vertical
[Hao,09a] [Hao,09b]	copper / polycarbonate	?x106x? Y	28 36	6 square 2x2	water	54.4	30-320 W	water / cold plate	5-25°C	BHM
[Hideyama,18]	ABS	34x160x? Y	25 25	7 square 1.3x1.3	HFE-7000	50	4-7 W	water / cold plate	4°C	BHM
[Ibrahim,17]	titanium	38.1x50.8x15.75 N	25.4 25.4	4x4 layers circular 1.52	acetone water n-pentane Novec 7200	80	0-50 W	water / aluminum block	≈ 20°C	BHM / H / THM
[Jang,19a]	aluminum / quartz glass	60x110x(0.5+?) Y	25 25	15 rect./alternate 0.5-1.5x0.5	FC-72	50	0-5 W	TEC	25-35°C	BHM / H / THM
[Jang,19b]*	graphite	60x110x0.5 N	25 110	14 rect./alternate 1.55-3.25x0.3	FC-72	50	0-5 W	air / natural convection	25°C	BHM / H / THM
[Jo,19]**	silicon / pyrex	67.5x28x(0.5+1.1) Y	10 10	5 semi-circular 0.835	ethanol	50	2-21 W	water / copper block	20°C	BHM

	Material / geometry				Operating conditions					
	Material	**Overall dimensions**	**Evap. / cond. lengths**	**Channels**	**Fluids**	**Filling ratio**	**Heat power applied**	**Cooling system**	***T sat°***	**Orientation / gravity field**
Reference	machined plate / covering plate	*wxLx(t m+t c)* (mm3) Visu. (Y/N)	*L ev* (mm) *L cd* (mm)	*N* Shape *D (mm) / axb*		%	(W) or (W/cm²)	fluid / cooling block		
[Jun,18]	silicon / pyrex	33.5x50x(1+0.7) Y	10 15	10 rectangular 1x0.5	ethanol	50	?	water / copper block	20°C	BHM / H
[Jung,20]**	polycarbonate	53.4x85.5x0.64 N	17.1 17.1	12-28 rect./alternate 0.82-3.25x0.3	HFE-7000	?	0-2.8 W/cm²	water / copper block	20°C	BHM / 45° bent / H
[Jung,21]**	silicon / glass	28x67.5x1.6 N	10 10	5 rectangular 1.1x0.5	ethanol	45	0-16 W	water / copper block	30°C	BHM
[Kamijima,20]**	silicon / glass	20x40x (0.525+0.525) Y	12 16	11 square 0.35x0.35	FC-72	39-63	2-24 W	water / copper block	20-40°C	BHM
[Kearney,14]*	FR4 / polycarbonate	158x575x(2.3+5) Y	50 50	26 rectangular 1.9x1.55	ethanol Novec 649 Novec 7200	30-70	0-2 W/cm²	water / cold plate	10°C	BHM / 45° / H
[Kearney,16]*	FR4 / polycarbonate	158x575x(2.3+5) Y	50 50	26 rectangular 1.9x1.55	Novec 649 Novec 774	30-70	0-2.5 W/cm²	water / cold plate	10°C	BHM
[Khandekar,02]	aluminum / polycarbonate	130x45x(3+3) Y	30 13.5	12 rectangular/circ. 2.2x2-1.5x1 / 2	water ethanol	0-70	0-70 W	water / cold plate	?	BHM / θ / H
[Kim,03]*	brass / glass	78x265x(15+12) Y	70 70	4-10 square 1.5x1.5	ethanol R-142b	40	0-1.2 W/cm²	water / cold plate	?	BHM
[Kim,20]**	silicon / pyrex	80x35x(1+0.7) Y	20 20	10 rectangular 1x0.5	ethanol FC-72 HFE-7000 R-134a R-245fa	50	9-21 W	water / copper block	(-10)-60°C	BHM
[Laun,14]*	aluminum	300x300x6 N	80 150	20 square 1.3x1.3	acetone	80	0-500 W	water / aluminum block	?	BHM / H / THM
[Lee,16]** [Lee,17]**	silicon / pyrex	16x50x(1+1) Y	10 15	5 square/circular *Dh* = 390 / 480 / 570 µm	FC-72	50	0-8.46 W	water / cold plate	20°C	BHM
[Lee,18]**	silicon / pyrex	16-44.5x50x(1+1) Y	10 15	5-10-15-20 square/circular *Dh* = 390 / 480 / 570 µm	FC-72	50	0-12 W	water / cold plate	20°C	BHM / H
[Li,13]	aluminum	61x180x? N	?	10 square/triangular 1x1 / *D h* = 0.58 - 1	acetone ethanol	38 50 70	0-100 W	air / aluminum fins	32°C	BHM
[Lim,18] [Lim,19]	silicon / glass	33.5x80x(0.5+0.8) Y	15 15	10 rect./alternate 1.5-0.5x0.5	HFE-7000	50	0-12 W	water / copper block	30°C	H
[Lin,08] [Lin,09]	PDMS PDMS + copper powder	50x56x5 Y	10 10	6 circular 2	ethanol methanol	60	0-8 W	water / copper block	15°C	BHM / H
[Manno,15]	copper / borosilicate	125x265x(5+5) Y	45 67	12 square 2x2	ethanol	50	0-100 W	water / copper block	20°C	BHM / H / E
[Markal,20a-b]*	copper / glass	55.5x116x(4+?) Y	20 40	8 rect./alternate 1-2x2	ethanol pentane eth./pent.	30 60	5-45 W	water / copper block	20°C	BHM / H
[Miyazaki,99]	copper / polycarbonate	120x285x(5+16) Y	?	25 rectangular ?	R-142b	42	0-80 W	water / cold plate	?	?
[Natsume,13]	?	95x225x5 N	30 30	11x2 layers square 1.5x1.5	H_2 Ne N_2	25-50	0-4 W	Cryocooler / copper block	15-30 K	BHM

	Material / geometry				Operating conditions					
	Material	**Overall dimensions**	**Evap. / cond. lengths**	**Channels**	**Fluids**	**Filling ratio**	**Heat power applied**	**Cooling system**	***T sat°***	**Orientation / gravity field**
Reference	machined plate / covering plate	*wxLx(t m+t c)* (mm3) Visu. (Y/N)	*L ev* (mm) *L cd* (mm)	*N* Shape *D (mm) / axb*		%	(W) or (W/cm²)	fluid / cooling block		
[Pagnoni,18a]*	copper / borosilicate	145x210x(2.5+5) Y	10 150	11 square 2.5x2.5	ethanol	55	0-200 W	water / copper block	20°C	BHM / H / E
[Pagnoni,18b]*	copper	120x200x(2+1) N	10 100	12 rectangular 1.6x1.7	ethanol FC-72	50	0-260 W	water / copper block	5-20-40°C	BHM / H / E
[Qu,07]	copper	25x60x6 N	?	8 square/triangular *D h* = 1 - 1.5	water	25-45	0-55 W	water / cold plate	?	BHM / H / THM
[Qu,10]** [Qu,12]**	silicon / pyrex	25x60x(0.5+0.525) Y	9.5 15	5-7-5 trapezoidal *D h* = 251 / 352 / 394 µm	water ethanol FC-72 R-113	0-73	0-11 W	water / cold plate	25°C	BHM / H
[Sedighi,18]*	aluminum / glass	148x346x(5+?) Y	80 80	4 square 2x2	methanol	40-70	0-200 W	water / cold plate	20°C	BHM?
[Smoot,11]	copper + copper porous rods	30x30x? N	20 10	7 square 0.794x0.794	acetone water	30-80	0-120 W	water / cold plate	20-60°C	BHM / H / THM
[Taft,13]* [Taft,15]*	aluminum	300x300x6 N	76 127	20 square 1.3x1.3	acetone	80	100-500 W	water / cold plate	?	BHM / H / THM
[Taft,19]	?	50.8x152.4x2 N	2x25.4 1 or 2x12.7	17 square 1x1	butane R134a	45	0-40 W	Cold plate	?	µg
[Takawale,19]*	copper / glass	101.4x193.6x(5+?) Y	32 65	17 square 1.2x1.2	ethanol	40 60 80	20-180 W	water / aluminum block	22°C	BHM
[Thompson,09]	copper?	63.5x101.6x2.54 N	25.4 76.2	15x2 layers square 0.762x0.762	acetone	80	0-200 W	water / aluminum block	20-60°C	BHM / E
[Thompson,11a]	copper	38.1x130.2x2.86 N	15 76	4x2 layers square 1.175x1.70	acetone water	73	0-300 W	water / aluminum block	20-60°C	BHM / H
[Thompson,11b] [Thompson,11c]	copper	74.5x136x3 N	38 38	6 square 1.5x1.5	water	70	0-250 W	water / aluminum block	20°C	BHM
[Winkler,20]*	copper	50x100x2-2.5 N	8-25 10-50	13-10 square 1x1/1.5x1.5	acetone	50	0-300 W	water / copper bl. - air / alu	20.5°C	BHM / H
[Wits,18]	stainless steel	50x200x? N	50 50	6 square 2x2	methanol water ammonia	40	0-100 W	TEC / water / cooling block	10°C	BHM / H
[Wu,16]	aluminum / plexiglas	54x168x? Y	35 40	4 square 2x2	ethanol / 0.1-0.3 wt. % C60	50	20-70 W	water / aluminum block	?	50°
[Yamagami,16]*	aluminum / polycarbonate	119x236x(3+?) Y	40 40	12 square 2x2	water water / 1-7.15% butan-	50	0-320 W	water / aluminum block	20°C	BHM
[Yang,09]*	aluminum / polycarbonate	120x180x(3+?) Y	30 60	20 - 33 square 2x2 - 1x1	ethanol	0 - 95	48-338 W	water / copper block	20°C	BHM / H / THM
[Yang,15]**	silicon / glass	35x40x1.25 Y	7 7	32 rect./alternate 0.5/0.3x0.25	methanol water	70 80	6-19 W	water / copper block	5°C	BHM / 45°
[Yoon,17]** [Yoon,18]**	silicon / pyrex	50x18.5x(1+0.7) Y	10 15	5 rectangular 1x0.5	ethanol	55	2-30 W	water / copper block	20°C	BHM
[Zabek,16]*	copper	120x200x3 N	10 80	12 rectangular 1.6x1.7	ethanol	50	120 W	water / aluminum block	20°C	BHM / 45°

Nomenclature of appendix A.2:

a: channel width

b: channel height

w: FPPHP width

L: length

t_m: machined plate thickness

t_C: covering plate thickness

ABS: Acrylonitrile Butadiene Styrene

PDMS: PolyDiMethylSiloxane

References used for the calculations carried out in appendix A.1:

* Normal FPPHPs

** Micro-FPPHPs

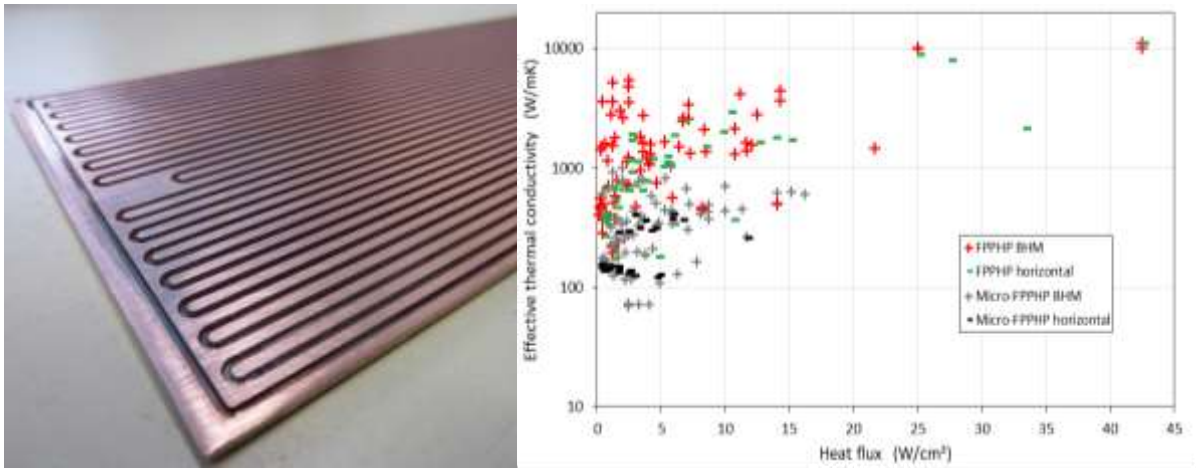

GRAPHICAL ABSTRACT